



1 **New Insights From The Jülich Ozone-Sonde Intercomparison**
2 **Experiments: Calibration Functions Traceable To One Ozone Reference**
3 **Instrument**

4 Herman G.J. Smit¹, Deniz Poyraz², Roeland Van Malderen², Anne M. Thompson^{3,4}, David W. Tarasick⁵, Ryan M.
5 Stauffer³, Bryan J. Johnson⁶, Debra E. Kollonige^{3,7}

6

7 ¹Forschungszentrum Jülich, Institute of Energy and Climate Research, IEK-8: Troposphere, Jülich, 52425, Germany

8 ²Royal Meteorological Institute of Belgium & Solar-Terrestrial Centre of Excellence, Uccle, Belgium

9 ³Atmospheric Chemistry and Dynamics Laboratory, NASA/GSFC, Greenbelt, MD, USA

10 ⁴University of Maryland Baltimore County, Baltimore, MD, USA,

11 ⁵Environment and Climate Change Canada, Downsview, ON, Canada

12 ⁶Global Monitoring Laboratory, NOAA Earth System Research Laboratory, Boulder, CO, USA

13 ⁷Science Systems and Applications, Inc, Lanham, MD, USA

14

15 *Correspondence to:* Herman G.J. Smit (h.smit@fz-juelich.de)

16



17 **Abstract**

18 Although in principle the ECC (Electrochemical Concentration Cell) ozonesonde is an absolute measuring device, in
19 practice it has several “artefacts” which change over the course of a flight. Most of the artefacts have been corrected in the
20 recommendations of the Assessment of Standard Operating Procedures for Ozone Sondes Report (GAW Report No. 268),
21 giving an overall uncertainty of 5-10% throughout the profile. However, the conversion of sampled ozone into the measured
22 cell current has not been fully quantified, resulting in time-varying background current and pump efficiencies. We describe
23 an updated methodology for ECC sonde data processing that is based on JOSIE 2009/2010 and JOSIE 2017-SHADOZ test
24 chamber data. The stoichiometry (O_3/I_2) factors and their uncertainties along with the fast and the slow reaction pathways for
25 the different sensing solution types used in the global ozonesonde network are determined. Experimental evidence is given
26 for treating the background current of the ECC-sensor as the superposition of a constant ozone independent component (I_{B0} ,
27 measured before ozone exposure in the sonde preparation protocol) and a slow time-variant ozone-dependent current
28 determined from the initial measured ozone current using a first-order numerical convolution. The fast sensor current is
29 refined using the time response determined in sonde preparation with a first order deconvolution scheme. Practical
30 procedures for initializing the numerical deconvolution and convolution schemes to determine the slow and fast ECC
31 currents are given. Calibration functions for specific ozonesondes and sensing solution type combinations were determined
32 by comparing JOSIE 2009/2010 and JOSIE-2017-SHADOZ profiles with the JOSIE ozone reference UV-photometer
33 (OPM). With fast and slow currents resolved and the new calibration functions, a full uncertainty budget is obtained. The
34 time responses correction methodology makes every ozonesonde record traceable to one standard, i.e. the OPM of JOSIE,
35 enabling the goal of a 5% relative uncertainty to be met throughout the global ozone network.

36

37



38 1 Introduction

39 Although it is a minor trace gas constituent of the Earth's atmosphere, ozone plays several essential roles in its chemistry and
40 physics. In the stratosphere, where about 90% of the total ozone amount resides, ozone protects life on Earth by absorbing
41 the harmful ultraviolet (UV) radiation from the sun, adding heat to the stratosphere. In the upper troposphere, ozone is an
42 important absorber of infrared radiation, acting as a powerful greenhouse gas (IPCC-Climate Change, 2013, 2023). Ozone is
43 the primary source of the hydroxyl (OH) radical in the troposphere, controlling the lifetime of hundreds of pollutants
44 (Seinfeld and Pandis, 2016), and determining its oxidizing capacity (Thompson, 1992). The stratosphere is a natural source
45 of tropospheric ozone but approximately half of the ozone in the troposphere is formed photochemically when combustion
46 (vehicular, industrial or pyrogenic) processes release NO_x , ($\text{NO} + \text{NO}_2 = \text{NO}_x$), carbon monoxide (CO) and hydrocarbons
47 (also referred to as volatile organic compounds (VOC) that react through free radical cycles in the presence of UV. VOC may
48 also originate from combustion or natural sources, the latter predominantly from vegetation and to a lesser extent from the
49 ocean. Surface ozone is considered a pollutant with adverse impacts on human and animal health (e.g., respiratory problems)
50 and on vegetation (Mills et al., 2018) and is a primary marker for "Air Quality," setting the scale for Good, Fair, and
51 Unhealthy definitions used by local Air Quality agencies (Garner and Thompson, 2013). The photochemistry of ozone
52 pollution or "smog" was worked out in the 1950s (Seinfeld and Pandis, 2016); surface ozone measurements became
53 widespread as regions or nations enacted regulations to mitigate episodes of high ozone.

54 Measurements of stratospheric ozone gained attention in the 1960s and 1970s when it was recognized that natural levels of
55 ozone were regulated by catalytic cycles involving nitrogen oxides (NO_x , N_2O_5 , NO_3 and HNO_3), hydrogen oxides (with H_2O
56 vapor a source of OH and HO_2 , $\text{HO}_x = \text{OH} + \text{HO}_2$) and halogens (XO and XO_2 , where X was Cl or Br derived from oceanic
57 methyl chloride and methyl bromide). Anthropogenic perturbations of these cycles were investigated when it was recognized
58 that emissions of N- and Cl-containing compounds by rockets and high-altitude aircraft could threaten stratospheric ozone
59 (Crutzen, 1970; Stolarski and Cicerone, 1974). A worse threat was hypothesized when it was realized that
60 chlorofluorocarbons (CFCs) present in the atmosphere (Lovelock et al., 1973), but relatively inert in the troposphere could
61 enter the stratosphere and destroy ozone photochemically there (Molina and Rowland, 1974). Perturbed stratospheric ozone
62 chemistry by CFCs was a cause for alarm, leading to first regulations in CFC usage in the 1970s. However, it was not until
63 ground-based total ozone monitoring (Farman et al., 1985) discovered catastrophic springtime ozone loss over Antarctica in
64 1984-1985 that international action was taken to phase out Ozone Depleting Substances through the 1987 signing of the
65 Montreal Protocol (UNEP-Ozone Secretariat, 14th edition, 2020). Implementation of the Montreal Protocol and its follow-on
66 Amendments require governments to monitor ozone, reporting every four years to the World Meteorological Organization
67 (WMO) and United Nations Environment Programme (UNEP) in Scientific Assessments on total column ozone, its vertical
68 distribution and attribution of long-term. Since 1991 there have been nine UNEP/WMO Scientific Assessments, with the
69 most recent report released in 2022 (WMO/UNEP, 2023).

70 Global monitoring of total ozone has relied on satellite instruments since the 1970s but ground-based instrumentation
71 deployed on all continents still provides ground-truth. In particular, ozonesondes are essential for satellite algorithms and
72 validation of satellite-derived profiles and reanalysis products (Wang et al., 2020; Thompson et al., 2022). Balloon-borne
73 ozonesondes, flown together with radiosondes, make relatively inexpensive, accurate, all-weather measurements of the
74 ozone concentrations from the ground to 30 km or higher, with ~100 m vertical resolution (Smit, 2014). The electrochemical
75 concentration cell (ECC) ozonesonde has been deployed for more than 50 years with ~60 stations currently launching on all
76 continents (GAW Report No.268, 2021; Thompson et al., 2022; Stauffer et al., 2022). Ozonesonde data constitute the most
77 important record for deriving ozone trends throughout both stratosphere and troposphere, particularly in the climate-sensitive
78 altitude region near the tropopause where satellite measurements are most uncertain. Strategic ozonesonde networks like
79 MATCH and IONS (Intensive Ozonesonde Network Studies) have been organized to support aircraft campaigns in



80 characterizing photochemical and dynamical interactions affecting vertical and regional ozone distributions (Thompson et
81 al., 2007a and 2011; Tarasick et al., 2010).

82 **1.1 Establishing Quality Assurance/Quality Control (QA/QC) practices for ozonesondes (1996-2021)**

83 Despite the advantages of ozonesonde profiles, there is a challenge in that each ozonesonde instrument is unique, typically
84 launched only once, and it must be carefully prepared prior to launch in order to obtain accurate data. Processing of the final
85 measurement is carried out using certain parameters determined pre-launch. In addition, there are two manufacturers of
86 ozonesondes that show systematic offsets relative to each other. Further biases in ozonesonde datasets can occur because
87 three variants of the sensing solution that produce the ECC current signal from the ozone are currently in use. The
88 ozonesonde community has created guidelines for operations and data processing applicable to the range of instrument and
89 sensing solution types used in the global ECC-sonde network. When the guidelines are followed it is possible for
90 consistently high-quality data to be collected across the global network.

91 The creation of guidelines or “best practices” has evolved over the past 20 years in a process referred to as the Assessment of
92 Standard Operating Procedures (SOP) for Ozonesondes (ASOPOS) and organized through the WMO Global Atmosphere
93 Watch (GAW). The key element of ASOPOS was the establishment of the World Calibration Centre for Ozone Sonde
94 (WCCOS) with a custom-designed Environmental Simulation Facility (ESF) at the Research Centre in Jülich, Germany, in
95 1995 (GAW Report No.104, 1994; Smit et al., 2000). The ESF consists of an absolute ozone measuring reference, a fast
96 response (2s), accurate (2-3%), dual beam UV-absorption ozone photometer (OPM) (Proffitt and McLaughlin, 1983)
97 attached to the chamber that enables control of pressure, temperature and ozone concentration simulating flight conditions of
98 an ozone sounding up to 35 km over ~ 2 hours (Smit et al., 2007). Up to four ozonesonde instruments at once can be
99 intercompared through this process. Simulations in the ESF included conditions of polar, midlatitude, subtropical and
100 tropical sonde launches. Other aspects of sonde operations, e.g., response times to rapid changes in ozone concentration, are
101 also tested in the ESF. Since 1996, nine Jülich OzoneSonde Intercomparison Experiment (JOSIE) campaigns have been
102 conducted at WCCOS and documented in a series of publications (Smit and Kley, GAW Report No. 130, 1998) for JOSIE-
103 1996; JOSIE-1998 (Smit and Sträter, GAW Report No. 157, 2004a), JOSIE-2000 (Smit and Sträter, GAW Report No. 158,
104 2004b; Smit et al., 2007; Thompson et al., 2007b); JOSIE-2009/2010; JOSIE-2017 (Thompson et al., 2019). The first three
105 JOSIEs, which tested several non-ECC instruments as well as Science Pump Corporation (SPC) and ENSCI ECC
106 instruments, showed the ECC-sonde to be more accurate. After JOSIE-2000 only ECC-sondes were tested in the WCCOS.
107 In 2004 a the WMO/BESOS (Balloon Experiment on Standards for OzoneSondes) field campaign, carried out in Laramie
108 (Wyoming, USA) deployed a large gondola with 18 ozonesondes and the OPM of WCCOS (Deshler et al., 2008) with results
109 similar to JOSIE-2000. These early experiments demonstrated that high precision and accuracy depend not only on sonde
110 manufacturer and sensing solution strength, but also on pre-launch preparation details. Smit et al. (2007) concluded that
111 standardisation of operating procedures for ECC sondes yields a precision better than $\pm (3-5) \%$ and an accuracy of about
112 $\pm(5-10)\%$ up to 30 km altitude.

113 In 2004 an expert team of ozonesonde operators, data providers and manufacturers formally instituted the ASOPOS to
114 analyse the results of BESOS and the JOSIE campaigns up to that time. The ASOPOS goal was to ensure consistency of data
115 quality across stations and within individual station time series by specifying how to prepare and operate the ozonesonde
116 instrument and to accurately process and report profile data. The first set of SOP recommended by ASOPOS, based on the
117 JOSIE campaigns from 1996 to 2000 and BESOS, was published online in 2012 and as GAW Report No. 201 in 2014 (Smit
118 and ASOPOS 1.0 Panel). To make (historical) ozonesonde time series records compliant with the ASOPOS standards, an



119 OzoneSonde Data Quality Assessment (O3S-DQA) activity was initiated in 2011 within the framework of SI2N¹, resulting in
120 procedures for “homogenizing” data and estimating uncertainties (Smit and O3S-DQA Panel, 2012; [https://www.wccos-](https://www.wccos-josie.org/o3s-dqa)
121 [josie.org/o3s-dqa](https://www.wccos-josie.org/o3s-dqa)); transfer functions in support of the guidelines were documented in Deshler et al. (2017). Within several
122 years roughly half of the global network stations had reprocessed their data (Tarasick et al., 2016; Van Malderen et al., 2016;
123 Thompson et al., 2017; Sterling et al., 2018; Witte et al., 2017, 2018, 2019; Ancellet et al., 2022). Comparisons between
124 original and homogenized data showed that significant systematic errors were eliminated, particularly where changes in
125 technique and/or equipment had been made.

126 The homogenised time series were based on having raw currents from the ozonesonde cells, a prerequisite for the analysis
127 and processing methods of the present paper. However, the ozonesonde community agreed that several issues were
128 unresolved. These included the complexity of the so-called “background current” characterized during the preparation and
129 the lack of traceability of the archived ozone profile to an absolute standard. A JOSIE-2017 campaign was designed to
130 address these concerns. In addition to the tests of prior JOSIEs, the 2017 tests focused on a single regime, tropical profiles, to
131 gather a larger set of statistics. A special challenge of tropical soundings is that near the tropopause the ozone signal to noise
132 is typically very small, giving artefact low readings (Vömel et al. 2020). JOSIE-2017 (also called JOSIE-SHADOZ) was
133 carried out with eight SHADOZ operators who supplied their home-prepared sensing solutions, following their own
134 preparation procedures for half the simulations (Thompson et al., 2019). The other half of the simulations tested a lower-
135 buffer variant of the sensing solution with the WMO/GAW SOP. The overall results of JOSIE-2017 resembled those of the
136 1996-2000 JOSIE and BESOS. In other words, the offsets of the various instrument-sensing solution types (SST) from the
137 OPM reference and associated biases of ECC sonde instruments and SST had not changed over more than 20 years.
138 An ASOPOS 2.0 Panel formed in 2018 to review the JOSIE-2017 campaign data along with lessons learned from
139 reprocessed datasets and the JOSIE 2009/2010 results. ASOPOS 2.0 published GAW Report No. 268, “Ozonesonde
140 Measurement Principles and Best Operational Practices” (Smit, Thompson and ASOPOS, 2021; hereafter referred to as
141 GAW Report No. 268) as an update to GAW Report No. 201. The newer report gives the same recommendations as GAW
142 Report No. 201 on sonde manufacturer-SST combinations, but stricter and more unified SOP. The latter consist of more
143 detailed recommendations based on physical principles of the ozonesonde measurement. More explicit procedures are given
144 for data quality indicators, hardware usage and maintenance and metadata. GAW Report No. 268 also specified for the first
145 time how to report ozone profiles traceable to the standard OPM. However, the issues of a time-varying background current,
146 specification of uncertainties in the ozone measurement (and related pump efficiencies) required analysis beyond GAW
147 Report No. 268 before consensus could be reached on data-processing recommendations. That is the scope of this paper.

148 **1.2 Addressing residual ozonesonde QA/QC issues from WMO/GAW 268. Outline of paper**

149 Chapter 3 of GAW Report No. 268 draws on the Tarasick et al. (2021) review of ozonesonde performance characteristics.
150 Both documents point out that the greatest barriers to reducing uncertainties in the final ozone measurement derive from (1)
151 the use of improper pump efficiencies and (2) a background current that varies with ozone exposure (hence with time) over
152 the course of the balloon ascent. The current paper revisits fundamentals of the ozonesonde measurement to overcome these
153 two shortcomings. The here reported methodology to resolve the fast and slow time responses builds on an earlier study by
154 Imai et al. (2013), and more recently on the work by Tarasick et al. (2021) and Vömel et al. (2020). We first give a more
155 detailed description of the physical and chemical origin of the ECC ozonesonde signal (Section 2), illustrated with laboratory
156 measurements from the Uccle, Belgium, ozonesonde station. Section 3 first corrects for the background signal composed of

¹ This is a joint initiative under the auspices of SPARC (Stratosphere–troposphere Processes And their Role in Climate), the International Ozone Commission (IO3C), the ozone focus area of the Integrated Global Atmospheric Chemistry Observations (IGACO-O3) programme, and the Network for Detection of Atmospheric Composition Change (NDACC). For simplicity, an acronym of acronyms, SI2N, was adopted.



157 (i) a constant physical component (IB_0) and (ii) a small and slow varying (time constant 25 min) chemical component that
158 varies with ozone exposure. The remaining fast component of the signal is then corrected by deconvolution with an
159 exponential decay with a time constant between 20 and 30s. Although the approach is similar to Vömel et al. (2020), an
160 advantage of our updated method is that it is developed from and applied to dedicated JOSIE chamber data (JOSIE
161 2009/2010) that used consistently prepared ozonesondes, with detailed in-flight and post-flight measurements and metadata.
162 Second, the simultaneous OPM measurements in the simulation chamber serve as reference data for determining key
163 parameters of the method, e.g. the contribution of the slow component to the overall signal. In Section 4, the OPM reference
164 data are used to evaluate the updated method with comparisons to the conventional method. For these analyses,
165 measurements from all JOSIE campaigns, covering a range of simulated environments are used. Comparing residuals of the
166 corrected ozonesonde profiles to the OPM profiles allows us to determine a set of the calibration functions for each
167 instrument-SST combination (Section 5) and to estimate uncertainties of the updated time response correction (TRC) method
168 (Section 6). The TRC method is implemented with actual sounding data in Section 7 for ascent and descent profiles at
169 tropical, mid-latitude and polar (Antarctic) stations and improvements with respect to the conventional approach are
170 quantified. A summary and outlook appear in Section 8.

171 2 Physical and Chemical Origins of the ECC Ozonesonde Signal

172 2.1 Principle of Operation

173 The ECC (=Electrochemical Concentration Cell) ozonesonde, developed by Komhyr (1969), uses an electrochemical method
174 to measure ozone which is based on the titration of ozone in a neutral buffered potassium iodide (NBKI) sensing solution
175 according to redox reaction:



179 A neutral $\text{pH} \approx 7$ is obtained through the addition of a phosphate buffer ($\text{NaH}_2\text{PO}_4 \cdot \text{H}_2\text{O}$ and $\text{Na}_2\text{HPO}_4 \cdot 12\text{H}_2\text{O}$)
180 The titration involves a coulometric method employing electrochemical cells to determine the amount of generated “free”
181 iodine (I_2) per unit time through conversion into an electrical current at a depolarizing cathode electrode. The actual ECC
182 component of the ozone sensor, made of Teflon or molded plastic, consists of two chambers. Each chamber contains a
183 platinum (Pt) mesh electrode that serves as cathode or anode. The chambers are immersed in a KI-solution of different
184 concentrations and linked together to provide an ion pathway and to prevent mixing of the cathode and anode concentrations.
185

186 Continuous operation is achieved by a small nonreactive gas sampling pump (Komhyr 1967) forcing ozone in ambient air
187 through the cathode cell that contains a lower-concentration KI-sensing solution, causing an increase of “free iodine” (I_2)
188 according to the redox reaction (1). Transported by the stirring action of the air bubbles, the free I_2 contacts the Pt-cathode
189 and convert to 2I^- through the uptake of two electrons. At the Pt-anode surface, I^- is converted to I_2 through the release of
190 two electrons. The overall cell reaction is:



194 The electrical current I_M (μA) generated in the external circuit of the electrochemical cell is directly related to the uptake rate
195 of ozone in the sensing solution. By knowing the gas volume flow rate $\Phi_{\text{P}0}$ [cm^3s^{-1}] of the air sampling pump and its
196 temperature T_P (K), the electrical cell current I_M (μA), after subtracting a background current I_B (μA), is converted to the
197 ozone partial pressure $P_{\text{O}3}$ (in mPa) (Komhyr 1969):



198

$$199 \quad P_{O_3} = 0.043085 * \frac{T_P}{(\eta_P * \eta_A * \eta_C * \Phi_{PO})} * (I_M - I_B) \quad (1)$$

200

201 The constant 0.043085 is determined by the ratio of the universal gas constant, R, to twice the Faraday constant, F, (because
202 two electrons flow in the electrical circuit from reaction (R2) (Komhyr 1969).

203 The overall efficiency of conversion consists of:

- 204 a) Pump efficiency, η_P , that declines at lower pressures. At reduced air pressures (< 100 hPa), the pump efficiency
205 declines due to pump leakage, dead volume in the piston of the pump, and the back pressure exerted on the pump
206 by the cathode cell (Komhyr 1967, Steinbrecht et al., 1998, Nakano and Morofuji, 2023).
- 207 b) Absorption (i.e capture) efficiency, η_A , for the transfer of the sampled gaseous ozone into the liquid phase. Although
208 evaporation reduces the amount of the sensing solution available for ozone uptake, η_A is not significantly affected
209 (Komhyr, 1971). Thus, η_A remains at 1.0, with an uncertainty of < ±1% (Tarasick et al., 2021; Davies et al., 2003).
- 210 c) Conversion efficiency, η_C , of the absorbed ozone in the cathode solution creating iodine that leads to the measured
211 cell current I_M . Historically, it has been assumed that η_C is unity at neutral pH (Saltzman and Gilbert, 1959;
212 Komhyr, 1969; Komhyr, 1986). However, there is now a great deal of evidence that this is not quite the case, as will
213 be discussed below.

214

215 Currently, there are two manufacturers of ECC ozonesondes, Science Pump Corporation and Environmental Science
216 Corporation, most recently producing the SPC-6A and EN-SCI-Z ozonesonde series, respectively. The designs of both ECC
217 types are similar but differences include: (i) the material of the electrochemical cell (Teflon for SPC-6A and molded plastic
218 for EN-SCI-Z); (ii) ion bridges (details are not known due to manufacturer proprietary issues); (iii) layout of the metal
219 frame. Since 2014, a modified ECC-type ozonesonde manufactured at the Institute of Atmospheric Physics (IAP), Beijing,
220 has been produced (Zhang et al., 2014a,b) but to date, few comparisons of the Chinese instrument with the well-
221 characterized SPC-6A and EN-SCI models have been carried out. Thus, profiles from Chinese instruments are not included
222 in the current study.

223

224 Three different aqueous sensing solution types (SST) are commonly used in the ECC-sonde cathode cells: (i) SST1.0: 1.0%
225 KI & full buffer; (ii) SST0.5: 0.5% KI & half buffer; (iii) SST0.1: 1.0% KI & 1/10th buffer (GAW Report No. 268),
226 respectively. In all cases a KI saturated cathode solution is employed in the anode cell. Laboratory studies by Johnson et al.
227 (2002) found that, depending on the concentration of the cathode sensing solution, the stoichiometric ratio of the ozone to
228 iodine conversion reaction (1) can increase from 1.00 up to 1.05-1.20. Johnson et al. (2002) determined that this increase is
229 caused primarily by the phosphate buffer and to a lesser extent depends on the KI concentration. No significant influence of
230 KBr-concentration was observed, although its role is not well understood. From JOSIE 2000 (Smit et al., 2007), BESOS
231 2004 (Deshler et al., 2008) and multiple other sounding tests (e.g. Deshler et al., 2016) it is known that there is a significant
232 difference in the ozone readings when sondes of the same type are operated with different sensing solutions, e.g. STT0.5 and
233 SST1.0. Both sonde types exhibit a systematic change of sensitivity, about 5-10% over the entire profile, when the sensing
234 solution is changed from SST0.5 to SST1.0. Johnson et al. (2002) demonstrated that this offset is mostly caused by the
235 phosphate buffer with a minor contribution from the KI- concentration. In addition, the EN-SCI sonde tends to measure
236 about 4-5 % more ozone than the SPC-sonde when operated with the same SST for reasons that are not understood.

237 2.2 Impact of Pump efficiency and Conversion Efficiency (Stoichiometry)

238 The accuracy of the ECC ozonesonde depends on the extent of the ozone-iodide reaction in the cathode cell and the
239 efficiency of the reduction of the iodine produced, which can be expressed primarily in the overall uncertainty based on the



240 contribution of the individual uncertainties of each parameter expressed in Eq. (1). Tarasick et al. (2021) quantified and
 241 reviewed the uncertainty budget of the measured partial pressure of ozone, confirming that the most critical parameters are
 242 the (background) current for the tropospheric part of the ozone profile and the pump and conversion efficiencies used in the
 243 post flight data processing for the stratospheric part of the ozone profile.

244
 245 Since JOSIE 1996 (Smit and Kley, 1998) it was recognized that, if the preparation and data correction procedures prescribed
 246 by Komhyr (1986) are used, an increase of the stoichiometric factor, presumably due to evaporation of the cathode sensing
 247 solution in the course of the sounding, may be compensated by a too low pump flow correction in the stratosphere above 20-
 248 25 km altitude. With new pump flow calibrations and stoichiometry investigations, Johnson et al. (2002) demonstrated that
 249 the pump efficiency tables reported by Komhyr (1986) and Komhyr et al. (1995) indeed compensate for the increase of the
 250 stoichiometric factor, i.e. the conversion efficiency. Commonly used pump efficiencies and their uncertainties recommended
 251 by ASOPOS 2.0 (GAW Report No. 268) are listed in Table 1.

252
 253 **Table 1:** Pump efficiencies (η_p) as a function of air pressure for ECC ozonesondes reported by (i) Komhyr (1986) and referred
 254 to as K86; (ii) Komhyr et al. (1995), called K95; (iii) Johnson et al. (2002), referred as NOAA/CMDL & UWYO at
 255 Univ.Wyoming; (iv) Nakano and Morofuji, 2023, at JMA.

256

| Pressure [hPa] | ECC (SPC-6a) Komhyr, 1986 K86-Efficiency | ECC (ENSCI) Komhyr et al., 1995 K95-Efficiency | ECC (CMDL) Johnson et al., 2002 | ECC (UWYO) Johnson et al., 2002 | ECC (JMA) Nakano and Morofuji, 2023 |
|----------------|--|--|---------------------------------|---------------------------------|-------------------------------------|
| 1000 | 1 | 1 | 1 | 1 | 1 |
| 100 | 0.989 ± 0.005 | 0.993 ± 0.005 | 0.968 ± 0.009 | 0.978 ± 0.011 | 0.978 ± 0.009 |
| 50 | 0.985 ± 0.006 | 0.982 ± 0.005 | 0.951 ± 0.011 | 0.964 ± 0.012 | 0.964 ± 0.011 |
| 30 | 0.978 ± 0.008 | 0.972 ± 0.008 | 0.935 ± 0.011 | 0.953 ± 0.015 | 0.948 ± 0.013 |
| 20 | 0.969 ± 0.008 | 0.961 ± 0.011 | 0.918 ± 0.012 | 0.938 ± 0.018 | 0.929 ± 0.014 |
| 10 | 0.948 ± 0.009 | 0.938 ± 0.021 | 0.873 ± 0.015 | 0.893 ± 0.026 | 0.883 ± 0.017 |
| 7 | 0.935 ± 0.010 | 0.920 ± 0.022 | 0.837 ± 0.019 | 0.858 ± 0.029 | 0.848 ± 0.020 |
| 5 | 0.916 ± 0.012 | 0.889 ± 0.021 | 0.794 ± 0.023 | 0.817 ± 0.034 | 0.807 ± 0.023 |

257

258 The pump efficiency tables reported by Johnson et al. (2002) and more recently by Nakano and Morofuji (2023) are both
 259 based on a large number of pump calibrations using complementary and well-established methods. Both tables are generally
 260 consistent within statistical uncertainty, but diverge significantly from the older Komhyr (1986) and Komhyr et al. (1995)
 261 tables. Although they have historically been called “pump efficiencies”, the Komhyr values in Table 1 are now recognized as
 262 empirical efficiencies, which combine pump efficiency and conversion efficiency for the standard buffered solutions SST1.0
 263 and SST0.5 (Tarasick et al., 2021). For consistency with long-term data records, the values reported by Komhyr (1986) and
 264 Komhyr et al. (1995) are recommended by ASOPOS 2.0 (GAW Report No. 268) for SPC-6A & SST1.0 and EN-SCI &
 265 SST0.5, respectively.

266

267 Normally, in the pH = 7 buffered KI sensing cathode the stoichiometry of the conversion (R1) of ozone into iodine is
 268 assumed to be 1.00 with an uncertainty of about ±0.03 (Dietz et al., 1973), while the initial absorption efficiency of gaseous



269 ozone into the sensing solution will be 1.00 with an uncertainty of 0.01. These values for η_A and η_C are used in the
270 conventional method of ozonesonde data processing as recommended by ASOPOS in GAW Report No. 268 and before in
271 GAW Report No. 201.
272

273 **2.3 Perspectives on the Background Current**

274 **2.3.1 I_{B0} and I_{B1} Conventions for Background Currents**

275 The ECC sensor background current, I_B , is defined as the residual current output by the cell when sampling ozone free air.
276 Since the 1990s during the preparation of the ECC sensor at the day of flight, two background currents, I_{B0} and I_{B1} ,
277 respectively, are measured: before and after exposure of a certain amount of ozone, usually about $5\mu\text{A}$ ozone equivalent for
278 about 10 minutes. Both background currents are measured after flushing the cell for 10 minutes with ozone free air. (GAW
279 Report No. 201 and GAW Report No. 268). Although small (typically $< 0.1\mu\text{A}$), the ECC sensor background current may be
280 of appreciable magnitude compared to the current when there is very low ozone such as in the tropical upper troposphere or
281 in the stratosphere above 5 hPa but also during ozone hole conditions in polar regions.
282

283 Background measurements of SPC-5A sondes operated with the SST 1.0 using ozone-free air, showed before about 1993,
284 typical values of $I_{B0} = 0.06\pm 0.02\mu\text{A}$ and $I_{B1} = 0.09\pm 0.02\mu\text{A}$, respectively (Smit, 2004c). After 1993 I_{B0} dropped to values of
285 $0.00\text{--}0.03\mu\text{A}$ and consequently I_{B1} dropped by about $0.06\mu\text{A}$. This may mean that the manufacturer made changes, most
286 likely cleaning or conditioning the electrodes or ion bridge (e.g. less leakage of I_2 into the cathode solution). In the past thirty
287 years, both SPC-6A and EN-SCI sondes show similar low I_{B0} and I_{B1} values when a high-quality gas filter flushes the cells
288 with ozone free “zero” air. However, the difference of $I_{B1}\text{--}I_{B0}$ of $\sim 0.03\text{--}0.04\mu\text{A}$ has stayed the same over decades. This is
289 actually the “chemical” contribution of the overall $\text{O}_3 + \text{KI}$ chemistry in the cathode cell to the measured background current
290 after zero-air flushing, whereas I_{B0} is independent of ozone exposure and assumed to be an inherent property of the ECC-
291 sensor. The latter has been demonstrated in several laboratory experiments (Smit et al., 2007; Vömel and Diaz, 2010), and in
292 this study (Sect.2.3.3).

293 **2.3.2 Constant Background Current?**

294 In the early days of the ECC there was no clear distinction between I_{B0} or I_{B1} to apply for I_B in Eq. (1). Komhyr (1969)
295 suggested that I_B resulted largely from a residual sensitivity of the ECC sensor to oxygen, such that I_B decreased with air
296 pressure in proportion to the rate at which oxygen entered the sensor. Thornton and Niazy (1982) showed in a laboratory
297 study that the primary source of the background current is from the removal of residual tri-iodide, normally present in the
298 cathode solution and not from the reaction of oxygen with iodide to produce tri-iodide nor from the direct reduction of
299 oxygen. Since 1975 the manufacturer (Science Pump Corporation) has preconditioned the ECC electrodes with iodide such
300 that the oxygen dependence has become vanishingly small and can be neglected (Thornton and Niazy, 1982).
301

302 Theoretically, an ECC sensor in electrochemical equilibrium will produce no current; any current in the absence of ozone or
303 other oxidants must be due to an imbalance of tri-iodide between the anode and cathode cells (Komhyr, 1969). Possible
304 causes of such an imbalance include (i) a leaky ion bridge, (ii) limited mass transfer of residual tri-iodide (I_3^-) in the cathode
305 solution (Thornton & Niazy, 1982), (iii) limited electron transfer at the cathode surface, (iv) an imbalance resulting from cell
306 conditioning or contamination, or (v) previous exposure to ozone. The first three cases represent a background current that
307 may be expected to remain roughly constant and should therefore be subtracted as a best approximation; however, the last
308 two cases, (iv) and (v), should decline according to the response time of the cell (Tarasick et al., 2021).
309



310 2.3.3 Past Ozone Dependent Background Current

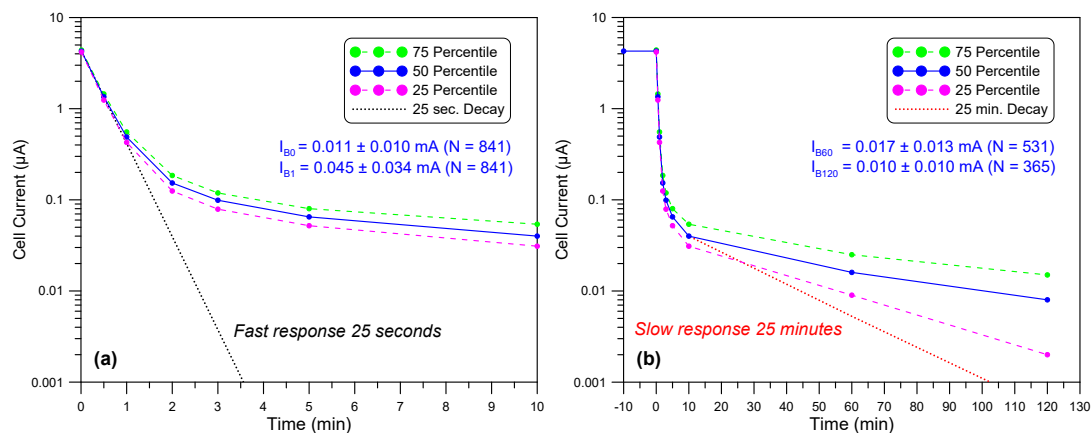
311 Based on simulation chamber experiments Smit et al. (1994) recommended using I_{B0} for the constant I_B subtraction, which
312 was confirmed in a field experiment by Reid et al. (1996). However, the results could not be confirmed in later JOSIE
313 experiments which demonstrated that the background current most likely varies with the past ozone measured, implying that
314 two background currents operate over the sonde operation (Smit and Sträter, 2004a,b; Smit et al., 2007): (i) one background
315 current I_{B0} , which is independent of ozone exposure and (ii) a second past ozone dependent background current that will vary
316 in the course of the sounding. This time variant ECC background current is assumed to result from a minor, but still slowly
317 decaying, contribution to the measured cell current. Based on laboratory experiments Johnson et al. (2002) and Vömel and
318 Diaz (2010) suggested that its origin is related with the ECC-chemistry having a fast (20-30 s) and an additional minor
319 pathway (reaction time constant ~20-30 min) that causes a memory effect, probably due to slow side reactions in the
320 oxidation of iodide by O_3 in the cathode sensing solution. In equilibrium this can lead to an overall stoichiometry factor,
321 O_3/I_2 , larger than 1.0. The magnitude of the excess stoichiometry depends strongly on the phosphate buffer concentration in
322 the cathode sensing solution. Vömel and Diaz (2010) suggested that, instead of a measured background current, it would be
323 better to use an appropriate solution dependent conversion efficiency and background current values in the basic ECC-
324 formula Eq. (1). For improved data processing the contributions of the slow (20-30 min) and fast (20-30 s) responses to the
325 overall measured ECC ozone signal need to be considered simultaneously using an appropriate response (memory) function.
326

327 Such a possible methodology may be the deconvolution of the measured ozone profile after determining the overall
328 frequency response of the combined sensor and air sampling system (De Muer and Malcorps, 1984). However, the method is
329 complicated and not practical to be apply to the global ozonesonde network. More accessible are first order numerical
330 schemes that deconvolve the fast response which were developed and tested by Imai et al. (2013) and Huang et al. (2015).
331 Tarasick et al. (2021) further developed one simple first order numerical scheme to resolve both the fast and slow time
332 responses of the ECC-sensor. Vömel et al. (2020) developed the methodology for quantifying the fast and slow currents in
333 more detail but several aspects were not fully considered and their methodology was not assessed with the most
334 comprehensive data base and for various pairs of sonde types and SSTs. This study remedies these gaps.
335

336 To investigate the chemical origins of the slow current, laboratory response-time tests for hundreds of ECC-ozone sensors
337 (EN-SCI, SST0.5) were made at the Uccle (Belgium) sounding station since August 2017 during every routine day-of-launch
338 preparations to measure the two time constants in the ECC signal. In this experiment, the following steps were taken to
339 record the ECC sensor current as function of time:

- 340 a. Before ozone exposure, flush the ECC-cell for 10 min with zero air: Record I_{B0} .
- 341 b. Expose the ECC-cell for 10 min to 5 μA ozone equivalent.
- 342 c. Flush the ECC-cell for 10 min with zero air: Record I_{B1} and stop flushing (pump inactive, short-circuit sensor leads)
- 343 d. No Flushing until $t=55$ min, then flush 5 min. zero air: Record I_{B60} and then stop flushing.
- 344 e. No Flushing until $t=115$ min, then flush 5 min with zero air: Record I_{B120} .

345 The steps (a) to (c) follow exactly GAW Report No. 201 and GAW Report No. 268 SOPs. However, after these steps, most
346 of the time between $t=10$ and 120 min., flushing with ozone-free air has stopped except for the 5-minute periods at $t=55$ min
347 and $t=115$ min. During the 5 minutes of flushing a short current increase was observed but it declined rapidly with a typical
348 “fast” $1/e$ response time of 25 seconds. The 120-min timing was chosen because this is the typical duration of the ascent of
349 an ozone sounding. Summaries of the observations for the fast and slow currents appear in Figure 1.



350

351 **Figure 1.** Relaxation of the ECC-cell current (logarithmic scale) flushed with purified ozone free air as function of time
 352 after the cells have been exposed for 10 minutes with 5 μA ozone. The sequence: (i) No flushing $t=10\text{-}55$ min.; (ii) Flushing
 353 $t=55\text{-}60$ min.; (iii) No flushing $t=60\text{-}115$ min.; (iv) Flushing $t=115\text{-}120$ min. Left diagram first 10 minutes relaxation (grey
 354 dotted line: $1/e$ decay of $I_M(t=0)$ with 25 s. time constant) and right diagram show the full two hours of relaxation (red
 355 dotted line: $1/e$ decay of I_{B1} ($t=10$ min.) with 25 min. time constant).

356

357 The observed relaxations in Figure 1 follow a typical superposition of two first order exponential decays of the fast and the
 358 slow component which can be expressed here as:

$$359 \quad I_M(t) = I_{F0} \text{Exp} \left[\frac{-t}{\tau_F} \right] + I_{S0} \text{Exp} \left[\frac{-t}{\tau_S} \right] + I_{B0} \quad (2)$$

360 where I_{F0} and I_{S0} are the fast and slow sensor current contributions, respectively, at the start of the response test at $t=0$.

361

362 Although, after $t=10$ min. until $t=120$ min. only two short periods of 5 minutes the cathode cell was flushed with ozone free
 363 air, the results are fairly consistent with the observations of Vömel and Diaz (2010), who flushed the cathode cell over the
 364 entire 120 minutes relaxation period. Clearly the relaxation of the slow component of the background is independent of the
 365 flushing, i.e. no stirring action in the cathode sensing solution, and therefore most likely has a chemical origin from a slow
 366 reaction pathway. The I_{B0} and I_{B1} shown in Fig.1 are typical of present-day ECC sondes (e.g. GAW Report No. 268). Further,
 367 the characteristic difference of I_{B1} and I_{B0} of about 0.03-0.04 μA has been observed over a large number of sondes (≈ 800)
 368 and is most likely the residual of the slow reaction pathway.

369

370 In contrast to Vömel and Diaz (2010), based on around 25 runs, in the more than 350 Uccle experiments the cell current do
 371 stabilize after 1-2 hours decay time to the background current before exposure to ozone, I_{B0} . As a matter of fact, assuming a
 372 25 min $1/e$ -decay from the mean $I_{B1} = 0.045$ μA at $t=10$ min, the I_{B60} and I_{B120} would decay on average down to 0.006 μA
 373 and 0.00055 μA , after 60 and 120 minutes, respectively. Actually, we recorded mean values of 0.017 μA and 0.01 μA ,
 374 respectively. The average differences of $I_{B60}-I_{B0}$ and $I_{B120}-I_{B0}$ are 0.008 μA and < 0.001 μA , respectively. Similar
 375 observations were made in 1993 in the simulation chamber at WCCOS, whereby four ECC sondes were flushed for more
 376 than 90 minutes with zero ozone air during the simulation of a tropical descent pressure profile. After a relaxation time of
 377 about 70 minutes the cell currents approximate constant values which are very close to the corresponding recorded I_{B0} (for
 378 details see Fig. S1 in the supplementary material). This means that after 1-2 hour of flushing the ECC-sensor with zero
 379 ozone, the remaining current is identical to I_{B0} , so that during the typical duration of the ascent of an ozone sounding, the



380 remaining current (I_{B0}) persists, which is not the result of a 25 min decay but has another origin. This inherent I_{B0} of the
 381 ECC-sensor, possibly caused by a small leakage of iodine (I_2) from the ion bridge into the cathode solution or by a mass-
 382 transfer limit in the solution or electron transfer at the cathode surface (Thornton and Niazy, 1982, 1983), is assumed
 383 constant over the 2 hours of an ozonesounding.

384

385 To understand the KI+O₃ chemistry and the impact of the phosphate buffer on the stoichiometry of the conversion of the
 386 sampled ozone into “free” iodine, Tarasick et al. (2019, 2021) reviewed many studies in which a variety of KI-solution
 387 strengths with different pH-buffers were investigated. The reaction mechanism of KI+O₃ in aqueous solution in presence of a
 388 phosphate buffer as investigated by Saltzman and Gilbert (1959) may explain the observations made here and are discussed in
 389 detail in Appendix A. In short, they proposed two reaction pathways: a primary reaction pathway without a buffer and the
 390 secondary pathway with a buffer. Experimentally, Saltzman and Gilbert (1959) showed that the impact of the slow reactions
 391 increases with the buffer concentration, whereas buffered solutions with no KI showed no evidence of any O₃ reactions. This
 392 means that the additional reactions with O₃ are secondary reactions after the initial O₃ + KI reaction. Saltzman and Gilbert
 393 further demonstrated that the secondary pathway can form additional free iodine, half of it reacting very fast (\ll than 1 sec,
 394 i.e. residence time of air sample in the cathode cell), the other half more slowly (~25 min). This means that the secondary
 395 reaction pathway can contribute both to the fast and slow ECC current, respectively. However, loss mechanisms may occur
 396 too. In summary, we do not know exactly the stoichiometry of the fast and slow reaction pathways leading to “free” iodine.”
 397 Therefore, we can only indirectly quantify these two stoichiometries that lead to the fast and slow cell current components
 398 observed, respectively. In other words, the measured cell current $I_M(t)$ is the superposition of

399

$$400 \quad I_M(t) = I_{P,F}(t) + I_{S,F}(t) + I_S(t) + I_{B0} \quad (3)$$

401 where

402 $I_{P,F}$ = sensor current contribution from fast primary reaction pathway.

403 $I_{S,F}$ = sensor current contribution from fast secondary reaction pathway.

404 I_S = sensor current contribution from slow secondary reaction pathway with a typical 20-25 min time response.

405 The contribution of the fast reaction pathways that form iodine fast is lumped together in the total fast sensor current
 406 component $I_F(t)$ with a typical time response of 20-30 s. The measured sensor current $I_M(t)$ is then expressed as:

$$407 \quad I_M(t) = I_F(t) + I_S(t) + I_{B0} \quad (4)$$

408 The overall stoichiometry S_T of the chemical conversion of O₃ into I₂ is the sum of the stoichiometry factors S_F and S_S of the
 409 fast and slow reaction pathways, respectively.

410

411 2.4 Formulating New Fast and Slow Components of the ECC Current

412 From the response tests (fast decay from 5 μ A down to 0.1-0.5 μ A within less than 1 minute) it can be concluded that S_F is
 413 close to one (0.9-1.1) and at least a factor 10-20 larger than S_S , which is small (0.01-0.10). The time scale of the slow current
 414 component ($\tau_S=25$ min) is about a factor of 60 slower than the dominating fast current component. This means that the slow
 415 current acts as a slowly time-varying background current. The latter can be treated as a superposition with the ozone-
 416 independent background I_{B0} to constitute to the total background, but given now as the time varying $I_B(t)$ in Eq. (1).

$$417 \quad I_B(t) = I_{B0} + I_S(t) \quad (5)$$

418 By substituting $I_M(t)-I_B(t)$ into Eq. (1) the partial pressure of ozone is now expressed as Eq. (6):

$$419 \quad P_{O_3} = 0.043085 * \frac{T_P}{(\eta_P * \eta_A + \eta_C * \Phi_{P0})} * I_F(t) \quad (6)$$

420 where the fast sensor current is expressed as:



421
$$I_F(t) = I_M(t) - I_S(t) - I_{B0} \tag{7}$$

422 The conversion efficiency may depend on sonde type and sensing solution type. It is largely related to the stoichiometry of
 423 the conversion of O₃ into I₂ from the primary fast reaction pathway and to a lesser degree on the secondary reaction pathway.

424 The partial ozone pressure can be determined from equation Eqs. (6)-(7) in two steps:

- 425 a. Determine the slow current as function of time. Because the past ozone exposure-dependent slow current
 426 component I_S(t) is much slower and smaller than the fast current component I_F(t), the slow current can be
 427 determined from the convolution of the measured current I_M(t) with the slow time constant τ_S=25 min.
 428 b. Calculate the fast current I_F(t) and then through deconvolution of I_F(t), resolve the time delay of the relatively fast
 429 time constant τ_F=20-30 seconds.

430 The fast as well as the slow reaction path are determined by a first order time response and can therefore be separated in a
 431 convolution part to determine I_S(t) and a deconvolution part to obtain the fast current component, I_{F,D}(t), respectively. The
 432 mathematical techniques used here to resolve the impacts of the slow and fast time constants, τ_S and τ_F, respectively, are
 433 based on the numerical scheme described by Miloshevich et al. (2004), and were first applied by Imai et al (2013) to resolve
 434 the time delay effects caused by the ECC fast response time. A first order response of a measured sensor signal U (here ECC
 435 ozone sensor current) that is approximately exponentially to a change in U, is described by the common “growth law
 436 equation”:

437
$$\frac{dU_m}{dt} = \frac{1}{\tau} * (U_a - U_m) \tag{8}$$

438 where U_m is the instantaneous measured signal, U_a is the ambient (“true”) signal that is driving the change in U_m, and τ is the
 439 time constant of the signal.

440 Integrating Eq.(8) over a small time step Δt_k = t_{k-1} - t_k gives the measured signal as a function of time:

441
$$U_m(t_k) = U_a(t_k) - \{U_a(t_k) - U_m(t_{k-1})\} * \text{Exp}\left(-\frac{\Delta t_k}{\tau}\right) \tag{9}$$

442 This assumes that the time step Δt_k is small relative to the response time τ. Further, it is assumed that the “true” (ambient)
 443 signal U_a is quasi-stationary during time step Δt_k such that U_a(t_k) = U_a(t_{k-1}). The exponential term is the response function.
 444 Eq. (9) can be expressed in a numerical convolution or de-convolution scheme. From Eq. (9) we can obtain I_S(t) and I_{F,D}(t),
 445 as follows:

446 **Case 1:** Slow current component derived from convolution (time constant τ_S) of the ambient sensor current I_a:

447 To obtain the slow current component (I_S), U_m in Eq. (9) is substituted by the slow fraction of I_a, represented here by the
 448 stoichiometry S_S multiplied with the ambient (“true”) ozone sensor current I_a. Eq. (9) can now be re-written into the
 449 integrating form:

450
$$I_S(t_k) = S_S * I_a(t_k) - \{S_S * I_a(t_k) - I_S(t_k - 1)\} * X_S \tag{10}$$

451 whereby the slow response function X_S is:

452
$$X_S = \text{Exp}\left(-\frac{\Delta t_k}{\tau_S}\right) \tag{11}$$

453



454 **Case 2: Deconvolution (time constant τ_F) of the fast signal I_F with τ_F :**

455 To obtain the deconvolved fast current component $I_{F,D}$, Eq. (9) should be solved to obtain $U_a (=I_{F,D})$, and U_m is substituted by
456 the fast fraction I_F . Eq. (9) can then be re-written into the differentiating form:

$$457 \quad I_{F,D}(t_k) = \frac{I_F(t_k) - I_F(t_{k-1}) \cdot X_F}{(1 - X_F)} \quad (12)$$

458 where the fast response function X_F is:

$$459 \quad X_F = \text{Exp}\left(-\frac{\Delta t_k}{\tau_F}\right) \quad (13)$$

460

461 Compared to Vömel et al. (2020), the recursive numerical convolution scheme proposed here (Eq.11) is the same, while the
462 deconvolution scheme (Eq.12) differs through the inclusion of the exponential fast response function X_F (Eq. 13) itself,
463 rather than its first order approximation. The latter allows larger time steps Δt_k , which may become significant for older
464 ozone sounding records that had data with resolution of 10 seconds or more.

465 **3 Resolving Slow- and Fast-Response Signals using JOSIE 2009/2010**

466 To resolve the slow and fast time responses of the measured ECC sensor current, the JOSIE measurements conducted in
467 several campaigns between 1996 and 2017 form an ideal dataset, because of several reasons. Firstly, all the ozonesonde
468 preparations and the measurements were carried out in a controlled environment. Secondly, the availability of simultaneous
469 reference measurements from a fast-response photometer OPM with high precision and accuracy provide an absolute
470 reference for the derived ozone profiles. Further, in the course of the simulation several response tests are performed in
471 which the ozonesondes and the OPM are exposed to zero-ozone air for a five minutes period (see Fig. 2). These response
472 tests enable us to determine the stoichiometry of the slow reaction pathway and subsequently the slow sensor current $I_s(t)$ as
473 a function of time. In this sense, the JOSIE 2009 and 2010 campaigns dataset is of particular interest, because all
474 experiments included four of those response tests in the simulation profiles themselves.

475

476 For the sake of clarity, it is to be noted that the here reported ozone readings of the OPM are already based on the new UV-
477 absorption cross-section, referred to as the CCQM.O3.2019 (BIPM, 2022; Hodges et al., 2019) value that is about 1.23%
478 lower than the former cross-section (Hearn et al., 1961) that was mostly used before in the global ozone ground based
479 monitoring networks. Consequently, all P_{O_3} measurements of the OPM reported here are about 1.23% larger than the values
480 reported before in earlier JOSIE-publications.

481 **3.1 JOSIE 2009/2010**

482 The JOSIE 2009 and 2010 protocols are similar to the JOSIE 1998 campaign (Smit and Sträter, 2004a; Smit et al., 2007). In
483 2009 a set of 40 brand new ECC sondes (20 SPC6A and 20 ENSCI) were tested; in 2010 the same set of ECC sondes, re-
484 furnished and tested under the same conditions, were evaluated against the same OPM reference. One aim of these
485 campaigns was to test the performance of brand new and refurbished ozonesondes. It was found that the re-used sondes
486 agree within 1%–2% with brand new sondes, although with a slightly lower precision of ~5% (see Fig. 3.1 in GAW Report
487 No. 268). The JOSIE 2009/2010 ozonesondes were prepared by only three operators, strictly following the same preparation
488 protocols, including the use of purified air from the same cylinders for the ozone-free air source. It can therefore be
489 considered as an ideal data set for well-prepared ozonesondes. All ozonesonde data were processed according to the
490 guidelines of GAW Report No. 268, which we denote as the “conventional” method hereafter. That means: (i) subtracting the
491 constant background current I_{B1} ; (ii) correcting the pump flow rate for the moistening effect; (iii) using the pump flow rate
492 efficiency correction tables Komhyr (1986) and Komhyr et al. (1995) for SPC and EN-SCI ozonesondes respectively; (iv)



493 converting the measured pump temperature to the internal pump body temperature, with an additional small pressure
 494 dependent correction (GAW Report No. 268); and (v) no total ozone normalisation. Note also that all simulations were
 495 identical in representing a typical mid-latitude ozone profile (Smit et al., 2007).
 496 During both campaigns, a total of 26 simulation runs were made, of which all but one had 4 ozonesondes simultaneously in
 497 the simulation chamber, giving a total amount of 103 ozonesonde profiles. However, 17 of those profiles were gathered
 498 using research-mode SSTs and are not included here. Fourteen simulations were carried out in December 2009, 2 in January
 499 2010, and 10 in August 2010.

500 3.2 Determination of Slow Current $I_s(t)$

501 3.2.1 Determination of Stoichiometry S_s

502 To determine the relative contribution S_s of the slow component in the ECC ozonesonde signal, in other words, the
 503 stoichiometry factor of the slow reaction pathway of conversion of O_3 into I_2 , the response tests of the JOSIE 2009/2010
 504 dataset are used. Four time response tests are included during these simulations at four different pressure levels, (RT1: 475-
 505 375 hPa, RT2: 100-85hPa, RT3: 20-15 hPa, RT4: 6-5 hPa), during which ozone-free air is provided in the simulation
 506 chamber for 5 minutes. A typical example of a JOSIE 2009 simulation run is given in Figure 2. After 5 minutes the fast
 507 sensor current has declined by more than 16 $1/e$ relaxation times and is vanishing small. This means that at the end of this
 508 time response test, the only contribution to the overall measured current $I_M(t)$, after correction for I_{B0} , comes from the
 509 remaining slow current component. At this moment, the fast co-existing OPM data (red in Fig. 2) provides the measure of
 510 the true value of the ozonesonde signal. The next paragraphs outline the different practical steps.

511 To obtain a direct measure of the true ECC-ozone sensor current, the OPM ozone partial pressure is converted to the generic
 512 OPM current (I_{OPM}) for each individual ozonesonde using sonde pump temperature, sonde pump flow rate and pump
 513 efficiency values of JMA (Nakano and Morofuji, 2023, See Table 1), as in Eq. (1).

514

$$515 \quad I_{OPM} = \frac{(\eta_P \cdot \eta_A \cdot \eta_C \cdot \Phi_{P_0})}{T_P \cdot 0.043085} * P_{O_3, OPM} \quad (14)$$

516

517 In other words, we are calculating the generic sensor current corresponding to the ozone equivalent measured by the OPM,
 518 as if it were the true ECC ozone current. This means that the generic I_{OPM} is taken as the actual reference (“true”) current for
 519 determining the slow stoichiometry factor S_s .

520

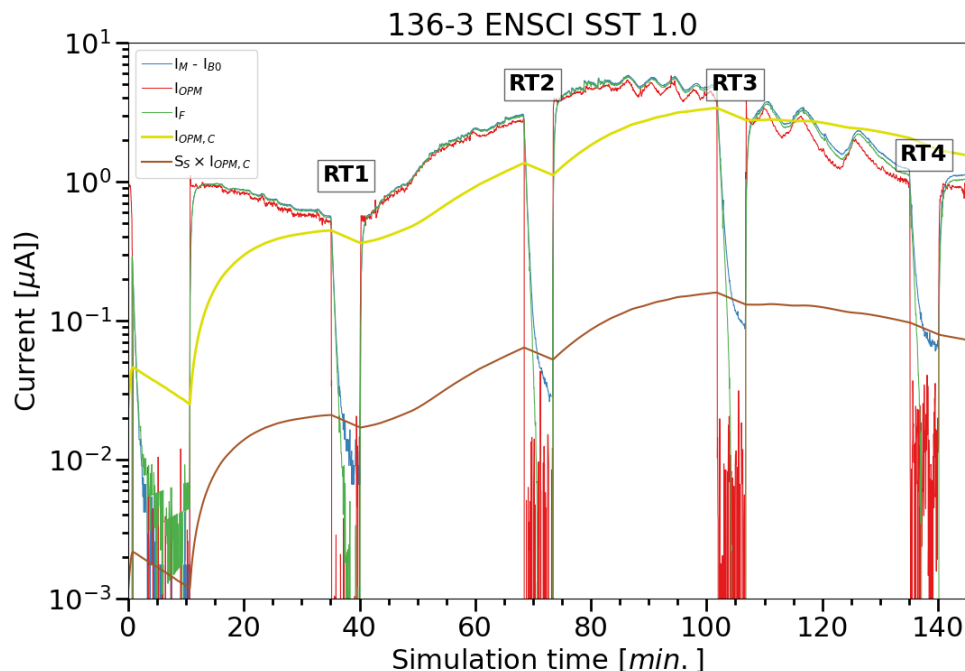
521 Additionally, the generic OPM current I_{OPM} (red in Fig. 2) is convolved into $I_{OPM,C}$ with an exponential time response with τ_s
 522 = 25 minutes using Eq. 9, to obtain a slow time response into the generic OPM current signal (yellow in Fig. 2).

$$523 \quad I_{OPM,C}(t_k) = I_{OPM}(t_k) - \{I_{OPM}(t_k) - I_{OPM,C}(t_k - 1)\} * X_S \quad (15)$$

524 Finally, the slow stoichiometry factor S_s is obtained by taking the ratio of the remaining ECC sensor current I_M minus the
 525 constant background current I_{B0} and the convolved OPM signal ($I_{OPM,C}$), at the end of the time response test intervals RT1,
 526 RT2, RT3, RT4, when only the slow component is expected to contribute to the sonde signal, such that

$$527 \quad S_s = \frac{(I_M(ECC) - I_{B0})}{I_{OPM,C}} \quad (16)$$

528



529

530

531 **Figure 2.** Example of a simulation run during JOSIE 2009 as a function of the simulation time, with the measured ECC
 532 current I_M minus I_{B0} (blue line), the generic OPM current I_{OPM} (red line), the 25 min convolved $I_{OPM,C}$ (yellow line) and the
 533 25 min convolved I_{OPM} adapted to $I_M - I_{B0}$ after the determination of the slow stoichiometry factor S_S or slow current $I_S (= S_S \times$
 534 $I_{OPM,C})$ (brown line) and the fast sensor current I_F (green line), obtained after correction of the measured sensor current I_M for
 535 the constant background current I_{B0} and the slow current contribution I_S

536

537 The ratios used to obtain the slow stoichiometry factor (S_S) values are calculated during the final 50 seconds of each time
 538 response test, RT1, RT2, RT3, RT4, respectively. Those values, obtained for all ozone profiles within each sonde type and
 539 SST combination, are shown in Fig. 3, together with median, 25th and 75th percentile values. The median S_S values and their
 540 Median Absolution Deviation (MAD) uncertainties are given in Table 2. Note that the determination of the mean S_S values
 541 (and their uncertainties) is very robust, and does not depend on the time response test interval or the slow time lag constant.
 542 We will come back to this in Sect. 6.2. Further it showed that by varying $\tau_s = 25$ min. by ± 5 min. the corresponding S_S
 543 values only changed by less than 5%, which is small compared to the MAD uncertainty of S_S (Table 2).

544

545 The most striking feature is that S_S only depends on the SST, not on the sonde type. This confirms our hypothesis on the
 546 origin of this slow component, as described in Section 2.4. For SST0.5 and SST1.0 there is an almost proportional relation
 547 between the magnitude of S_S and the buffer strength, independent of the KI concentration (or percentage). This result has
 548 been explained by the secondary reaction pathway of the reaction mechanism after Saltzman and Gilbert (1959), whereby the
 549 extra slow stoichiometry contribution is caused by the buffer (Appendix A). However, a comparable result does not hold for
 550 SST0.1 (Table 2). One would expect that for the low buffered case (SST0.1) S_S should be much smaller than for the SST0.5.
 551 This is not true; S_S is even slightly larger. It seems that for the SST0.1, other competing reaction mechanisms may occur,
 552 which do depend on the KI concentration, and may generate free iodine on a 25-minute time scale. Such a hypothetical



553 mechanism may also explain the fact that for low or no buffered SST we still measure I_{B1} background currents with values of
 554 0.01-0.03 μA larger than I_{B0} as measured in JOSIE 2000 (no buffer SST; Smit and Sträter, 2004b) and JOSIE 2017 (SST0.1;
 555 Thompson et al., 2019). A speculative mechanism is that the electronically excited oxygen singlet molecule formed in (R3)
 556 of the primary reaction pathway of the O_3+KI chemistry (Appendix A) may, in addition to de-activation in (R4), react with
 557 H_2O and produce hydrogen peroxide (H_2O_2) (e.g. Xu et al., 2002). The formed H_2O_2 would oxidize KI to produce free
 558 iodine, but on a time scale of 25 minutes which could contribute to the slow current $I_S(t)$. Further studies are required to
 559 understand the underlying chemical processes.

560

561 **Table 2:** Median and their Median Absolute Deviation (MAD) uncertainty values of the slow stoichiometry factor S_S
 562 obtained from JOSIE 2009 and 2010 for SPC and EN-SCI ozonesondes operated with the sensing solution types SST0.5 and
 563 SST1.0. The stoichiometry factor S_S for EN-SCI/SST0.1 has been determined with the same approach but using laboratory
 564 measurements at Uccle with an ozone reference instrument (see Appendix B). *: the same value for SPC/SST0.1 has been
 565 adopted as for EN-SCI 1.0%-0.1B. N_S is the number of sonde profiles.

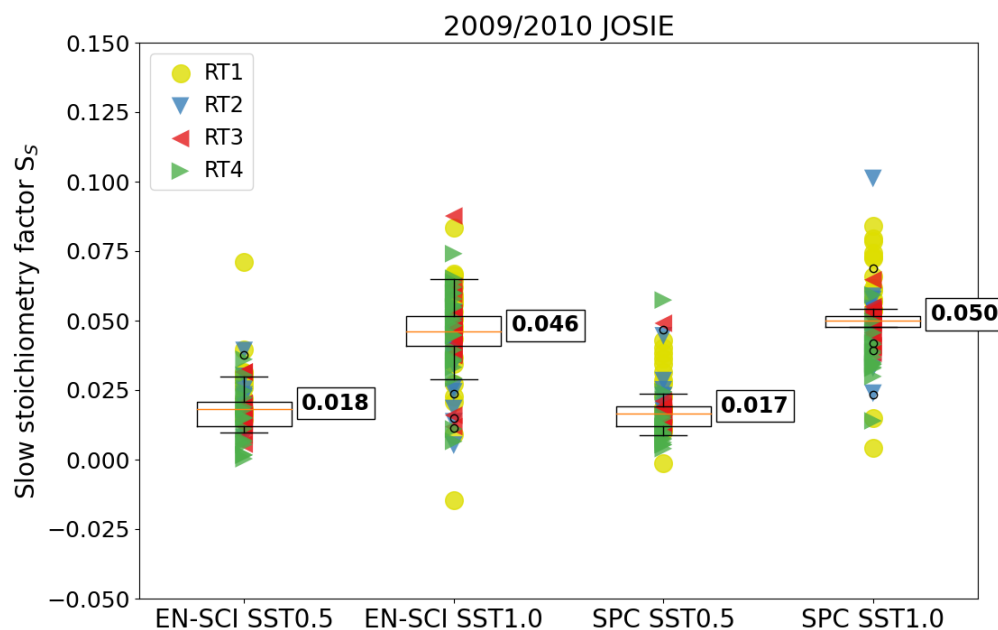
566

| Sonde Type | SST1.0 | SST0.5 | SST0.1 |
|------------|--------------------------------|--------------------------------|-------------------------------|
| SPC | 0.050 ± 0.002 ($N_S=16$) | 0.017 ± 0.004 ($N_S=21$) | $0.023 \pm 0.005^*$ |
| EN-SCI | 0.046 ± 0.006 ($N_S=23$) | 0.018 ± 0.004 ($N_S=15$) | 0.023 ± 0.005 ($N_S=8$) |

567

568 The stoichiometry factors S_S (Table 2) to determine the slow current $I_S(t)$ are substantially lower than the so called “steady
 569 state bias factors” applied by Vömel et al. (2020). These steady state bias factors were determined as the overall excess
 570 stoichiometry to one from laboratory experiments with a fixed ozone exposure during several hours (Figs. 3 & 4 in Vömel
 571 and Diaz, 2010). In this study we derived for SST1.0 $S_S = 0.046-0.050$ which is only half the 0.09 value of Vömel et al.
 572 (2020). For SST0.5 and SST0.1, our respective $S_S = 0.017-0.018$ and 0.023 values are also smaller than their 0.024 and 0.031
 573 steady-state bias factors. Using the same laboratory procedures as Vömel et al. (2010), Johnson et al. (2002) reported an
 574 excess overall stoichiometry of ~ 0.07 for SST1.0. The lower factors obtained in this study, particularly for SST1.0, might
 575 also be related to the different methodology followed for determining S_S . Here, S_S values are determined from the response
 576 of a downward step under zero-ozone conditions. In Johnson et al. (2002), and Vömel and Diaz (2010) the excess
 577 stoichiometry factors were determined from the relatively small differences observed between the ECC sonde and a
 578 reference UV-photometer after a 60-min upward step ozone exposure. The latter requires very accurate generation of ozone
 579 values with a precision better than 1% to determine the relatively small excess stoichiometry factors involved. Note also that
 580 for the earlier studies reference ozone readings are based on older UV absorption cross sections that are now corrected by
 581 1.23% to be compatible with the new UV absorption cross-section applied to the OPM. Accordingly, the steady state bias
 582 factors of Johnson et al. (2002) and Vömel et al. (2020) should be decreased by subtracting 0.012. The resulting S_S values
 583 would then approach the S_S values obtained here for SST0.1 and SST0.5, and better approximate the SST1.0 S_S values.

584



585

586 **Figure 3.** Whisker plots of the slow stoichiometry factor S_s as the ratio of the measured I_M minus I_{B0} to the 25 min
 587 convolved OPM current ($I_{OPM,C}$) obtained from JOSIE 2009 and 2010 for EN-SCI and SPC ozonesondes operated with the
 588 SST0.5 and SST1.0. The yellow dots and triangle symbols (blue, red and green) represent the individual values obtained
 589 from the four response tests RT1, RT2, RT3 and RT4, respectively. Thus, every ozonesonde profile is represented four times
 590 in the graph. Whisker plots are represented by median plus the 25th and 75th percentiles (respectively, orange and black
 591 horizontal lines for each instrument-SST combination).

592

593 Another difference between the new methodology and that of Vömel & Diaz (2010) is that we subtract I_{B0} from the
 594 ozonesonde signal prior to determining the stoichiometry. However, we also determined the S_s values without correction of
 595 I_{B0} ; the results appear in Fig. S2 in Supplementary Material. It is noted that these S_s values increase for all sensing solution
 596 types by only 0.005-0.009. For SST0.5 and SST0.1, they approach the Vömel & Diaz (2010) values, but the substantially
 597 lower S_s values for SST1.0, as derived here (Table 2) cannot be explained exclusively by subtracting I_{B0} . Furthermore,
 598 comparing Fig. 3 with Fig. S2, also demonstrates that the subtraction of the I_{B0} value makes the determination of the S_s
 599 values even more independent of the selected RT intervals, which is not the case without this prior subtraction (e.g. the RT1
 600 values being significantly larger than the other RT values).

601

602 The factors reported by Johnson et al. (2002) and Vömel & Diaz (2010) are based on a limited sample of experiments (three
 603 different sondes using three different solutions for a total of 22 runs in Vömel & Diaz, 2010) in contrast to the large
 604 statistical sample in this study (Table 2). The difference between the two approaches – in terms of exposure to ozone or not –
 605 may be then explained by assuming that when the overall excess stoichiometry originates from the secondary reaction
 606 pathway, only half of it contributes to the slow cell current $I_s(t)$ and with the other half contributing to the fast cell current
 607 $I_f(t)$. For SST05 and this SST1.0 this can be understood by the type of reaction mechanisms of the secondary reaction
 608 pathway as proposed by Saltzman and Gilbert (1959): in this case, the extra stoichiometry caused by the buffer could be still



609 for 50% contributing to the relatively fast signal (R7) and 50% to the slow signal (R8) (see Appendix A). This would mean
610 that the stoichiometry of the secondary reaction pathway could be two times the stoichiometry factor S_s of the slow ECC
611 current $I_s(t)$ determined here from the response tests RT1 to RT4 after $I_F(t) = 0$. However, for the S_s values for the SST0.1,
612 even slightly larger than for SST0.5, explanations would be more speculative. More analysis and new JOSIE trials, for
613 example in the JOSIE simulation chamber, might be required to find the cause of varying factors among the different studies
614 and SSTs.
615

616 3.2.2 Initial Condition of Slow Current $I_s(t)$

617 With the derived S_s values, the slow component of the sonde signal (I_s) is computed by convolution with the slow time
618 constant $\tau_s = 25$ min., as in Eq. (10) (brown line in Fig. 2). Note that, in practise, to determine $I_s(t)$, the measured current $I_M(t)$
619 minus I_{B0} can be taken instead of the true generic ozone current $I_{OPM}(t)$, because their differences are rather small (less than
620 5-10%), at the same time the slow stoichiometry factors S_s are also smaller than 0.1. From here on, we will use the measured
621 current $I_M(t)$ minus I_{B0} to determine the slow current $I_s(t)$ along with the S_s values listed in Table 2.
622

623 As Eq. (10) is a recursive expression, the initial conditions of I_s reflect prior ozone exposure during pre-launch preparations,
624 although decaying exponentially in time. Exposure to ozone values during pre-launch will cause non-zero I_s values at the
625 beginning of the simulation, impacting the boundary layer ozone profile (e.g., Fig. 10 in Vömel et al., 2020). Ideally, the
626 convolution of the slow component of the sonde signal is computed taking the pre-launch measurements into account. These
627 pre-launch measurements are available for JOSIE 2009/2010 (as in Fig. 4), but this is often not the case for operational
628 soundings. Using those JOSIE 2009/2010 pre-launch simulation data (with negative simulation times in Fig. 4), we found
629 that the best approximation of the true I_s (red dashed line in Fig. 4, taking all the pre-launch measurements into account) is
630 obtained if $I_s(t_0)$ equals $(I_{B1} - I_{B0})$ multiplied with the exponential decay factor $X_s = \text{Exp}[-\Delta t / \tau_s]$, where Δt is the time interval
631 between the measurement of I_{B1} and the start of the launch (green dashed line in Fig. 4). It is important to mention here the
632 good agreement of the measured I_{B1} value (yellow horizontal line in Fig. 4, subtracted by I_{B0}) with the convolved, pre-
633 launch, slow component I_s (dashed red line) at $t = -2500$ seconds (time mark No.2 in Fig. 4). This reinforces the selection of
634 the $I_{B1} - I_{B0}$ measurement as a good pre-launch representation of the slow component of the ECC signal.
635

636 To apply this method in the ozonesonde network, it is essential to record the time difference between the I_{B1} measurement
637 and the sonde launch. In GAW Report No. 268, the recording of the I_{B1} timestamp is included in the SOP for ozonesonde
638 preparations. For the JOSIE 2009/2010 data, we will use this exponential decay method for the initial condition of the
639 convolved slow component at $t=0$. For the initial condition of the slow component $I_s(t_0)$ we investigated two other
640 alternatives:

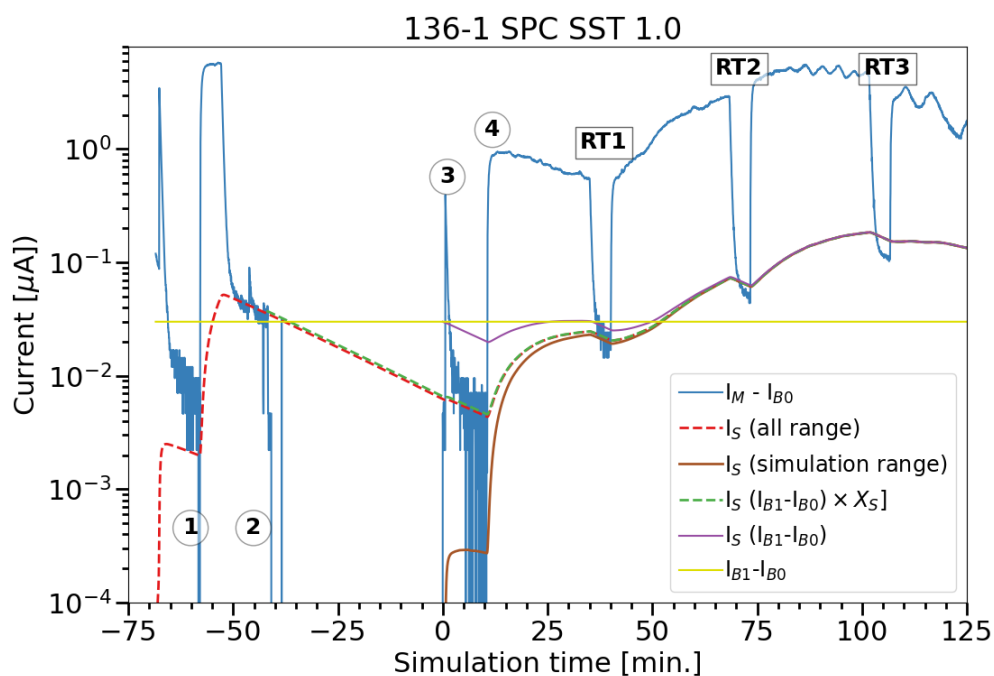
- 641 • $I_s(t_0) = I_{B1} - I_{B0}$, denoted by the horizontal yellow line in Fig. 4, which results in a slow component I_s marked by the
642 purple solid line, which clearly overestimates the true I_s in the beginning of the profile (up to about 3500 s).
- 643 • $I_s(t_0) = 0$, for which the corresponding I_s , represented by the brown solid line in Fig. 4, underestimates the true I_s
644 up to about a simulation time of 2200s for the JOSIE 2009/2010 representative example here.

645 For stations with a time gap of several hours between the I_{B1} measurement and the launch time, the current will have been
646 fallen back to the I_{B0} (see the Uccle example in Fig. 1), resulting, after subtraction of I_{B0} , in this particular case $I_s(t_0) = 0$.
647

648 A better understanding of the ECC time response provided a justification for quality control indicators on the I_{B0} ($< 0.03 \mu\text{A}$)
649 and I_{B1} ($< 0.07 \mu\text{A}$) in GAW Report No. 268. In practice, often higher background currents I_{B0} and I_{B1} are recorded at the
650 sounding sites at the day of the launch. These high background currents are typically caused by the use of an inadequate gas



651 filter in the test unit, e.g. the filter provides ozone free air, but does not trap water vapour and contaminants in the laboratory
 652 air that is filtered into the preparation equipment. A poor filter combined with a leaky photolysis cuvette producing ozone by
 653 UV-photodissociation of oxygen with a Hg-discharge lamp can contaminate the air flow to produce in high background
 654 current measurements. It appears that UV irradiation can produce substances that cause reactions similar to KI and O₃. There
 655 are some indications (Newton et al., 2016) that high backgrounds may display be due to processes with 1/e-decay times ~ 25
 656 min like the slow cell current $I_S(t)$. Nevertheless, more research is necessary to investigate the cause and the time behaviour
 657 of these high background currents in the course of the sounding in order to correct for this artifact properly. As stated by
 658 ASOPOS 2.0 (WMO/GAW Report No. No. 268) the use of proper gas filters to provide ozone free, dry and purified air in
 659 practice at the sounding site, is very essential in general, but also when applying the data processing proposed here.



660

661

662 **Figure 4.** Convolved slow ECC current obtained from different initialization scenarios as function of the simulation time.
 663 (details see text). The dashed red line is the convolved ECC current obtained from the measured I_M minus I_{B0} , hereby
 664 including all pre-launch measurements (with negative simulation times). Time stamps 1-4: 1= record I_{B0} ; 2= record I_{B1} ;
 665 3=turn on pump motor (at simulation time $t=0$); 4= start ozone profile of simulation. RT1, RT2, RT3 are the first three in-
 666 flight time response tests.

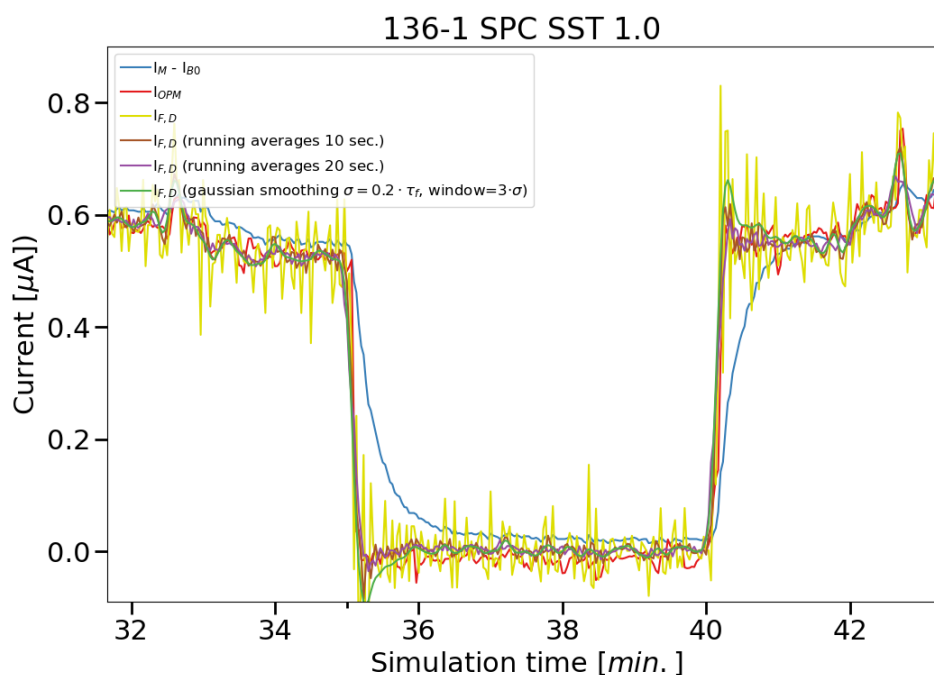
667

668 3.3 Determination of the Fast ECC Ozone Sensor Current, $I_F(t)$

669 After determining the slow component of the signal due to the secondary reaction pathway, we can subtract it from the
 670 overall measured current $I_M - I_{B0}$ to end up with the fast component I_F (Eq. 7), as shown by the green line in Fig. 2. From the
 671 fast component $I_F(t)$, we can remove the time lag introduced by the 1/e time response of about 20-30 seconds through
 672 deconvolution of $I_F(t)$ according to Eq. (12). In this paper, we use $\tau_F = 25 \pm 4$ seconds for EN-SCI, and $\tau_F = 21 \pm 4$ seconds
 673 for SPC ozonesondes, which are the average fast time responses determined from all the simulation time response tests (RT1,



674 RT2, RT3, RT4) during JOSIE 2009/2010. The response times of the EN-SCI sondes are typically about 4 seconds larger
 675 than the SPC-6A sondes due to the slightly lower pump flow rates and slightly larger volume of the cathode cell of the EN-
 676 SCI sondes (Smit and Sträter, 2004a). In general, we found that the fast response times in upward as well in downward
 677 direction agree within 1-2 seconds. Moreover, τ_F only varies marginally in flight with a slight decrease of less than 5-10 %
 678 between the surface (RT1) and the upper part of the sounding (RT4). The in-flight τ_F values also agree very well with the τ_F
 679 values determined from the response tests made during the pre-flight preparation of the ECC sensor, which confirmed earlier
 680 observations made during JOSIE (Smit and Sträter, 2004a). A close-up of the first time response interval RT1 is provided in
 681 Fig. 5, in which also the deconvolved fast component is shown in yellow.



682
 683

684 **Figure 5.** Example of a downward and upward response of a simulation run in the tropospheric part of the vertical profile to
 685 show the impact of resolving the fast response effects on the measured cell current I_M minus I_{B0} ($I_M - I_{B0}$; blue solid line). The
 686 fast, deconvolved current $I_{F,D}$, without smoothing, is shown in yellow, and with a moving average smoothing over a time
 687 interval of 10 and 20s in brown and purple, respectively. The Gaussian smoothing applied on $I_{F,D}$ and used in this paper is
 688 marked by the green line. For reference, the OPM current is shown in red.

689

690 Note that the deconvolution procedure introduces a substantial amount of noise in the data. To reduce this noise, the
 691 deconvolved current signal should be smoothed. We therefore used a smoothing with a Gaussian filter with width equal to
 692 20% of the time lag constant τ_F as in Vömel et al. (2020), their equations (10) and (11). Compared to other common
 693 smoothing techniques, e.g. running averages with a time window of 10 seconds (see brown line in Fig. 5), this Gaussian
 694 filter still has a slight phase shift with respect to the true signal (I_{OPM} , in red in Fig. 5), but outperforms other tested
 695 smoothing algorithms in terms of reducing the noise level. The final smoothed deconvolved signal is shown in green in Fig.
 696 5. It is obvious that, after correcting for the slow and the fast times responses in the signal, the resulting current better agrees
 697 with the OPM current than the original measured current. It even exhibits small-scale features that are also present in the



698 fast(er) response OPM measurements. Small differences still remain that indicates the conversion efficiency, i.e.
699 stoichiometry of the fast reaction, slightly deviates from one.

700 **4. Comparison of Ozone Profiles Based on the Conventional Versus Updated Time Responses Correction Method**

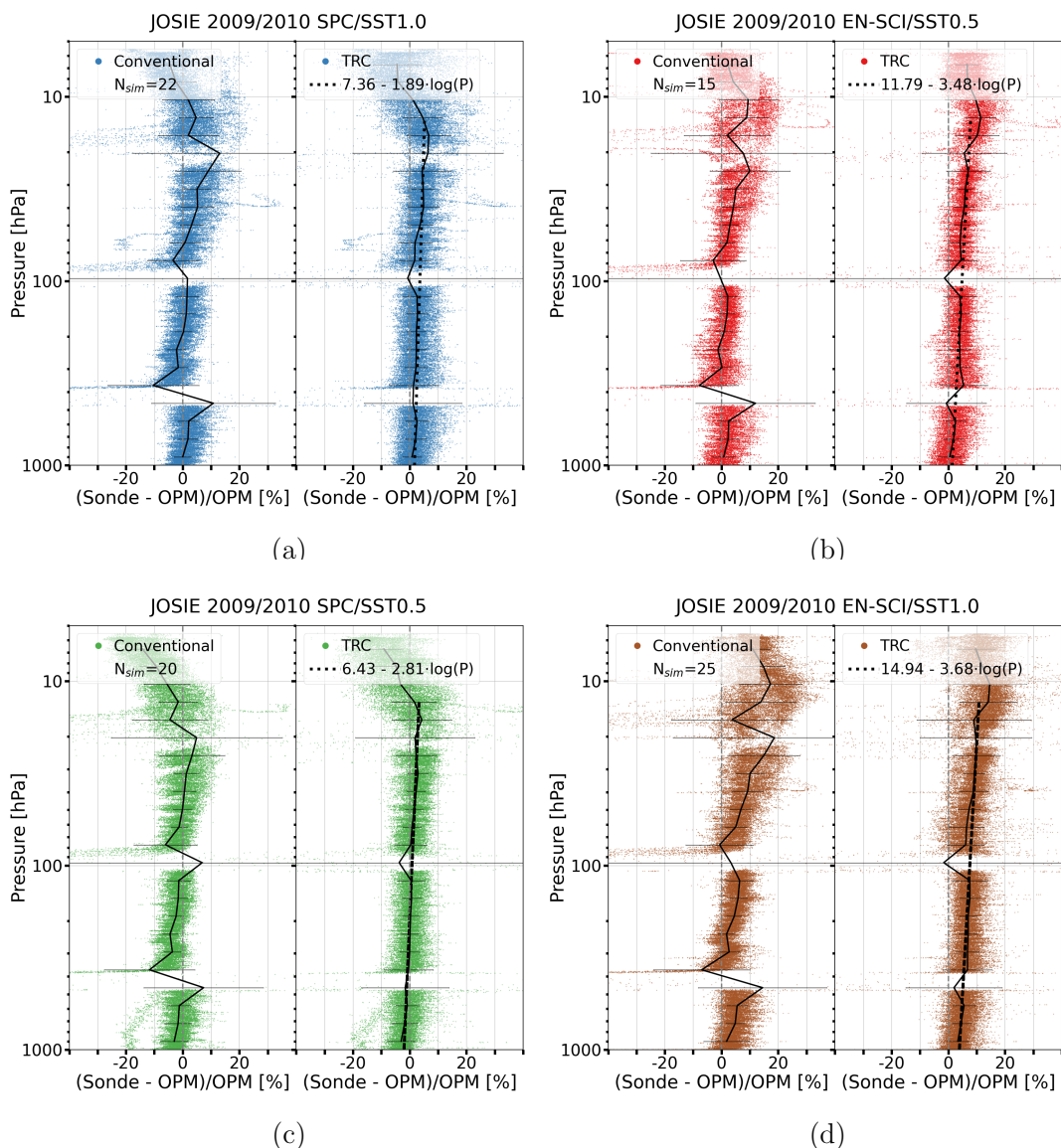
701 To test the Time Responses Correction (abbreviated here as TRC) methodology as described in the previous chapter and a
702 first version in Vömel et al. (2020), we apply the methodology on individual ozonesonde profiles of the different JOSIE
703 simulations and compare those corrected profiles with the corresponding OPM measurements. This method involves the use
704 of the stoichiometry factors S_S from Table 2 for the different ozonesonde-SST pairs and the application of the measured
705 pump efficiency factors of Nakano and Morofuji (2023) (Table 1). As opposed to this TRC method, ozone partial pressures
706 from profiles are determined according to the “conventional method”, as recommended in ASOPOS (GAW Report No. 201;
707 GAW Report No. 268), e.g. using the constant background I_{B1} correction with the Komhyr et al. (1986, 1995) efficiency
708 factors (Table 1). Both sets of processed profiles are compared to the OPM reference values which are enhanced by 1.23%
709 compared to earlier JOSIE publications due to the newly revised ozone absorption cross-section at 254 nm wavelength
710 (Hodges et al., 2019). In 2024-2025 the new cross-section will be introduced into the global ozone observation networks
711 using UV-photometry (BIPM, 2022). The comparisons are made for two different JOSIE campaigns: (i) JOSIE 2009/2010
712 with mid-latitude profiles and well-established ozonesonde preparation procedures, and (ii) the JOSIE 2017 campaign with
713 mostly tropical profiles and good ozonesonde preparation procedures.

714 All here presented comparisons of the TRC with the conventional method are processed as function of flight time. However,
715 to present the results as vertical profiles, they are mapped on a pressure grid with successive pressure levels of $P_i=0.98 \times P_{i-1}$
716 between 1000 and 5-6 hPa. Hereby, all presented JOSIE experiments are based on a pressure, temperature and ozone profile
717 simulating a balloon ascent velocity of about 5 m/s, such that a quasi-realistic linking between the simulated flight time and
718 pressure scale is obtained.

719 **4.1 Ozone Profiles from JOSIE 2009-2010 for SST1.0 and SST0.5**

720 In Figure 6, the relative differences with the OPM for the conventionally (left diagrams) and TRC (right diagrams) processed
721 ozonesonde profiles of JOSIE 2009/2010, respectively, are shown for each pair of sonde (SPC6A or EN-SCI) and solution
722 type (SST0.5 or SST1.0), respectively, including the mean (black solid lines) and its 1σ -standard deviation. The absolute
723 ozone partial pressure differences are presented in the supplementary material (Fig. S3).

724



725

726 **Figure 6** JOSIE 2009/2010: Relative differences with the OPM for the conventional (left diagrams) and TRC (right
 727 diagrams) processed ozonesonde profiles for four pairs of sonde type and SST shown as scatter plots in four different colors
 728 in the panels a-d: SPC6A/SST1.0 (a: blue dots), EN-SCI/SST0.5 (b: red dots), SPC6A/SST0.5 (c: green dots), and EN-
 729 SCI/SST1.0 (d: brown dots), respectively. In each diagram for both methods the mean and 1σ -standard deviation of the
 730 relative differences are included (solid black line). The black dashed lines in the TRC-diagrams are the linear regressions of
 731 the difference of the ozonesonde to the OPM as function of the pressure (on a logarithmic scale). A summary plot is provided
 732 in Fig. S4, and absolute differences are available in Fig. S3 of the Supplementary material.

733

734 For the conventional method, large relative deviations from the OPM exist in the pressure intervals response-time tests (in
 735 particular RT1, RT2, RT3) take place during a simulation. This can be explained by the difference in response time between
 736 the OPM and the ozonesondes and the fact that when ozone concentrations are close to zero, the relative differences will be



737 magnified. The TRC method is able to correct well for the time response differences, as illustrated by the small relative
738 differences, although with higher uncertainty (1σ -standard deviation) compared to adjacent pressure levels. A major
739 improvement of the TRC methodology compared to the conventional corrections is the fact that the relative differences with
740 respect to the OPM are almost pressure-independent, hence past ozone exposures. Up to about 13 hPa ($Z\approx 30$ km), only a
741 slightly increasing bias with decreasing pressure exists between the overall mean of the TRC-corrected ozonesondes and
742 OPM for the JOSIE 2009/2010 sample (black dashed linear regression lines in Fig. 6).

743

744 At pressures lower than 13 hPa the SPC sondes exhibit a declining behaviour, which is discussed in the next section. Overall,
745 both EN-SCI SST0.5 and SPC SST1.0 agree very well within a few percent, with the TRC methodology using the correct
746 pump efficiencies (see also Fig. S4). Consistent with earlier JOSIE and BESOS campaigns (Smit et al., 2007; Deshler et al.,
747 2008), for both sonde types, SST0.5 gives around 3-5% lower ozonesonde readings than SST1.0, whereas, for both SSTs,
748 SPC ozonesondes read ~ 3 -5% lower than EN-SCI.

749

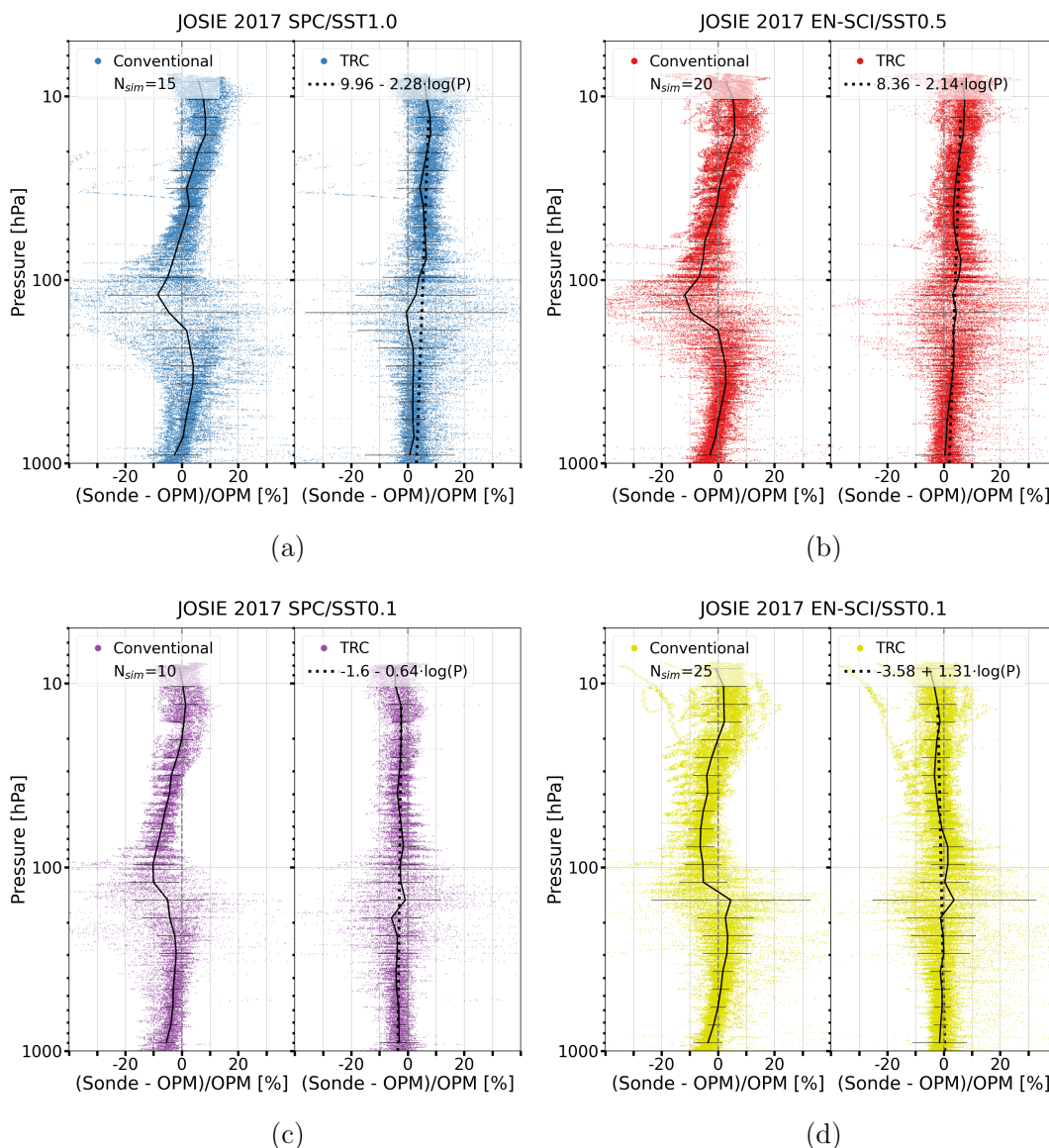
750 **4.2 Ozone Profiles from JOSIE 2017 for SST1.0, SST0.5, and SST0.1**

751 During the JOSIE 2017 campaign, tropical ozone profiles were simulated for three different SSTs: SST1.0, SST0.5 and
752 SST0.1 (Thompson et al., 2019). No time-response tests were performed during these simulations. Therefore, for SST1.0 and
753 SST0.5, the stoichiometry factors, S_s , derived from the JOSIE2009/2010 data have been applied. However, the SST0.1
754 solution was not tested during the JOSIE 2009/2010 campaign. Therefore, for this SST, we determined the stoichiometry
755 factors S_s with the same method as described in Sect. 3.2.1, but with time-response tests during ozonesonde laboratory
756 measurements with a calibrated ozone analyser (details in Appendix B). The derived S_s factor is 0.023 ± 0.005 . For the
757 JOSIE 2017 campaign data, the initial value of the slow current component I_s at the start of the simulation at $t=0$ (Sect.
758 3.2.2) has been chosen to equal 0 (i.e. equal to I_{B0} before subtracting I_{B0}), as there were usually a few hours between the end
759 of the day of launch preparations and the start of the simulation, such that I_{B1} has decayed to I_{B0} . The Uccle experiments
760 (Fig. 1) illustrated that the measured current with a zero-air source falls after two hours back to the I_{B0} value measured at the
761 beginning of the preparation.

762

763 The differences of the JOSIE 2017 ozonesonde profiles with the corresponding OPM profile using the conventional and TRC
764 data processing methodologies are shown in Figure 7; the absolute differences appear in Fig. S5. The most prominent feature
765 for the conventional corrections, sonde type-SST combinations, is the dependence of the OPM differences on pressure or
766 measured ozone amounts: the mean relative differences are largest (as well as the corresponding standard deviations) just
767 below the tropopause at ~ 200 hPa, where the ozone partial pressures are minimal; the mean relative differences increase with
768 decreasing pressure in both troposphere and stratosphere (also obvious in Fig. S6). The conventional method deviates strong
769 from the OPM in the upper troposphere at about 100 hPa for the tropical ECC ozone profiles. In contrast, when the TRC-
770 method is applied to the data, the pressure/ozone amount dependence of the relative difference almost completely disappears.
771 For the standard EN-SCI/SST0.5 and SPC/SST1.0, there remains a slightly increasing bias with decreasing pressure (black
772 dashed lines), while for the SST0.1 ozonesonde simulations, there is a tendency for decreasing (negative) relative differences
773 with decreasing pressure. For both SPC and EN-SCI, SST0.1 ozone measures about 10% lower than OPM in the
774 stratosphere, compared to the recommended SOP (SPC/SST1.0 and EN-SCI/SST0.5).

775



776

777 **Figure 7.** JOSIE 2017: Differences with the OPM for the conventionally (left) and TRC (right) processed ozonesonde
 778 profiles for the four sonde-SST pairs as scatter plots: SPC6A/SST1.0 (a: blue dots), EN-SCI/SST0.5 (b: red dots),
 779 SPC6A/SST0.1 (c: purple dots), EN-SCI/SST0.1 (d: yellow dots). In each diagram for both methods, mean and 1σ -standard
 780 deviations are solid black lines. The black dashed lines in the TRC-diagrams are the linear regressions of the sonde-OPM
 781 differences as a function of the pressure on a logarithmic scale. A summary plot appears in Fig. S6 and absolute differences
 782 are in Fig. S5 of Supplementary material.

783

784 When comparing the mean relative OPM offsets after processing the ozonesonde measurements with TRC methodology for
 785 the two JOSIE campaigns, i.e. Figs. 6 and 7 (also in Figs. S4 and S6), we note that the network standards SPC/SST1.0 and
 786 EN-SCI/SST05 are a few percent larger in the stratosphere for the “tropical” JOSIE 2017 campaign. That is, those mean
 787 relative differences are manifest in both cases as a slightly decreasing relative bias with increasing pressure during both



788 campaigns. These differences are independent of post-ozone exposure and profile type (mid-latitude or tropical), in contrast
789 to the conventional methodology which exhibits this past ozone memory effect. A striking disagreement between the profile-
790 OPM offsets between JOSIE 2009/2010 and 2017 occurs at the lowest pressure range, lower than ~13 hPa. For the JOSIE
791 2009/2010 data, the mean relative differences with the OPM display a stronger pressure dependence in this lowest pressure
792 range, distinctly different for both sonde types, in contrast to the JOSIE 2017 mean relative OPM differences. The origin of
793 this different behaviour above 13 hPa lies most likely in pump temperature differences between the simulated profiles.
794 Whereas the mean pump temperature is close to 21°C in this pressure range in JOSIE 2009/2010, it is near 15°C for the
795 tropical profiles in JOSIE 2017. Simultaneous temperature measurements during JOSIE 2017 revealed that the cell
796 temperatures are about 5 to 10°C lower than the corresponding pump temperatures, depending on the sonde type.
797 Specifically the differences between pump and cell temperature are more at the high end range of this temperature interval
798 for EN-SCI sondes, and at the low end range for the SPC due to differences in thermal contact between cells and pump. With
799 these cell temperatures and taking the boiling temperatures at those low pressures into account, it turns out that the solutions
800 in the SPC sondes tested in JOSIE 2009/2010 may already start boiling at higher ambient air pressures than during JOSIE
801 2017. Cell weights were measured before and after all simulations for both campaigns. The weight loss due to
802 evaporation/boiling of the sensing solution was considerably higher during JOSIE 2009/2010 than in JOSIE 2017: about a
803 factor 2 for EN-SCI/SST0.5 and even a factor 3 for SPC/SST1.0. Although at these reduced ambient air pressures the
804 absorption efficiency is not critical (Tarasick et al., 2021), the sensing solutions losses of the sondes may have become so
805 large during JOSIE 2009/2010 that the absorption efficiency has been declined. This may explain the underestimation of the
806 ozone concentrations at low pressures for the JOSIE 2009/2010 profile simulations, in particular for SPC ozonesondes.
807

808 4.3 Differences Between Different Pairs of Sonde Type and SST

809 For each pair of ozone sonde type and SST for JOSIE 2009/2010, JOSIE 2017 and combined JOSIE 2009/2010 and 2017
810 (for SPC/SST1.0 and EN-SCI/SST0.5) a linear regression has been calculated as a function of pressure on a logarithmic
811 scale for the TRC sonde-OPM relative differences within ±30% for pressures up to 13 hPa. These linear regression lines are
812 shown in Figs. 6 and 7 as black dashed curves in the TRC diagrams for the different sonde-SST pairs; they agree well with
813 the corresponding averages (black solid lines in TRC diagrams). All TRC-sonde/SST pair relative difference scatterplots
814 display variations within 3-7% with altitude between the surface at P=1000 hPa and the upper end of the profile at P=10 hPa,
815 as can be seen in Table 3 that displays the relative sonde-OPM differences at the intercepts P=1000 hPa and P=10 hPa of the
816 linear regression. Table 3 illustrates the same typical differences of 3-5% for the same sonde type but different SST1.0 or
817 SST0.5, as first observed in JOSIE 2000 (Smit et al., 2007). Figures S4 (a & b) and S6 (a and b) show the persistence of
818 these systematic differences in detail for the conventional and TRC method as function of pressure (i.e. altitude). The low
819 buffered (SST0.1) EN-SCI or SPC-6A sondes slightly underestimate ozone by a few percent compared to the OPM. It is
820 noteworthy that the EN-SCI/SST0.1 OPM offsets decrease over the course of the sounding, in contrast to all other sonde-
821 SST pairs for which the relative differences increase (Table 3: last column).

822

823



824 **Table 3.** Relative differences of the sonde to the OPM at the P= 1000 hPa and P=10 hPa intercepts of the linear regression as
 825 a function of $\text{Log}_{10}(P)$ obtained from the different JOSIE data sets (Figs. 6-7) and for the sonde pairs SPC-6A and EN-SCI
 826 with different sensing solutions SST1.0, STT0.5 and SST0.1. Included are also the relative differences between EN-SCI and
 827 SPC6A sondes when operated at the same SST (last three rows).
 828

| Data set | Number of Samples | Rel. Differences in % Sonde to OPM at intercept P=1000 hPa | Rel. Differences in % Sonde to OPM at intercept P=10 hPa | Rel. Differences in % Sonde to OPM between P is 1000 and 10 hPa |
|---------------------------|-------------------|--|--|---|
| SPC-6A /SST1.0 | | | | |
| JOSIE 2009/2010 | 23 | 1.69 | 5.47 | 3.8 |
| JOSIE 2017 | 11 | 3.12 | 7.68 | 4.6 |
| JOSIE 2009/2010 + 2017 | 34 | 2.26 | 6.44 | 4.2 |
| SPC-6A /SST0.5 | | | | |
| JOSIE 2009/2010 | 20 | -2.0 | 3.62 | 5.6 |
| SPC-6A /SST0.1 | | | | |
| JOSIE 2017 | 6 | -3.52 | -2.24 | 1.8 |
| EN-SCI /SST1.0 | | | | |
| JOSIE 2009/2010 | 25 | 3.89 | 11.26 | 7.4 |
| EN-SCI /SST0.5 | | | | |
| JOSIE 2009/2010 | 15 | 1.35 | 8.30 | 7.0 |
| JOSIE 2017 | 20 | 1.93 | 6.21 | 4.3 |
| JOSIE 2009/2010 + 2017 | 35 | 1.72 | 7.02 | 5.3 |
| ENSCI /SST0.1 | | | | |
| JOSIE 2017 | 20 | 0.35 | -2.27 | -2.6 |
| SST EN-SCI – SPC6A | | | | |
| SST1.0 | | 1.63 | 4.82 | 3.2 |
| SST0.5 | | 3.92 | 3.40 | -0.5 |
| SST0.1 | | 3.87 | 0.03 | -3.4 |



829 **5 Conversion Efficiency of TRC Method Calibrated to OPM**

830 In the previous section it was shown that the TRC-method resolves the dependence of the measured ozonesonde profile from
 831 the past exposure of ozone, whereas the deconvolution of the remaining fast ozone sensor current resolves effectively the
 832 impact of gradients in the profile caused by the 20-30 sec time response of the ECC-sensor. The sonde to OPM comparisons
 833 presented in section 4 for the mid-latitude profiles of JOSIE 2009/2010 (Fig. 6) and tropical profiles of JOSIE 2017 (Fig. 7)
 834 demonstrate that the TRC results are independent of the shape of the simulated ozone profiles, in contrast to the results
 835 obtained by the conventional method (e.g. Smit et al., 2007; Deshler et al., 2008, 2017; Thompson et al., 2019). Further, the
 836 TRC results show a strong consistency of the mean relative differences with the OPM for the different sonde types-SST
 837 combinations across the different (grouped) JOSIE campaigns (see also Figs. S4 and S6). Therefore, those relative mean
 838 differences can be characterized by the linear regression curves as a function of $\text{Log}_{10}(P)$ in Figs 6-7 and directly linked to
 839 the OPM. As such, these linear regression lines (hereafter referred to as “calibration curves”) could be applied as the final
 840 correction step of the TRC methodology, tracing the ozonesonde measurements back to the OPM as the reference
 841 instrument.
 842

843 **5.1 Parameterisation of the Overall Conversion Efficiency η_c**

844 The linear regressions of the relative differences of the sonde to the OPM (Figs. 6-7) of the TRC method can be interpreted
 845 as the correction term of the overall conversion efficiency η_c when deviating from one for each of the different pairs of
 846 sonde type and SST. The overall conversion efficiency η_c in Eq. (6) can be expressed as a function of the ambient air
 847 pressure of the vertical sounding:

$$848 \eta_c(P) = 1 + F_c(P) \tag{17}$$

849 where $F_c(P)$ is the so-called correctional term of η_c as a function of the ambient air pressure P, which is parameterised by the
 850 linear regression fit of the relative sonde-OPM deviations as a function of $\text{Log}_{10}(P)$ and substituted in Eq. (17). This means
 851 that the overall conversion efficiency $\eta_c(P)$, calibrated to the OPM, has the following parameterisation

$$852 \eta_c(P) = 1 + a + b \cdot \text{Log}_{10}(P) \tag{18}$$

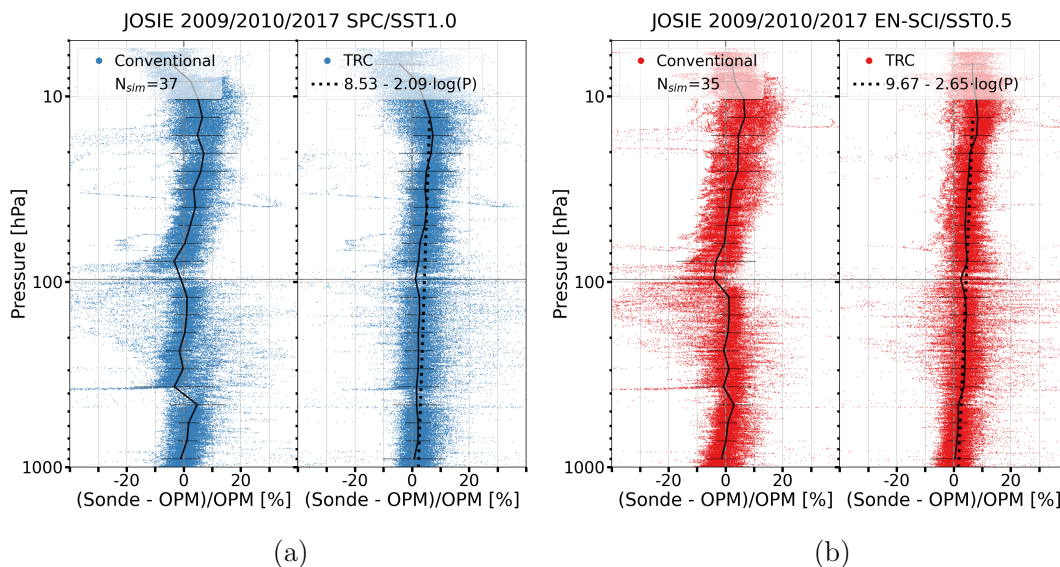
853 The linear regression curves derived for the different pairs of SPC-6A, EN-SCI with SST1.0, SST0.5, or SST0.1 obtained
 854 for the different JOSIE campaigns are shown in the TRC diagrams of Figs. 6-7 by the dashed black line. From Fig. 6-7 and
 855 Table 3, it is obvious that the relative OPM offsets (and the resulting linear regressions) for the same pairs of sonde and
 856 SST05 or SST1.0 are very similar in JOSIE 2009/2010 and JOSIE 2017. Thus, to achieve the best statistics, the results for
 857 those campaigns are lumped together in Fig. 8.

858
 859 The results of the parameterisation of $\eta_c(P)$, i.e. the offset a and the slope b (Eq.18), including their uncertainties Δa and the
 860 slope Δb , respectively, are listed for the different pairs of sonde type and SSTs as JOSIE (2009/2010 + 2017) in Table 4. The
 861 sonde/SST pairs operated with SST0.5 and SST1.0 cover mid-latitude as well as tropical ozone profile conditions, i.e. the
 862 resulting $\eta_c(P)$ functions are independent of the ozone profile. Based on this, we expect that the $\eta_c(P)$ for the SST0.1, which
 863 could only be derived in this study for the tropical JOSIE-2017 conditions, can also be applied to non-tropical ozone profiles.
 864 Likewise, we expect that the $\eta_c(P)$ determined from JOSIE 2009 only for the SPC/SST0.5 and EN-SCI/SST1.0 pairs are
 865 valid for tropical ozone profiles.

866
 867 The calibration functions are presented here (Table 4) as a function of pressure, but this does not mean that they are really
 868 pressure-dependent. However, the goal is to provide a practical empirical representation of the overall performance of the
 869 ozonesonde, ascending with a balloon at ~5m/s. The calibration functions can thus be interpreted as the correction term of



870 the overall conversion efficiency of the ECC sonde when deviating from one, but the origins are still uncertain. Most likely
 871 the term relates to the unknown stoichiometry of the fast chemical reactions converting ozone into free iodine, in other
 872 words, the fast ECC current I_f . This is supported by the shape of the vertical profiles of the absolute P_{O_3} -differences of the
 873 ECC sonde compared to the OPM for the TRC, shown for the JOSIE 2009/2010, JOSIE 2017 and for the JOSIE 1996-2002
 874 data (described in section 5.2), in the middle diagrams of Figures S3, S5 and S7, respectively. Indeed, in the middle
 875 stratosphere, the shapes of the residual currents compared to the OPM are more or less in phase with the simulated ozone
 876 profiles. This is most pronounced for the JOSIE-2017 tropical profiles (Fig. S5) and might indicate that these residual
 877 currents result from the fast chemical conversion and not from the 25-min delayed slow reaction. In the latter case, a phase
 878 shift between the residual currents and the ozone profile would be expected. The observed increase with altitude of typical 3-
 879 7% in the calibration functions (Tables 3 & 4) might derive from a small slightly increasing change stoichiometry of the fast
 880 O_3 conversion due to an increase of KI concentration and buffer strength caused by evaporation during the sounding.
 881



882

883

884 **Figure 8.** JOSIE 2009/2010 and 2017: Relative differences with the OPM for the conventional (left diagrams) and TRC
 885 (right diagrams) processed ozonesonde profiles for two pairs of sonde type and SST shown as scatterplots for
 886 SPC6A/SST1.0 (a: blue dots) and EN-SCI/SST0.5 (b: red dots), respectively. In each diagram for both methods the mean
 887 and 1σ -standard deviation are included (solid black line). The black dashed lines in the TRC-diagrams are the linear
 888 regressions of the differences of the ozonesonde to the OPM as function of the pressure (on a logarithmic scale).

889

890 Although the cell temperatures of the ozonesondes (both SPC6A/SST1.0 and EN-SCI/SST0.5) in JOSIE. 2009/2010 were
 891 about 10 °C higher than in JOSIE 2017 there are no direct indications that there is any cell temperature dependence of the
 892 calibration functions. This is demonstrated by the fact that SPC6A/SST1.0 and EN-SCI/SST0.5 for both campaigns show
 893 very similar OPM deviations over the course of the sounding when compared at the intercept points at $P=1000$ and 10 hPa
 894 (Table 3). However, temperature dependence cannot be completely excluded, in as much as the chemical reactions involved
 895 in the $KI+O_3$ chemistry may have significant temperature dependencies. Again, further in-depth investigations are needed.

896

897



898 **Table 4.** Parameterisation (offset a and slope b) of the calibrated conversion efficiency $\eta_c(P)$ (Eq. 18) for the different pairs
 899 of SPC-6A or ENSCI with SST1.0, SST0.5, or SST01 derived from the results of JOSIE 2009/2010 and JOSIE 2017.
 900 Included are the uncertainties Δa and Δb of the offset a and slope b in Eq. 15, respectively. The parameterisation of $\eta_c(P)$
 901 is valid from $P=1000$ hPa until $P=13$ hPa ($Z\approx 30$ km) for SPC, and for EN-SCI to 10 hPa ($Z\approx 32-33$ km).
 902

| Sonde Type / SST | Number of Samples | TRC-Conversion Efficiency $\eta_c(P) = 1 + a + b \cdot \text{Log}_{10}(P)$ Eq. (18) | | JOSIE Data Set |
|------------------|-------------------|---|-----------------------------------|--------------------------|
| | | Offset $a \pm \Delta a$ | Slope $b \pm \Delta b$ | |
| SPC-6A /SST1.0 | 34 | $(8.53 \pm 0.07) \times 10^{-2}$ | $(-2.09 \pm 0.03) \times 10^{-2}$ | JOSIE (2009/2010 + 2017) |
| SPC-6A /SST0.5 | 20 | $(6.43 \pm 0.08) \times 10^{-2}$ | $(-2.81 \pm 0.04) \times 10^{-2}$ | JOSIE 2009 |
| SPC-6A /SST0.1 | 6 | $(-1.60 \pm 0.12) \times 10^{-2}$ | $(-0.64 \pm 0.05) \times 10^{-2}$ | JOSIE 2017 |
| EN-SCI /SST1.0 | 25 | $(14.94 \pm 0.07) \times 10^{-2}$ | $(-3.68 \pm 0.03) \times 10^{-2}$ | JOSIE 2009 |
| EN-SCI /SST0.5 | 35 | $(9.67 \pm 0.06) \times 10^{-2}$ | $(-2.65 \pm 0.03) \times 10^{-2}$ | JOSIE (2009/2010 + 2017) |
| EN-SCI /SST0.1 | 20 | $(-3.58 \pm 0.09) \times 10^{-2}$ | $(1.31 \pm 0.04) \times 10^{-2}$ | JOSIE 2017 |

903
904

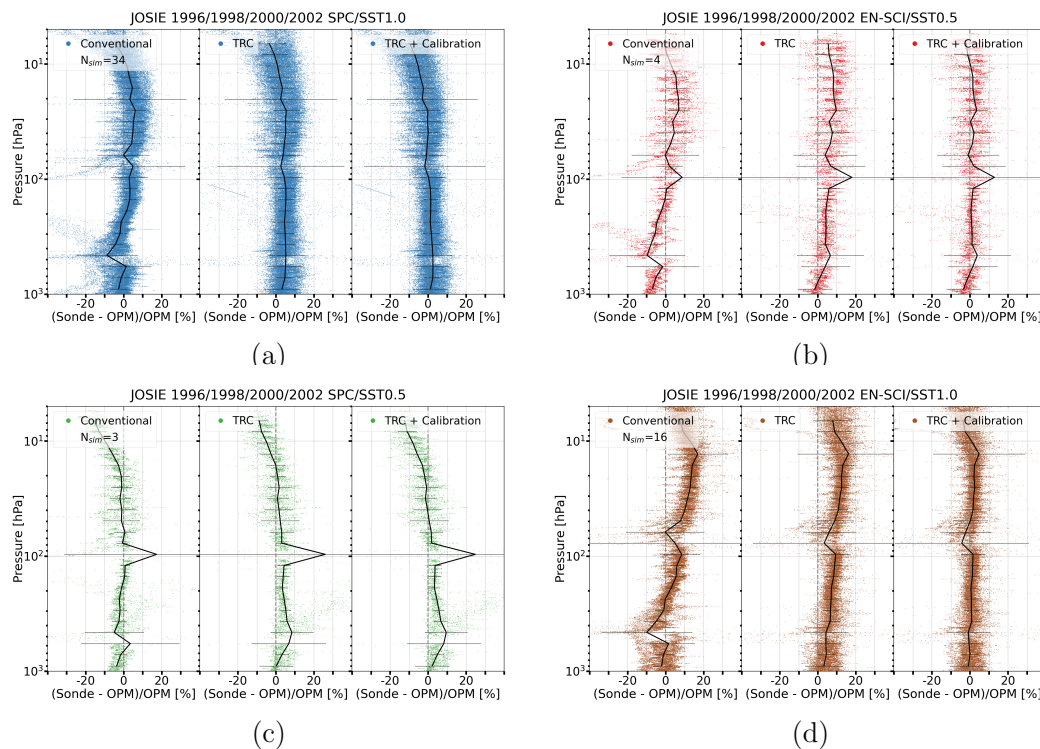
905 **5.2 Application to JOSIE 1996 + 1998 + 2000 + 2002 data**

906 The calibrated $\eta_c(P)$ functions derived from JOSIE 2009/2010 and JOSIE 2017 (Table 4) for the different sonde/SST pairs
 907 are applied to TRC processed ozonesonde data of JOSIE 1996 + 1998 + 2000 + 2002, in Figure 9, again as relative
 908 differences to the OPM. The JOSIE 1996 + 1998 + 2000 datasets and results were described in detail by Smit and Kley
 909 (1998) and Smit and Sträter (2004a, 2004b) and analysed by Smit et al. (2007). For JOSIE 1996, we excluded data from
 910 NOAA and CNRS because their operating procedures deviated too greatly from the Komhyr (1986) procedures; JOSIE 2002
 911 was a small campaign in which only 3 simulation runs were made with 10 SPC/SST1.0 sondes. The setup of the earlier
 912 campaigns was similar to the JOSIE 2009/2010 or JOSIE 2017 experiments. In the earlier campaigns mostly mid-latitude
 913 ozone profiles were simulated with the same four combinations of EN-SCI or SPC with either SST0.5 or SST1.0 (although
 914 the sample sizes with SST0.5 were rather small). The largest difference between JOSIE 2009/2010 and the early JOSIE
 915 campaigns lies in the preparation of the ozonesondes: in JOSIE 2009/2010, the same SOPs were followed by the three
 916 operators; ozonesondes “flown” in the earlier JOSIE-campaigns being prepared by different teams of people with a variety
 917 of SOPs.

918
 919 The comparisons with the OPM in Fig.9 are displayed for the TRC results, once not calibrated ($\eta_c(P) = 1.00$, middle
 920 diagrams) and once calibrated ($\eta_c(P)$ from Table 4, right diagrams), while the results for the conventional method (left
 921 diagrams) are included. From the figure it is obvious that independent of the sonde type (SPC-6A or EN-SCI) or sensing
 922 solution type (SST1.0, SST0.5), after applying $\eta_c(P)$ the residual average curves (black solid lines) are within less than $\pm 1\%$
 923 deviation from the “zero” over the entire vertical profile until 7-10 hPa. This means that with the TRC, combined with the
 924 use of the specific $\eta_c(P)$ for the various sonde-SST pairs, there are no longer systematic bias effects in the measured vertical
 925 ozonesonde profiles with respect to the OPM as a function of pressure (i.e. altitude). The use of the calibrated TRC can be a
 926 powerful tool to homogenize long term ozone records in the global ozonesonde network, so that these are now traceable to
 927 one reference standard, i.e. the OPM at the WCCOS. The application of the TRC with the use of the calibration functions on
 928 the JOSIE 2009/2010 and JOSIE 2017 datasets is also illustrated in the figures S3, and S5 in the Supplementary Material,



929 showing the vertical profiles of the absolute differences of the sondes with the OPM for the conventional method, TRC and
 930 TRC + Calibration. This information is also provided for the absolute differences for the early JOSIE campaigns in Fig. S7.
 931



932
 933
 934 **Figure 9.** JOSIE 1996 + 1998 + 2000 + 2002: Relative differences [%] with the OPM for the “conventional” (left diagrams
 935 of panels a-d), “TRC” (middle diagrams of panels a-d), and “TRC + application of calibration functions” (right diagrams of
 936 panels a-d) processed ozonesonde profiles for four pairs of sonde type and SST, shown as scatter plots in four different
 937 colors in the panels a-d: SPC6A/SST1.0 (a: blue dots), EN-SCI/SST0.5 (b: red dots), SPC6A/SST0.5 (c: green dots), and
 938 EN-SCI/SST1.0 (d: brown dots), respectively. In each diagram for both methods the mean and 1σ -standard deviation of the
 939 relative differences are included (solid black line). The absolute difference plots are available in the Supplementary Material
 940 (Fig. S7), and a summary plot of the relative differences in Fig. S8.
 941
 942



943 **6. Contribution Individual Correction Steps and Uncertainty Budget of the TRC Method**

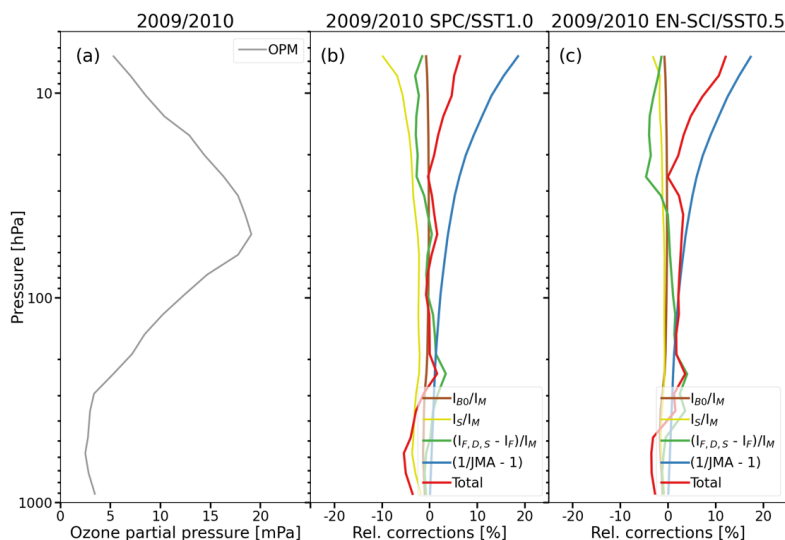
944 In this section we quantify the impact of the individual corrections made in the TRC method and estimate their uncertainty
945 contributions to the overall uncertainty of the ozone partial pressure derived from the measured ECC-ozone sensor current.
946

947 **6.1 Contribution of Correction Steps of TRC-Method for Mid-Latitude and Tropical Conditions**

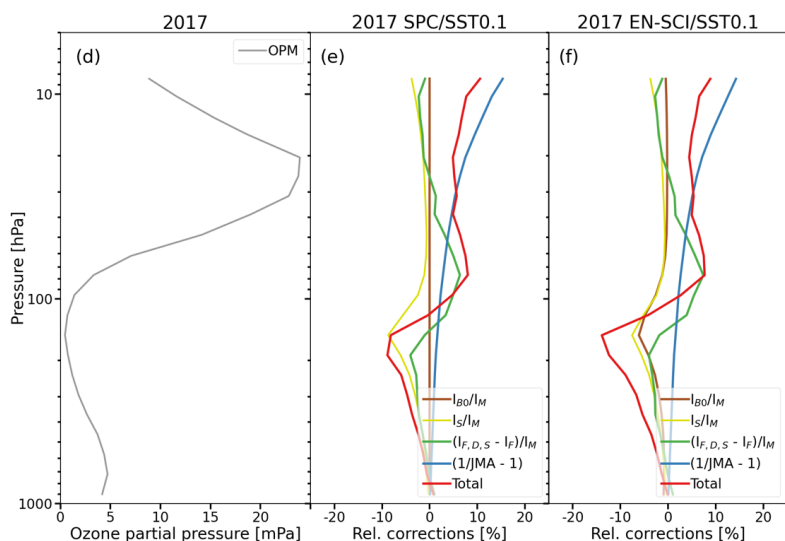
948 To derive from the measured cell current I_M the partial ozone pressure in the ambient air the TRC method includes four
949 different corrections: (i) constant background current I_{B0} ; (ii) slow cell current I_S ; (iii) time lag of fast current I_F : deconvolved
950 fast cell current (incl. smoothing); (iv) new pump efficiency (Nakano et al., 2023). The impact of the different corrections on
951 the measured cell current as a function of pressure (i.e. $\text{Log}^{10}(P)$) are shown in Figure 10 for mid-latitude (JOSIE
952 2009/2010) and tropical (JOSIE 2017) vertical profile conditions for the standard sonde type –SST pairs, SPC6A/SST1.0 and
953 EN-SCI/SST0.5, respectively.

954
955 A first, obvious, observation to make is that the corrections for a decreasing pump efficiency are for all sonde type- SST
956 pairs identical and at pressures smaller than 100 hPa increase slowly but significantly from 1 % at $P=100$ hPa to 12% at $P =$
957 10 hPa and to almost 20 % at $P = 5$ hPa. In the upper part of the profile (above 25 hPa) it is the dominating correction. In the
958 lower part, below 100 hPa, the constant background I_{B0} (brown line) and the past ozone dependent slow cell current I_S
959 (yellow line) are the major corrections, particularly in the upper tropical troposphere, with its very low ozone concentrations
960 (panels E and F). Here, those corrections can amount up to about 10-15%, depending on e.g. the amplitude of the measured
961 I_{B0} values. In this context, we also note that, because of the larger S_S values for SPC6A/SST1.0, the past ozone dependent
962 slow current (I_S) correction will be about a factor 2 larger than the I_S correction for the ENSCI/SST0.5, in all diagrams of
963 Fig. 10. On top of this effect, for SPC6A/SST1.0 JOSIE 2009/2010 (diagram b in Fig. 10), above 10 hPa, the relative I_S
964 correction is even rapidly increasing in absolute value due to the limited performance of the SPC6A sonde due to substantial
965 losses of the sensing solution caused by boiling effects, as explained before in section 4.2. The impact of the time lag
966 correction of the fast current is of the order of $\pm 5\%$, and of course strongly dependent on the local vertical ozone gradient.
967 Therefore, it can even become the dominant correction in the tropical UTLS region (between 5-10%), with its strong vertical
968 ozone gradient (diagrams e-f). Finally, we mention that very similar results are obtained for the ozonesonde types combined
969 with SST0.1, which are shown in the supplementary material (Fig. S9).

970



971



972

973

974 **Figure 10.** Relative corrections of TRC method for typical mid-latitude (upper diagrams A, B, C: JOSIE 2009/2010) and
 975 tropical (diagrams d, e, f: JOSIE 2017) ozonesonde profiles, respectively, showing the influence of the different correction
 976 steps for the new TRC method for SPC SST1.0 (diagrams b and e) and EN-SCI SST0.5 (diagrams c and f). The total
 977 correction (red line) consists of: (i) I_{B0} (brown line); (ii) I_S (yellow/green line); (iii) De-convolution I_F (green line); (iv) Pump
 978 efficiency (blue line: Nakano et al., 2023).



979 **6.2 Uncertainty Budget of the TRC Method**

980 For the conventional method a detailed uncertainty budget has been studied by Tarasick et al. (2021) and described in detail
 981 in the GAW 268 Report (Eq. E-3-1), together with practical guidelines to determine the overall uncertainty from the
 982 individual instrumental and procedural contributions. It is assumed that the uncertainties are random, uncorrelated, and
 983 normally distributed and following Gaussian statistics. In case of the TRC, the overall relative uncertainty of P_{O_3} is derived
 984 from Eq. (7), which has slightly changed compared to formula E-3-1 in GAW#268 (2021) as follows:

$$985 \frac{\Delta P_{O_3}}{P_{O_3}} = \sqrt{\left(\frac{\Delta \eta_P}{\eta_P}\right)^2 + \left(\frac{\Delta \eta_A}{\eta_A}\right)^2 + \left(\frac{\Delta \eta_C}{\eta_C}\right)^2 + \left(\frac{\Delta I_F}{I_F}\right)^2 + \left(\frac{\Delta T_P}{T_P}\right)^2 + \left(\frac{\Delta \Phi_{P_0}}{\Phi_{P_0}}\right)^2 + \sum \varepsilon_i^2} \quad (19)$$

986 The additional term ε_i represents additional random uncertainties (Tarasick et al., 2021); in case of the TRC these can be e.g.
 987 the relative uncertainty contributions by the used numerical schemes of either the convolution to obtain $I_S(t)$ or the
 988 deconvolution of $I_F(t)$ and its additional smoothing.

989 To determine the uncertainty budget for TRC in Eq. (19) the uncertainty contributions $\Delta \eta_P$, $\Delta \eta_A$, ΔI_M , ΔI_{B_0} , ΔT_P , and $\Delta \Phi_{P_0}$
 990 are exactly the same as in GAW Report No. 268 (2021) following the guidelines in its Annex-C. However, the recipes to
 991 determine the uncertainty contributions of the time varying $I_F(t)$, and the pressure dependent $\eta_C(P)$ (See Table 4) differ from
 992 GAW#268:

994 Uncertainty contribution ΔI_F :

995 From Eq. (7) the relative uncertainty of the fast sensor current $I_F(t)$ can be derived:

$$996 \frac{\Delta I_F}{I_F} = \sqrt{\frac{(\Delta I_M)^2 + (\Delta I_{B_0})^2 + (\Delta I_S)^2}{(I_M - I_{B_0} - I_S)^2}} \quad (20)$$

997 Here $\Delta I_{B_0} \approx 0.01 \mu A$, obtained from the I_{B_0} time series from Uccle. $I_S(t)$ estimations by varying the slow time constant with
 998 $\Delta \tau_S = \pm 5$ minutes has shown that $\Delta \tau_S$ only has a minor contribution to $\Delta I_S(t)$ of less than 1%, while a potential contribution
 999 of the numerical convolution scheme itself is vanishing small. It is obvious that $\Delta I_S(t)$ is predominantly determined by the
 1000 uncertainty ΔS_S of the stoichiometry S_S of the slow reaction path (Table 2)

$$1001 \Delta I_S(t) \approx \frac{\Delta S_S(t)}{S_S(t)} \cdot I_S(t) \quad (21)$$

1002 The impact of the slow time constant τ_S on the stoichiometry S_S and its uncertainty ΔS_S is also insignificant, as we assessed
 1003 by varying with $\Delta \tau_S = \pm 5$ minutes. Further, any contribution of the numerical schemes of deconvolution and its additional
 1004 smoothing to the uncertainty of I_F have been checked and appeared to be vanishingly small (< 0.5%).

1006 Uncertainty contribution $\Delta \eta_C$:

1007 The conversion efficiency $\eta_C(P)$ (Eq. 18) has been calibrated to the OPM such that its uncertainty $\Delta \eta_C(P)$ includes also the
 1008 uncertainty of the $P_{O_3,OPM}$ measurement by the OPM as follows

$$1009 \frac{\Delta \eta_C(P)}{\eta_C(P)} = \sqrt{\frac{(\Delta a)^2 + (\text{Log}_{10}(P) \cdot \Delta b)^2}{(\eta_C(P))^2} + \left(\frac{\Delta P_{O_3,OPM}(P)}{P_{O_3,OPM}(P)}\right)^2} \quad (22)$$

1010 Hereby $\frac{\Delta P_{O_3,OPM}(P)}{P_{O_3,OPM}(P)}$ is the relative uncertainty of the $P_{O_3,OPM}$ measurement of the OPM which is estimated to be better than 2
 1011 % at $P > 10$ hPa, and with lower pressures slightly increasing to 3 % until $P = 5$ hPa through potential small wall losses at
 1012 these pressures. The reported relative uncertainty values here for the OPM are about 1.5 % better than the values mentioned
 1013 before by Proffitt et al. (1983) because of the seven times smaller uncertainty of the new UV-absorption cross-section
 1014 (Hodges et al., 2019) compared to the former cross-section (Hearn et al., 1961) that was used before to derive the P_{O_3}
 1015 measurement of the OPM.

1016



1017 The overall uncertainty budget for the TRC method is summarized in Table 5. Figure 11 shows the contributions of the
 1018 different uncertainty sources to the uncertainty budgets for the SPC6A/SST1.0 and EN-SCI/SST0.5 when applying the TRC
 1019 method for a typical mid-latitude and tropical ozone profile as used in JOSIE 2009/2010 and JOSIE 2017, respectively. The
 1020 results for SPC6A/SST0.5 and EN-SCI/SST1.0 for JOSIE 2009/2010 and the low buffered SPC6A/SST0.1 and EN-
 1021 SCI/SST0.1 for JOSIE 2017 are shown in Figure S10 in Supplementary Material. For the sake of clarity, the uncertainty
 1022 contributions due to (i) ascent rate variation, (ii) pressure uncertainty, (iii) total ozone normalization factor are not included
 1023 here, as these are beyond the scope of this study. However, the characteristics of these uncertainty contributions, as reported
 1024 by Tarasick et al. (2021) and GAW Report No. 268, would not change the uncertainty budget of the TRC method itself.

1025

1026 **Table 5.** Sources of ozonesonde profile uncertainty and their estimated magnitudes for the TRC method. All quoted
 1027 uncertainties are one standard deviation (1σ). (*) To approximate ΔS_s as a one standard deviation uncertainty the MAD
 1028 values (only covering 25-75 percentiles) in Table 2 have been multiplied by 1.5 to become compatible with the Gaussian
 1029 error propagation applied here.

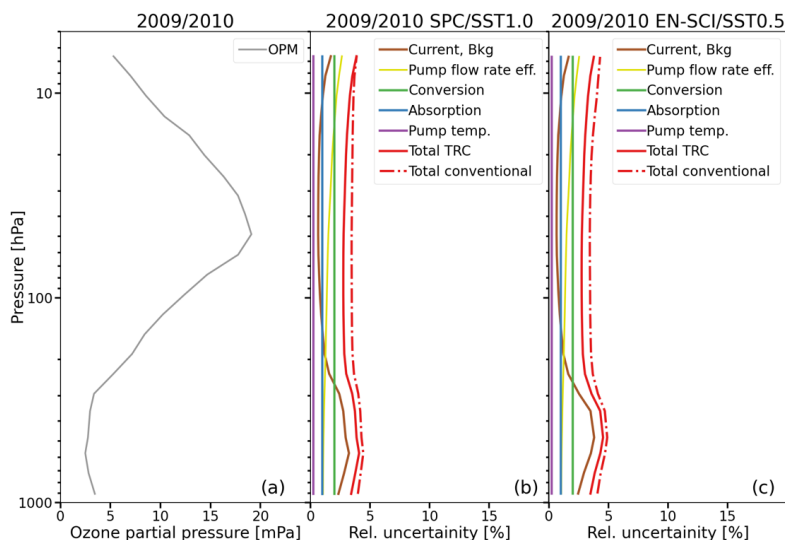
1030

| Source | Uncertainty | Reference |
|---|---|----------------------------|
| Pump flow rate Φ_{p0} | Φ_{p0} [E-3-3] and $\Delta\Phi_{p0}$ [E-3-9] | GAW Report No. 268 (2021) |
| Pump temperature T_P | T_P | GAW Report No. 268 (2021) |
| Pump efficiency $\eta_P(P)$ | $\eta_P(P)$ and $\Delta\eta_P(P)$ in Table 1: JMA-efficiency | Nakano and Morofuji (2023) |
| Absorption efficiency η_A | $\eta_A = 1.00$ and $\Delta\eta_A = 0.01$ | GAW Report No. 268 (2021) |
| Measured cell current $I_M(t)$ | $\Delta I_M(t) = \pm 0.005 \mu A$ at $I_M(t) < 1.00 \mu A$ $\Delta I_M(t) = \pm 0.5\%$ of $I_M(t)$ at $I_M(t) > 1.00 \mu A$ | GAW Report No. 268 (2021) |
| Background current I_{B0} | $\Delta I_{B0} = 0.01 \mu A$ | GAW Report No. 268 (2021) |
| Slow cell current $I_S(t)$ | Different sonde Type and SST: $\Delta I_S(t) = \frac{\Delta S_S(t)}{S_S(t)} \cdot I_S(t)$ from Eq. (21) S_S and ΔS_S from Table 2 (*) | This study |
| Fast cell current $I_F(t)$ | $I_F(t)$ from Eq. (7) and $\frac{\Delta I_F}{I_F}$ from Eq. (20) | This study |
| Conversion efficiency $\eta_C(P)$ | Different sonde type and SST: $\eta_C(P)$ from Table 3 and $\frac{\Delta\eta_C(P)}{\eta_C(P)}$ from Eq. (22) | This study |
| Partial pressure ozone by OPM: $P_{O_3, OPM}$ | $\Delta P_{O_3, OPM} : 2\%$ at $P > 10$ hPa 2% to 3% at P from 10 hPa to 5 hPa | This study |

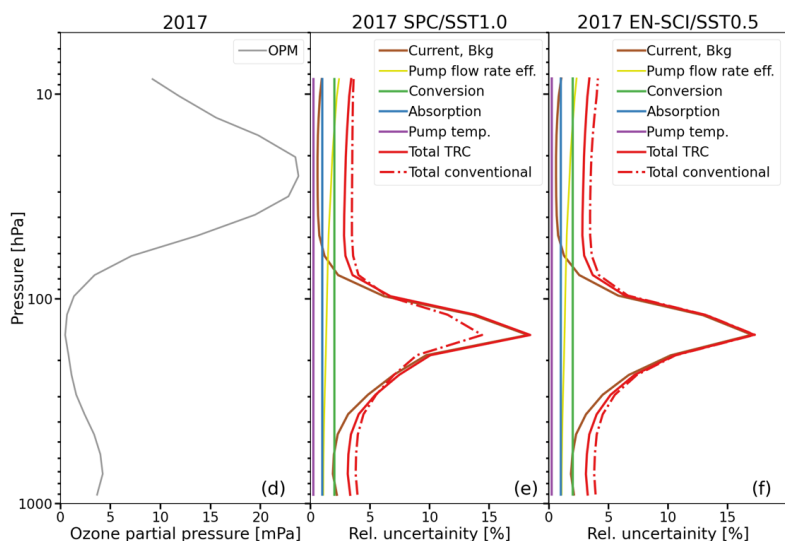
1031

1032

1033 In both the mid-latitude and tropical case (Fig. 11) it is seen that the (“background”) current in the troposphere and the
 1034 conversion efficiency in the stratosphere are the dominant uncertainty sources. For the conventional method the conversion
 1035 efficiency is based on the assumption that the overall stoichiometry factor is 1.00 with an uncertainty of 0.03 (Dietz et al.
 1036 1973), and obviously also the dominant uncertainty source in the stratosphere. However, in this study we have shown that
 1037 the overall stoichiometry can significantly differ from unity, which makes the overall uncertainty for the conventional
 1038 method rather optimistic. For the TRC-method $\Delta\eta_C(P)$ is mostly determined by the 2-3% uncertainty of the OPM as the
 1039 reference to obtain the $\eta_C(P)$ calibration functions (Table 4). In the troposphere, the contribution of I_S correction in the TRC
 1040 method is mostly smaller than the I_{B1} correction in the conventional method, particularly in the tropics.



1041



1042

1043 **Figure 11.** Uncertainty budgets of a mid-latitude (diagrams a, b, c; JOSIE 2009/2010) and tropical (diagrams d, e, f; JOSIE
 1044 2017) ozonesonde profile, showing the influence of the different uncertainty source terms listed in Table 5 for the TRC
 1045 method for SPC/SST1.0 (diagrams b and e) and EN-SCI/SST0.5 (diagrams c and f). Total uncertainty (red solid line)
 1046 consists of (i) Corrected cell current (brown line: $I_M - I_{B0} - I_S$ (TRC)); (ii) Pump flow (yellow/green line: flow rate +
 1047 efficiency); (iii) Conversion efficiency (green line); (iv) Absorption efficiency (blue line); (v) Pump temperature (purple
 1048 line). In addition, total uncertainty conventional method (dashed red line).



1049 However, both their contributions to the uncertainty are of the order of 0.01-0.02 μA , but on a relative scale they become
1050 strongly dependent on the magnitude of the ozone partial pressures, particularly in the upper tropical troposphere. In the
1051 stratosphere the contributions of the different uncertainties do not vary much and the overall uncertainty stays well below our
1052 5% target.

1053 It is to be noted that in the Tropics in the upper troposphere the partial pressure of ozone P_{O_3} can be in remote air conditions
1054 very low of the order of 0.1-0.3 mPa while the detection limit of the ECC-sensor is of the order of 0.01-0.02 μA , which
1055 corresponds to ozone levels of about 0.04-0.08 mPa. It is obvious that at these very low ozone levels the ECC-sonde
1056 performance is strongly restricted to its detection limit, which of course can have a significant and large impact on the
1057 overall uncertainty of the P_{O_3} ozonesonde measurements.

1058

1059 7. Implementation of the New Time Responses Correction Into Field Operation

1060 A detailed procedure for applying the TRC method in practice is described in Appendix C. In this section, we apply the new
1061 methodology developed in the previous sections to ozonesonde profile data from three different stations: (i) a mid-latitude
1062 site (Uccle); (ii) a tropical station (American Samoa), and (iii) an ozone hole profile from the South Pole station in the
1063 Antarctic. At those sites, we selected ascent and the corresponding descent profiles, such that the new methodology to
1064 resolve time response effects in the ECC signal can be assessed by comparing the ascent and descent profile of the same
1065 flight.

1066 For the ozonesonde profiles of the three stations, we first determined the slow component $I_S(t)$ by convolution of the
1067 measured cell current $I_M(t)$ with an exponential decay with a time constant $\tau_S = 25$ minutes (Eq. 10) and conversion
1068 efficiencies $S_S = 0.018$ for SST0.5 (Uccle) and $S_S = 0.023$ for SST0.1 (Samoa & South Pole). For the I_S at time $t = 0$ of the
1069 launch, (i) zero is used at Uccle, as the last exposure to ozone usually occurs at least one hour prior to launch and the
1070 measured value will fall back to I_{B0} , and (ii) we use $I_{B1} - I_{B0}$ multiplied by the exponential decay factor $X_S = \text{Exp}[-\Delta t / \tau_S]$, for the
1071 other two stations, with $\tau_S = 25$ min and $\Delta t = 30$ min (South Pole) and 90 min (Samoa). Those time intervals are the typical
1072 time differences between the I_{B1} measurement and launch time at those sites. This slow component is then subtracted from
1073 the measured cell current I_M , together with the background current I_{B0} . The remaining signal is the fast component, which is
1074 deconvolved to correct for the fast time response τ_F . For this latter, the time lag measurements before launch at the stations
1075 (e.g. time to drop from 4 to 1.5 μA) are taken. The smoothing of $I_{F,D}$ is done by applying a Gaussian filter prior to the time
1076 lag correction using a width equal to 20% of the fast time lag constant (as in Vömel et al., 2020). The final currents are then
1077 converted to ozone partial pressures using the calibration functions in Table 4 as conversion efficiency, taking the Nakano
1078 and Morofuji (2023) pump efficiency correction factors into account, correcting the pump temperature and the pump flow
1079 rates as in GAW#268 (2021). For the conventional method, the GAW recommendations have been followed rigorously,
1080 instead of subtracting I_{B0} (Uccle) and I_{B2} (Samoa and South Pole) as background currents.

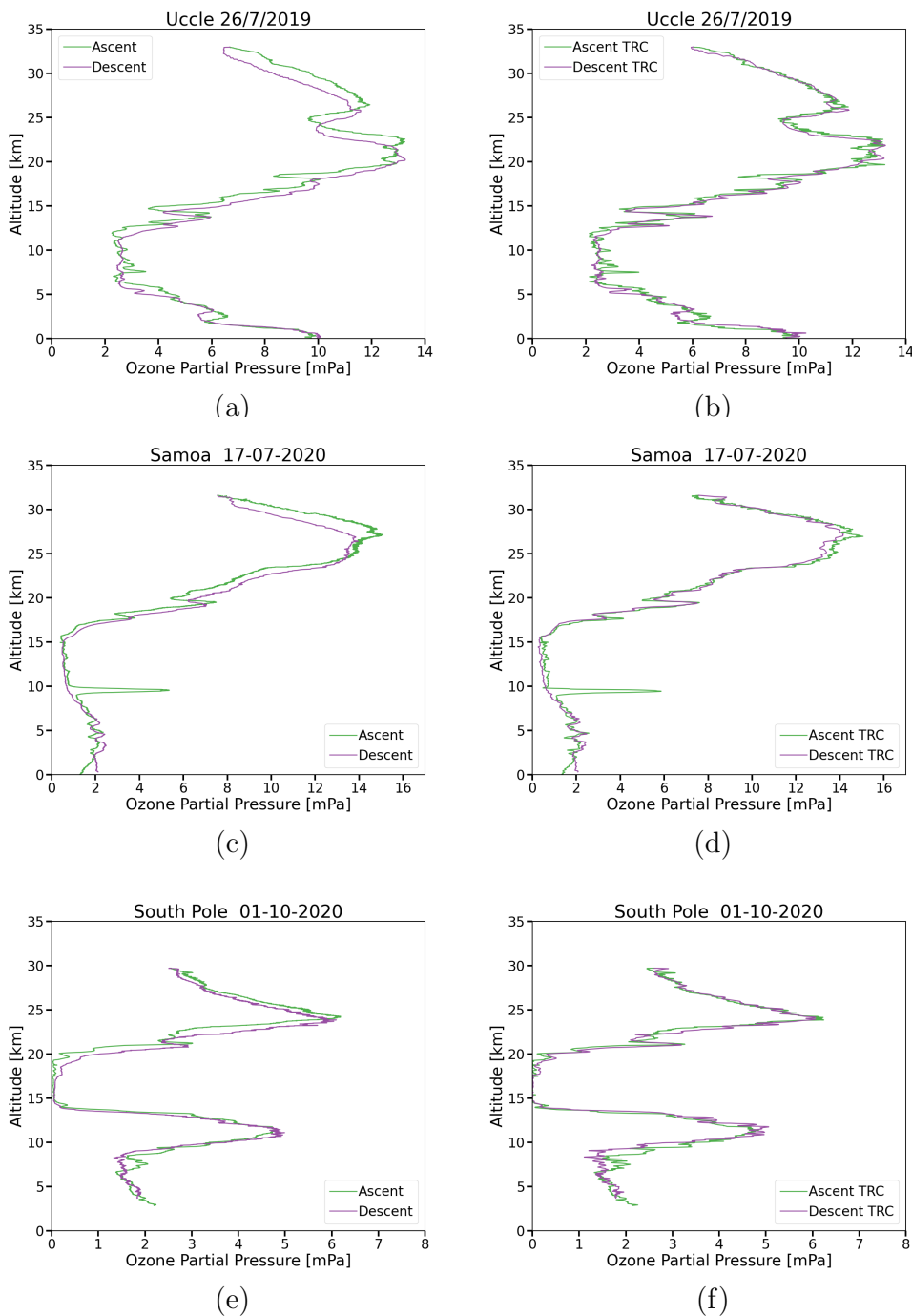
1081

1082 In Fig. 12, the profiles corrected with the conventional method are on the left side, while the implementation of the “new”
1083 TRC + calibration function on the profiles is shown on the right side. It should immediately strike the eye that the agreement
1084 between the ascent and descent profiles is much improved after applying in particular the fast time response deconvolution
1085 with the new method, and this for the three different sites. But also the profile shape, e.g. around the ozone peak maximum at
1086 the Uccle and Samoa profiles, corresponds much better with each other for the ascent and descent profiles for the new
1087 method. The slow time response correction contributes to a certain extent as well to this better profile shape agreement.

1088



1089



1090

1091

1092 **Figure 12.** Comparison of vertical ozone profiles obtained during ascent (green solid line) and descent (purple solid line) at

1093 three different ozonesounding stations (Uccle, Samoa, and South Pole) by applying once the conventional method (left

1094 diagrams) and the TRC method (right diagrams).



1095 A nice illustration of the impact of the slow time response correction is also found in the upper troposphere of the Samoa
1096 ozone profile. The upper tropospheric ozone concentrations are significantly decreased in both the ascent and descent
1097 profiles after applying this correction, while still agreeing very well. The strong reduction of upper-tropospheric ozone
1098 concentrations can be ascribed to correct for previous exposure to relatively high ozone amounts from the lower troposphere
1099 plus the (artificial) ozone spike for the ascent profile and from the ozone maximum for the descent profile.

1100
1101 The TRC figures are remarkable in amplifying the features after correcting for the fast time constant. We already noted that
1102 this new method is able to resolve some features in the ozonesonde data that were effectively present in the (faster) OPM
1103 ozone measurements in the JOSIE simulations. As noted by Vömel et al. (2020), the noise amplitude of the fast response
1104 time-lag-corrected data is comparable to that of the original data, but its spectral characteristics are different as a result of the
1105 smoothing algorithm. As a result, individual data points are heavily influenced by the noise characteristics of the smoothed
1106 data. This is demonstrated by the ozone spike in the Samoa ascent, which has a larger peak amplitude for the new method.
1107

1108 8. Summary and Conclusions

1109 The ECC ozonesonde, in principle an absolute measuring device, encounters in the course of its flight several imperfections,
1110 e.g. changing pump and conversion efficiency, that need to be corrected for. In the actual processing chain, the used “pump
1111 efficiency” tables (Komhyr 1986, Komhyr et al., 1995) in fact represent an overall correction, empirically tweaked to
1112 coincident total ozone measurements, that includes both a measured pump flow efficiency and an estimate of the
1113 stoichiometry increase over the flight (GAW Report No.268, 2021). However, the availability of recent measured ECC pump
1114 flow efficiencies (Nakano & Morofuji, 2023), confirming earlier measurements, together with the knowledge that the ECC
1115 sonde response (chemical reactions pathways) is driven by a slow and fast component (Vömel et al., 2020, Tarasick et al.,
1116 2021), call for a new approach. Vömel et al. (2020) also questioned the term “background current” in the ECC processing.
1117

1118 This study describes the concepts and the development of an updated methodology of ECC sonde data processing that
1119 applies a better correction of the ozone exposure dependent stoichiometry of the O_3+KI titration reaction in the
1120 electrochemical cell of the ECC-sonde through the use of true pump efficiencies combined with resolving the time responses
1121 of the slow ($\cong 25$ min) and fast ($\cong 20-25$ sec) components of the measured ECC-ozone sensor current. Experimental evidence
1122 is given to treat the measured ECC-sensor current as the superposition of a (i) dominant fast ozone current I_F ; (ii) slow time-
1123 variant, past ozone-exposure dependent, current I_S ; (iii) a constant ozone-independent background current I_{B0} .

1124

1125 The Time Responses Correction (TRC) method developed here is briefly described in three steps:

- 1126 I. The slow cell current component as a function of flight time is determined from the measured ozone sensor current,
1127 after correction for the constant background current I_{B0} , by using a first order numerical convolution scheme (Eq.
1128 (10). Hereby, the in-flight time response tests of JOSIE 2009/2010 have been used to quantify the stoichiometry
1129 (O_3/I_2) factors S_S (and their uncertainties) of the slow reaction pathways for both sonde types, SPC and EN-SCI, and
1130 two different sensing solution types, SST0.5 and SST1.0. In separate laboratory upward and downward response
1131 time experiments S_S and ΔS_S of the low buffered combination of EN-SCI with SST0.1 have been determined using
1132 exactly the same approach as in JOSIE 2009/2010.
- 1133 II. By subtracting the constant background current before exposure of ozone (I_{B0}) and the time variant slow sensor
1134 current I_S from the measured ECC-sensor current I_M , the remaining fast sensor current I_F has been resolved from the



1135 20-30 s. time response by using a first order deconvolution scheme (Eq. 12). Essential thereby is that the resulting
1136 deconvolved fast current $I_{F,D}$ is smoothed adequately to eliminate the high frequency noise into $I_{F,D,S}$.
1137 III. From $I_{F,D,S}$ and using the correct pump efficiency (Table 1: Nakano and Morofuji, 2023) the partial pressure of
1138 ozone measured by the ECC-sonde is determined (Eq. 6). Additionally, using the conversion efficiency table 4
1139 (“calibration functions”), the ozonesonde measurement is referred to the reference of the ozonesonde network, i.e.
1140 the photometer in the simulation chamber of the WCCOS in Jülich
1141
1142 Because the numerical convolution scheme used here is a recursive expression, the initial condition of I_S at the launch carries
1143 the past exposure of the pre-launch preparations. In laboratory experiments it was shown that after I_{B1} has been recorded
1144 during the pre-flight preparation and the ECC pump is not running anymore, I_S will further decay exponentially at the slow
1145 time constant $\tau_S=25$ min. By knowing the time span between recording of I_{B1} and turning-on the pump just before launch I_{B1}
1146 can be used to derive the initial value of I_S at the launch. Therefore, it is essential that during the pre-flight preparations both
1147 background currents before (I_{B0}) and after (I_{B1}) exposure of ozone are being recorded, including the timestamp at recording
1148 I_{B1} and activating the pump just before launch of the sonde. Similarly, our understanding of this slow time constant justifies
1149 the use of limiting values for I_{B0} and after I_{B1} in the operational preparation of ozone soundings, with filters providing a good
1150 quality zero ozone air source.
1151
1152 The slow stoichiometry factor S_S of the slow conversion of O_3 into I_2 and their MAD-uncertainties (Table 2) are each based
1153 on a statistically relevant number of samples. S_S depends on the different SSTs used (Table 2), but is not dependent on the
1154 sonde type, which indicates that the secondary reaction pathway is not responsible for the systematic 4-5 % relative
1155 differences existing between EN-SCI and SPC when operating with the same SST. However, a direct quantitative relation of
1156 the buffer strength and the magnitude of S_S only holds for the full buffered SST1.0 ($S_S \approx 0.046-0.050$) and the half-buffered
1157 SST0.5 ($S_S \approx 0.017-0.018$), but not for the low-1/10th buffered SST0.1 ($S_S \approx 0.023$). For SST0.1 significant lower S_S values
1158 would be expected, which might indicate that, in lower buffered sensing solutions, another competing chemical reaction
1159 scheme may occur that produce also free iodine at a 25 minutes time scale and contributes to I_S . This may be the reason that
1160 for non-buffered or low-buffered sensing solutions I_{B1} values of 0.01-0.04 μA are still recorded.
1161
1162 S_S values reported in Table 2 are significantly smaller than the so-called “steady bias factor” values applied by Vömel et al.
1163 (2020), which are the overall excess stoichiometry derived from steady state experiments under ozone exposure (Vömel and
1164 Diaz, 2010). The difference may be explained by the overall excess stoichiometry originating from the secondary reaction
1165 pathway is only partly contributing to the slow I_S and the other part is still contributing to the fast I_F (Appendix A). Further,
1166 in contrast to this study, Vömel et al. (2020) do not correct for I_{B0} before determining I_S and calculating I_F . These two
1167 different approaches in the methodology (e.g. I_{B0} subtraction and different stoichiometry factors S_S for the slow current I_S)
1168 will of course lead to different results when comparing the sondes to the OPM. To demonstrate the impact of these different
1169 assumptions between both correction schemes we have processed the JOSIE 2009/2010 and JOSIE 2017 according the TRC-
1170 scheme used by Vömel et al. (2020). The comparisons are shown in the supplementary material in the figures S4 and S6 for
1171 JOSIE 2009/2010 and JOSIE 2017, respectively. The impact of subtracting I_{B0} is generally small and only of significance in
1172 the upper troposphere in the Tropics, where including the I_{B0} subtracting leads to better agreement with the OPM. The
1173 impact of larger S_S values for SST1.0 and SST0.5 will lower the differences to the OPM above 100 hPa, but there still
1174 remains a significant deviation from the OPM. In the upper troposphere, the larger S_S gives negative deviations, particularly
1175 in the Tropics.
1176



1177 Different JOSIE data sets (JOSIE 2009/2010, JOSIE 2017, and JOSIE 1996 + 1998 + 2000 + 2002) have been used
1178 compare the relative differences of the sonde to the OPM obtained with the Time Responses Correction (TRC) versus the
1179 conventional methodology of post flight data processing (GAW Reports No. 201 and 268). Hereby, it is very important to
1180 mention that, in contrast to the conventional methodology, the relative differences obtained with TRC are almost
1181 independent of the past ozone exposure and increases only a few percent with altitude (or lower pressure). This is most
1182 pronounced in the tropical ozone profiles at 200-100 hPa pressure in the upper troposphere with very low ozone values and
1183 the steep vertical ozone gradient when entering into the lower stratosphere. The typical systematic relative differences of 3-
1184 5% for the same sonde type but different SST1.0 or SST0.5 as observed since JOSIE 2000 are still preserved in the TRC.
1185
1186 The different behavior between JOSIE2009/2010 and JOSIE2017 in the relative differences of the TRC corrected sonde
1187 profiles with the OPM for pressures smaller than about 13 hPa can be ascribed to different pump temperatures used for the
1188 mid-latitude and tropical profiles in the resp. campaigns. During JOSIE2009/2010, the higher pump temperatures led to a
1189 higher boiling rate in this pressure range, which has been observed by the higher solution weight losses.
1190 The TRC mean relative differences of the sonde with the OPM show a strong consistency for the different pairs of sonde
1191 type and SST and can be therefore represented by a linear regression as function of Log_{10} of the pressure. This linear
1192 regression can be interpreted as the calibration function of the correctional term of the conversion efficiency when deviating
1193 from one (Eq. 18). The calibration functions introduced here for the various sonde-SST combinations, parameterized as a
1194 function of ambient air pressure in Table 4, are independent of the ozone exposure, and thus invariant to the measured ozone
1195 profile itself. The use of these calibration functions will allow us to get the global ozonesonde records traceable to one
1196 common standard, i.e. the OPM of the WCCOS. The origin of these calibration functions remain speculative, but there are
1197 some experimental indications that they are linked to the unknown stoichiometry of the fast chemical conversion of O_3 into I_2
1198 and not caused by an underestimation of the slow cell current I_s .
1199
1200 The overall uncertainty of combining the TRC with the use of the calibration functions is about 3-4 % throughout the entire
1201 ozone profile, except for the upper troposphere, where the overall uncertainty can increase up to 10% for very low ozone
1202 amounts, particularly in the tropics. The major uncertainty sources in the upper troposphere are the constant background
1203 current I_{B0} and the slow current I_s (i.e. S_s), despite the correction of the slow current for the past ozone exposure in the TRC.
1204
1205 The TRC have been tested in practice (practical guidelines in Appendix C) for three different vertical ozone profiles
1206 measured during ascent and descent at a mid-latitude site, a tropical station and during an ozone hole at the South Pole. The
1207 resolving power of the fast deconvolution numerical scheme is thereby clearly demonstrated by resolving the strong delay
1208 shift in the descent ozone profile compared with the ascent ozone profile before and after applying the TRC. However, the
1209 examples also clearly demonstrate the importance of careful and proper smoothing of the deconvolved ozone profile. To
1210 apply the TRC method to the time series of an ozonesonde site, a proper determination of I_{B0} and I_{B1} is required. Improper
1211 filters might increase those background currents by several orders of magnitude, compromising the subtraction by the (too
1212 high) I_{B0} value throughout the entire profile and at the beginning of the profile due to the high initial value for $I_s(t_0)$. Some
1213 more analysis is needed to formulate alternative approaches for these cases. As stated also by ASOPOS 2.0 (GAW Report
1214 No. 268) the use of proper gas filters to provide ozone free, dry and purified air in practice at the sounding site, is very
1215 essential in general, but also when applying the TRC data processing.
1216
1217 An important outcome of this study is also that the contribution of the slow current I_s is not as prominent as previously
1218 thought because TRC demonstrates that the secondary pathway involving the buffer can also contribute to the fast
1219 stoichiometry factor to increase the fast current I_F so that the uncalibrated conversion efficiency exceeds one, which is most



1220 likely the case for SST1.0 and SST0.5. This in contrast to SST0.1, where the slow current has most likely a different
1221 chemical origin and not an additional contribution to I_F , occurs so that the fast stoichiometry (i.e. conversion efficiency) does
1222 not exceed one and is even a few percent lower. The underlying chemical mechanisms remain speculative in some cases and
1223 the stoichiometry of the fast O_3+KI chemistry cannot be quantified explicitly but only expressed implicitly in the conversion
1224 efficiency with the introduction of calibration functions (Table 4). These calibration functions can improve the
1225 homogenization of long term ozonesonde records of the global network, making the data traceable to one ozone standard, the
1226 OPM at the WCCOS at Jülich (Germany). Our OPM reference values have been scaled up 1.23% compared to earlier JOSIE
1227 publications because of the revised UV ozone absorption cross-section at 254 nm (BIPM, 2022; Hodges et al., 2019). The
1228 latter adjustment is being introduced in the global ozone network in 2024/2025.

1229

1230 Some specific recommendations for further research include:

- 1231 1. Regular JOSIE-campaigns at WCCOS (Jülich, Germany) are essential to check the long-term stability of the
1232 calibrations functions reported in this study (Table 4) and to guarantee the long term traceability of global
1233 ozonesonde records to the OPM-standard.
- 1234 2. More research is needed to understand the slow stoichiometry S_s factors in more detail, particularly for the low or
1235 no buffered sensing solutions for which the underlying chemical processes are not understood at all. A key question
1236 hereby is also the role of KBr in the sensing solutions. This should be in conjunction with understanding the
1237 differences observed between the methods to derive S_s from either a zero-ozone or ozone exposure time response
1238 experiment. Dedicated laboratory experiments in the WCCOS simulation chamber can accomplish this
- 1239 3. More detailed understanding of the chemical reaction mechanisms that are responsible for the fast and slow cell
1240 current response of the ECC-sensor, and their interaction. This should include determining the temperature
1241 dependency of the $KI+O_3$ chemistry.
- 1242 4. Better knowledge of the time behaviour of the high background currents I_{B0} and I_{B1} that are often measured in
1243 practice at the sounding sites when not using proper gas filters. Experiments are necessary to describe and
1244 eventually correct for this high I_{B0} and I_{B1} caused using inadequate gas filters because re-processing ozonesonde
1245 records often means correcting very high I_{B0} and I_{B1} .

1246 This study did not solve the systematic 3-5% offsets in measured ozone between EN-SCI and SPC instruments when
1247 operating with the same SST. However, we showed that the S_s values are comparable for both sondes with the same SST,
1248 which means the differences are not caused by the slow chemistry. More research here is essential.

1249 Acknowledgements

1250 For the JOSIE 2009/2010 we are very grateful to Marcel Berg (FZJ/IEK-8, Germany) and Dr. Johannes Staufer (ETHZ,
1251 Switzerland) for the pre-flight preparation of the ozonesondes. Many thanks to Dr. Holger Vömel for stimulating discussions
1252 in preparing the manuscript. Also many thanks to the people who supplied ECC-sondes to be “flown” in the simulation
1253 chamber in JOSIE 2009/2010 and 2017. For JOSIE 2009/2010 we thank: Dr. Bryan Johnson (NOAA-GML, USA), Francis
1254 Schmidlin (NASA/Goddard/Wallops Flight Facility, USA), Dr. Hugo De Backer (RMI, Belgium), Dr. Rene Stübi (Meteo
1255 Suisse., Switzerland), Dr. Rigel Kivi (FMI, Finland), Dr. Richard Querel (NIWA, New Zealand), Dr. Matt Tully (BOM,
1256 Australia), Dr. Emilio Cuevas (AEMET, Spain). Sondes for JOSIE-2017 were supplied by FZJ/IEK-8, NOAA/GML and
1257 NASA/Goddard. Researchers from FZ-J, NASA/Goddard, NOAA/GML, MeteoSwiss, RMI (Belgium), KNMI
1258 (Netherlands), JMA (Japan), Environment & Climate Change Canada along with 8 SHADOZ operators contributed time to
1259 JOSIE-2017. We thank the United Nations Environmental Programme, WMO, EN-SCI and SPC for supporting the



1260 participation of the SHADOZ personnel in JOSIE-2017. JOSIE 2009/2010 and 2017 were sponsored by WMO/GAW and
1261 Forschungszentrum Jülich (FZJ) and NASA/GSFC.

1262 **Competing interests**

1263 R. Van Malderen is a member of the editorial board of Atmospheric Measurement Techniques. The peer review process will
1264 be guided by an independent editor. The authors have no other competing interests to declare.

1265 **References**

- 1266 Ancellet, G., Godin-Beekmann, S., Smit, H. G. J., Stauffer, R. M., Van Malderen, R., Bodichon, R., and Pazmiño, A.:
1267 Homogenization of the Observatoire de Haute Provence electrochemical concentration cell (ECC) ozonesonde data record:
1268 comparison with lidar and satellite observations, *Atmos. Meas. Tech.*, 15, 3105–3120, [https://doi.org/10.5194/amt-15-3105-](https://doi.org/10.5194/amt-15-3105-2022)
1269 [2022](https://doi.org/10.5194/amt-15-3105-2022), 2022.
- 1270 BIPM, 2022: [https://www.bipm.org/documents/20126/27085544/RapportBIPM-2022-02.pdf/f93def70-2544-ff13-ac63-](https://www.bipm.org/documents/20126/27085544/RapportBIPM-2022-02.pdf/f93def70-2544-ff13-ac63-3bc73f36688e)
1271 [3bc73f36688e](https://www.bipm.org/documents/20126/27085544/RapportBIPM-2022-02.pdf/f93def70-2544-ff13-ac63-3bc73f36688e).
- 1272 Crutzen, P.J.: The influence of nitrogen oxides on the atmospheric ozone content, *Quart. J. Roy. Met. Soc.*, 96, No. 408, 320–
1273 325, <https://doi.org/10.1002/qj.49709640815>, 1970.
- 1274 Davies, J., McElroy, C.T., Tarasick, D.W., and Wardle, D.I.: Ozone capture efficiency in ECC ozonesondes: Measurements
1275 made in the laboratory and during balloon flights, EAE03-A-13703, in *Geophysical Research Abstracts*, Vol. 5, 13703, EGS-
1276 AGU-EUG Joint Assembly, Nice, France, 6–11 April 2003, 2003.
- 1277 De Muer, D., & Malcorps, H.: The frequency response of an electrochemical ozone sonde and its application to the
1278 deconvolution of ozone profiles, *J. Geophys. Res.*, 89, 1361–1372, 1984.
- 1279 Deshler, T., Mercer J., Smit, H.G.J., Stübi, R., Levrat, G., Johnson, B.J., Oltmans, S.J., Kivi, R., Davies, J., Thompson, A.M.,
1280 Witte, J., Schmidlin, F.J., Brothers, G., Sasaki, T.: Atmospheric comparison of electrochemical cell ozonesondes from
1281 different manufacturers, and with different cathode solution strengths: The Balloon Experiment on Standards for
1282 Ozonesondes, *J. Geophys. Res.*, 113, D04307, <https://doi.org/10.1029/2007JD008975>, 2008.
- 1283 Deshler, T., Stübi, R., Schmidlin, F. J., Mercer, J. L., Smit, H.G.J., Johnson, B.J., Kivi, R. and Nardi, B., 2017: Methods to
1284 homogenize ECC ozonesonde measurements across changes in sensing solution concentration or ozonesonde manufacturer,
1285 *Atm. Meas. Tech.*, 10, 2012–2043, [doi:10.5194/amt-10-2021-2017](https://doi.org/10.5194/amt-10-2021-2017), 2017.
- 1286 Dietz, R. N., Pruzansky, J., & Smith, J. D.: Effect of pH on the stoichiometry of the iodometric determination of ozone. *Anal.*
1287 *Chem.*, 45, 402–404, 1973.
- 1288 Farman, J.C., Gardener, B.G., and Shanklin, J.D.: Large Losses of total ozone in Antarctica reveal seasonal ClOx/NOx
1289 interaction, *Nature*, 315, 207-210, 1985.
- 1290 Garner, G. G., and Thompson, A. M.: Ensemble statistical post-processing of the National Air Quality Forecast Capability:
1291 Enhancing ozone forecasts in Baltimore, Maryland. *Atmos. Environ.*, **81**, 517–522, doi:10.1016/j.atmosenv.2013.09.020,
1292 2013.
- 1293 GAW Report No. 104: Report of the Fourth WMO Meeting of Experts on the Quality Assurance/Science Activity Centres
1294 (QA/SACs) of the Global Atmosphere Watch, WMO Global Atmosphere Watch Report Series, No. 104, World
1295 Meteorological Organization, Geneva, 1995.
- 1296 GAW Report No. 201, Smit, H.G.J., and the ASOPOS Panel: Quality Assurance and Quality Control for Ozonesonde
1297 Measurements in GAW, WMO Global Atmosphere Watch Report Series, No. 201, World Meteorological Organization,
1298 Geneva, [Available online at https://library.wmo.int/doc_num.php?explnum_id=7167], 2014.



- 1299 GAW Report No. 268, Smit, H.G.J., Thompson, A.M., and the ASOPOS 2.0 Panel: Ozonesonde Measurement Principles and
1300 Best Operational Practices, WMO Global Atmosphere Watch Report Series, No. 268, World Meteorological Organization,
1301 Geneva, [Available online at https://library.wmo.int/doc_num.php?explnum_id=10884], 2021.
- 1302 Hearn, A.G.: Absorption of ozone in ultra-violet and visible regions of spectrum, *Proc. Phys. Soc.*, 78, 932–940, 1961.
- 1303 Hodges, J.T., Viallon, J., Brewer, P.J., Drouin, B.J., Gorshelev, V., Janssen, C., Lee, S., Possolo, A., Smith, M.A.H., Walden,
1304 J., Wielgosz, R.I.: Recommendation of a consensus value of the ozone absorption cross-section at 253.65 nm based on a
1305 literature review, *Metrologia*. 56: 034001. <https://iopscience.iop.org/article/10.1088/1681-7575/ab0bdd>, 2019.
- 1306 Huang, L.J., Chen, M.J., Lai, C.H., Hsu, H.T. and Lin, C.H.: New Data Processing Equation to Improve the Response Time
1307 of an Electrochemical Concentration Cell (ECC) Ozonesonde. *Aerosol Air Qual. Res.* 15: 935-944.
1308 <https://doi.org/10.4209/aaqr.2014.05.0097>, 2015.
- 1309 Imai, K., Fujiwara, M., Inai, Y., Manago, N., Suzuki, M., Sano, T., Mitsuda, C., Naito, Y., Hasebe, F., Koide, T., Shiotani,
1310 M.: Comparison of ozone profiles between Superconducting Submillimeter-Wave Limb-Emission Sounder and worldwide
1311 ozonesonde measurements, *J. Geophys. Res. Atmos.*, 118, 12,755– 12,765, doi:[10.1002/2013JD021094](https://doi.org/10.1002/2013JD021094), 2013.
- 1312 IPCC-Climate Change 2013: The Physical Science Basis. Contribution of Working Group I to the Fifth Assessment Report
1313 of the Intergovernmental Panel on Climate Change [Stocker, T.F., Qin, D., Plattner, G.-K., Tignor, M., Allen, S.K.,
1314 Boschung, J., Nauels, A., Xia, Y., Bex, V. and Midgley, P.M. (eds.)]. Cambridge University Press, Cambridge, United
1315 Kingdom and New York, NY, USA, 1535 pp, 2013.
- 1316 IPCC-Climate Change 2021: The Physical Science Basis. Contribution of Working Group I to the Sixth Assessment Report
1317 of the Intergovernmental Panel on Climate Change [Masson-Delmotte, V., Zhai, P., Pirani, A., Connors, S.L., Péan, C.,
1318 Berger, S., Caud, N., Chen, Y., Goldfarb, L., Gomis, M.I., Huang, M., Leitzell, K., Lonnoy, E., Matthews, J.B.R., Maycock,
1319 T.K., Waterfield, T., Yelekçi, O., Yu, R., and Zhou, B. (eds.)]. Cambridge University Press, Cambridge, United Kingdom and
1320 New York, NY, USA, In press, doi:10.1017/9781009157896, 2022.
- 1321 Johnson, B.J., S.J. Oltmans, Vömel, H., Smit, H.G.J., Deshler, T. and Kroeger, C.: ECC Ozonesonde pump efficiency
1322 measurements and tests on the sensitivity to ozone of buffered and unbuffered ECC sensor cathode solutions, *Journal of*
1323 *Geophysical Research*, 107, D19, <https://doi.org/10.1029/2001JD000557>, 2002.
- 1324 Komhyr, W.D.: Nonreactive gas sampling pump, *Rev. Sci. Instr.*, 38, 981–983, 1967.
- 1325 Komhyr, W.D.: Electrochemical concentration cells for gas analysis, *Ann. Geoph.*, 25, 203–210, 1969
- 1326 Komhyr, W.D. and T.B. Harris: Development of an ECC Ozonesonde, NOAA Technical Report, ERL 200-APCL 18, 1971.
- 1327 Komhyr, W.D.: Operations handbook - Ozone measurements to 40 km altitude with model 4A-ECC ozone sondes, NOAA
1328 Technical Memorandum, ERL-ARL-149, 1986.
- 1329 Komhyr, W.D., Barnes, R.A., Brothers, G.B., Lathrop, J.A. and Opperman, D.P.: Electrochemical concentration cell
1330 ozonesonde performance evaluation during STOIC 1989, *J. Geophys. Res.*, 100, 9231–9244, 1995.
- 1331 Lovelock, J.E., Maggs, R.J., Wade, R.J.: Halogenated Hydrocarbons in and over the Atlantic, *Nature*, 241, 194-196,
1332 <https://doi.org/10.1038/241194a0>, 1973.
- 1333 Miloshevich, L. M., Paukkunen, A., Vomel, H., and Oltmans, S. J.: Development and validation of a time lag correction for
1334 Vaisala radiosonde humidity measurements, *J. Atm. Ocean. Tech.*, 21, 1305-1327, 2004.
- 1335 Mills, G., Pleijel, H., Malley, C.S., Sinha, B., Cooper, O.R., Schultz, M.G., Neufeld, H.S., Simpson, D., Sharps, K., Feng, Z.,
1336 Gerosa, G., Harmens, H., Kobayashi, K., Saxena, P., Paoletti, E., Sinha, V. and Xu, X.: Tropospheric Ozone Assessment
1337 Report: Present-day tropospheric ozone distribution and trends relevant to vegetation. *Elem Sci Anth*, 6: 47. DOI:
1338 <https://doi.org/10.1525/elementa.302>, 2018.
- 1339 Molina, M., Rowland, F. Stratospheric sink for chlorofluoromethanes: chlorine atom-catalysed destruction of
1340 ozone. *Nature* 249, 810–812, <https://doi.org/10.1038/249810a0>, 1974.



- 1341 Nakano, T. and Morofuji, T.: Development of an automated pump-efficiency measuring system for ozonesondes utilizing an
1342 airbag-type flowmeter, *Atm. Meas. Tech.*, 16, 1583–1595, <https://doi.org/10.5194/amt-16-1583-2023>, 2023.
- 1343 Newton, R., Vaughan, G., Ricketts, H.M.A., Pan, L.L., Weinheimer, A. J. and Chemel, C., 2016: Ozonesonde profiles from
1344 the West Pacific Warm Pool: Measurements and validation, *Atm. Chem. Phys.*, 619–634, [doi:10.5194/acp-16-619-201](https://doi.org/10.5194/acp-16-619-201),
1345 2016.
- 1346 Proffitt, M.H. and McLaughlin, R.J.: Fast response dual-beam UV-absorption photometer suitable for use on stratospheric
1347 balloons, *Rev. Sci. Instr.*, 54, 1719–1728, 1983.
- 1348 Reid, S.J., Vaughan, G., Marsh, A.R. and Smit, H.G.J.: Intercomparison of ozone measurements by ECC sondes and
1349 BENDIX chemiluminescent analyser, *J. Atmos. Chem.*, 25, 215–226, 1996.
- 1350 Saltzman, B.E. and Gilbert, N.: Iodometric micro-determination of organic oxidants and ozone, resolution of mixtures by
1351 kinetic colorimetry, *Anal. Chem.*, 31, 1914–1920, 1959.
- 1352 Seinfeld, J.H., Pandis, S.N.: *Atmospheric Chemistry and Physics (From Air Pollution to Climate Change, 3rd Edition*, 1152
1353 pp., ISBN-13: 978-111894740, John Wiley and Sons, Inc., New York, 2016.
- 1354 Smit, H.G.J., Sträter, W., Kley, D. and Proffitt, M.H.: The evaluation of ECC ozonesondes under quasi flight conditions in the
1355 environmental simulation chamber at Jülich, in *Proceedings of Eurotrac symposium 1994*, edited by P.M. Borell et al., SPB
1356 Academic Publishing B.V., The Hague, The Netherlands, 349–353, 1994.
- 1357 Smit H.G.J and Kley, D.: JOSIE: The 1996 WMO International Intercomparison of Ozonesondes Under Quasi Flight
1358 Conditions in the Environmental Simulation Chamber at Jülich, *WMO Global Atmosphere Watch Report Series*, No. 130,
1359 WMO/TD No. 926, World Meteorological Organization, Geneva, 1998.
- 1360 Smit H.G.J., Sträter, W., Helten, M. and Kley, D.: Environmental Simulation Facility to Calibrate Airborne Ozone and
1361 Humidity Sensors. *Jül Berichte*, No. 3796, Forschungszentrum Jülich, 2000.
- 1362 Smit, H.G.J.: Ozonesondes, in *Encyclopedia of Atmospheric Sciences*, Second Edition, edited by G.R. North, J.A. Pyle, and
1363 F. Zhang, Vol 1, pp. 372–378, Academic Press, London, 2014.
- 1364 Smit, H.G.J., and Sträter, W.: JOSIE-1998, Performance of ECC Ozone Sondes of SPC-6A and ENSCI-Z Type, *WMO*
1365 *Global Atmosphere Watch Report Series*, No. 157, WMO/TD No. 1218, World Meteorological Organization, Geneva, 2004a.
- 1366 Smit, H.G.J., and Sträter, W.: JOSIE-2000, Jülich Ozone Sonde Intercomparison Experiment 2000, The 2000 WMO
1367 International Intercomparison of Operating Procedures for ECC Ozonesondes at the Environmental Simulation Facility at
1368 Jülich, *WMO Global Atmosphere Watch Report Series*, No. 158, WMO TD No. 1225, World Meteorological Organization,
1369 Geneva, 2004b.
- 1370 Smit, H.G.J.: Tropospheric Ozone as a Tracer to Investigate Deep Convection and its Influence on the Humidity in the
1371 Marine Tropics, PhD Thesis, University of Wuppertal, [on-line available: [https://elekpub.bib.uni-](https://elekpub.bib.uni-wuppertal.de/ubwhsmig/content/titleinfo/3555358)
1372 [wuppertal.de/ubwhsmig/content/titleinfo/3555358](https://elekpub.bib.uni-wuppertal.de/ubwhsmig/content/titleinfo/3555358)], 2004c.
- 1373 Smit, H.G.J., Sträter, W., Johnson, B.J., Oltmans, S.J., Davies, J., Tarasick, D.W., Högger, B., Stübi, R., Schmidlin, F.J.,
1374 Northam, T., Thompson, A.M., Witte, J.C., Boyd, I. and Posny, F.: Assessment of the performance of ECC ozonesondes
1375 under quasi-flight conditions in the environmental simulation chamber: Insights from the Jülich Ozone Sonde
1376 Intercomparison Experiment (JOSIE), *Journal of Geophysical Research*, 112, D19306, [doi:10.1029/2006JD007308](https://doi.org/10.1029/2006JD007308), 2007.
- 1377 Smit, H.G.J., and O3S-DQA Panel: Guidelines for Homogenization of Ozonesonde Data, SI2N/O3S-DQA Activity as part of
1378 “Past Changes in the Vertical Distribution of Ozone Assessment”, available at <https://www.wccos-josie.org/en/o3s-dqa/>,
1379 2012.
- 1380 Stauffer, R.M., Thompson, A.M., Kollonige, D.E., Tarasick, D.W., Van Malderen, R., Smit, H.G.J.: An examination of the
1381 recent stability of ozonesonde global network data. *Earth and Space Science*, 9, e2022EA002459.
1382 <https://doi.org/10.1029/2022EA002459>, 2022.



- 1383 Steinbrecht W., Schwartz, R. and Claude, H.: New pump correction for the Brewer-Mast ozone sonde: Determination from
1384 experiment and instrument intercomparisons, *J. Atm. Ocean. Tech.*, 15, 144–156, 1998.
- 1385 Sterling, C.W., Johnson, B.J., Oltmans, S.J., Smit, H.G.J., Jordan, A.F., Cullis, P.D., Hall, E.G., Thompson, A.M. and Witte,
1386 J.C.: Homogenizing and estimating the uncertainty in NOAA's long-term vertical ozone profile records measured with the
1387 electrochemical concentration cell ozonesonde, *Atm. Meas. Tech.*, 11, 3661–3687, [https://doi.org/10.5194/amt-11-3661-](https://doi.org/10.5194/amt-11-3661-2018)
1388 [2018](https://doi.org/10.5194/amt-11-3661-2018), 2018.
- 1389 Stolarski, R. S. and Cicerone, R. J.: Stratospheric Chlorine: a Possible Sink for Ozone, *Can. J. Chem.*, 1610-1615,
1390 <https://doi.org/10.1139/v74-233>, 1974.
- 1391 Tarasick, D.W., Jin, J.J., Fioletov, V.E., Liu, G., Thompson, A.M., Oltmans, S.J., Liu, J., Sioris, C.E., Liu, X., Cooper, O.R.,
1392 Dann, T. and Thouret, V.: High-resolution tropospheric ozone fields for INTEX and ARCTAS from IONS ozonesondes, *J.*
1393 *Geophys. Res.*, 115, D20301, <https://doi.org/10.1029/2009JD012918>, 2010.
- 1394 Tarasick, D.W., Davies, J., Smit, H.G.J. and Oltmans, S.J.: A re-evaluated Canadian ozonesonde record: measurements of the
1395 vertical distribution of ozone over Canada from 1966 to 2013, *Atm. Meas. Tech.*, 9, 195–214, [doi:10.5194/amt-9-195-2016](https://doi.org/10.5194/amt-9-195-2016),
1396 2016.
- 1397 Tarasick, D., Galbally, I.E., Cooper, O.R., Schultz, M.G., Ancellet, G., Leblan, T., Wallington, T.J., Ziemke, J., Liu, X.,
1398 Steinbacher, M., Staehelin, J., Vigouroux, C., Hannigan, J.W., Garcia, O., Foret, G., Zanis, P., Weatherhead, E.,
1399 Petropavlovskikh, I., Worden, H., Osman, M., Liu, J., Chang, K.-L., Gaudel, A., Lin, M., Granados-Muñoz, M., Thompson,
1400 A.M., Oltmans, S.J., Cuesta, J., Dufour, G., Thouret, V., Hassler, B., Trickl, T. and Neu, J.L.: Tropospheric Ozone
1401 Assessment Report: Tropospheric ozone from 1877 to 2016, observed levels, trends and uncertainties. *Elementa: Science of*
1402 *the Anthropocene*, 7:39. <https://doi.org/10.1525/elementa.376>, 2019.
- 1403 Tarasick, D.W., Smit, H.G.J., Thompson, A.M., Morris, G.A., Witte, J.C., Davies, J., Nakano, T., Van Malderen, R., Stauffer,
1404 R.M., Deshler, T., Johnson, B.J., Stübi, R., Oltmans, S.J. and Vömel, H., 2021: Improving ECC ozonesonde data quality:
1405 Assessment of current methods and outstanding issues, *Earth and Space Science*, 8, e2019EA000914,
1406 <https://doi.org/10.1029/2019EA000914>, 2021.
- 1407 Thompson, A.M.: The oxidizing capacity of the Earth's atmosphere: Probable past and future changes. *Science*, 256, 1157–
1408 1165, <https://doi.org/10.1126/science.256.5060.1157>, 1992.
- 1409 Thompson, A.M., Stone, J.B., Witte, J.C., Miller, S.K., Pierce, R.B., Chatfield, R.B., Oltmans, S.J., Cooper, O.R., Loucks,
1410 A.L., Taubman, B.F., Johnson, B.J., Joseph, E., Kucsera, T.L., Merrill, J.T., Morris, G.A., Hersey, S., Forbes, G., Newchurch,
1411 M.J., Schmidlin, F.J., Tarasick, D.W., Thouret, V. and Cammas, J.-P.: Intercontinental Chemical Transport Experiment
1412 Ozonesonde Network Study (IONS) 2004: 1 Summertime upper troposphere/lower stratosphere ozone over northeastern
1413 North America, *J. Geophys. Res.*, 112, D12S12, [doi:10.1029/2006JD007441](https://doi.org/10.1029/2006JD007441), 2007a.
- 1414 Thompson, A.M., Witte, J.C., Smit, H.G.J., Oltmans, S.J., Johnson, B.J., Kirchhoff, V.W.J.H. and Schmidlin, F.J.: Southern
1415 Hemisphere Additional Ozonesondes (SHADOZ) 1998–2004 tropical ozone climatology: 3. Instrumentation, station-to-
1416 station variability, and evaluation with simulated flight profiles, *J. Geophys. Res.*, 112, D03304, [doi:10.1029/2005JD007042](https://doi.org/10.1029/2005JD007042),
1417 2007b.
- 1418 Thompson, A.M., Oltmans, S.J., Tarasick, D.W., von der Gathen, P., Smit, H.G.J. and Witte, J.C.: Strategic ozone sounding
1419 networks: Review of design and accomplishments, *Atm. Env.*, 45, 2145–2163, [doi:10.1016/j.atmosenv.2010.05.002](https://doi.org/10.1016/j.atmosenv.2010.05.002), 2011.
- 1420 Thompson, A.M., Witte, J.C., Sterling, C., Jordan, A., Johnson, B.J., Oltmans, S.J., Fujiwara, M., Vömel, H., Allaart, M.,
1421 Piters, A., Coetzee, G.J.R., Posny, F., Corrales, E., Andres Diaz, J., Félix, C., Komala, N., Lai, N., Maata, M., Mani, F.,
1422 Zainal, Z., Ogino, S.-Y., Paredes, F., Luiz Bezerra Penha, T., da Silva, F.R., Sallons-Mitro, S., Selkirk, H.B., Schmidlin, F.J.,
1423 Stübi, R. and Thiongo, K.: First reprocessing of Southern Hemisphere Additional Ozonesondes (SHADOZ) ozone profiles
1424 (1998–2016). 2. Comparisons with satellites and ground-based instruments, *J. Geophys. Res.*, 122,
1425 <https://doi.org/10.1002/2013JD019771>, 2017.



- 1426 Thompson, A.M., Smit, H.G.J., Witte, J.C., Stauffer, R.M., Johnson, B.J., Morris, G.A., von der Gathen, P., Van Malderen,
1427 R., Davies, J., Piters, A., Allaart, M., Posny, F., Kivi, R., Cullis, P., Nguyen T.H. Ahn, Corrales, E., Machinini, T., DaSilva,
1428 F.R., Paiman, G., Thiong'o, K., Zainal, A., Brothers, G.B., Wolff, K.R., Nakano, T., Stübi, R., Romanens, G., Coetzee,
1429 G.J.R., Diaz, J.A., Mitro, S., 'bt Mohamad, M. and Ogino, S.-Y.: Ozonesonde quality assurance: The JOSIE-SHADOZ
1430 (2017) experience, *Bull. Amer. Met. Soc.*, 100, <https://pubmed.ncbi.nlm.nih.gov/33005057/>, 2019.
- 1431 Thompson, A.M., Stauffer, R.M., Wargan, K., Witte, J.C., Kollonige, D.E., and Ziemke, J.R.: Regional and Seasonal Trends
1432 in Tropical Ozone From SHADOZ Profiles: Reference for Models and Satellite Products, *J. Geophys. Res.*, 126,
1433 <https://doi.org/10.1029/2021JD03469>, 2021.
- 1434 Thompson, A.M., Smit, H.G.J., Kollonige, D.E., Stauffer, R.M.: Ozonesondes: Instrumentation and Data Application, In:
1435 *Field Measurements for Passive Environmental Remote Sensing* (Ed. Nalli, N.R.), 458 pp., 1st Edition, ISBN 13- 978-
1436 0128239537, Elsevier, Amsterdam, 2022.
- 1437 Thornton, D.C., and Niazy, N.: Sources of background current in the ECC ozonesonde: Implication for total ozone
1438 measurements, *J. Geophys. Res.*, 87, 8943–8950, 1982.
- 1439 Thornton, D.C. and Niazy, N.: Effects of solution mass transport on the ECC ozonesonde background current, *Geophys. Res.*
1440 *Let.*, 10, 148–15, 1983.
- 1441 UNEP-Ozone Secretariat, Handbook for the Montreal Protocol on Substances that Deplete the Ozone Layer, 14th Edition,
1442 ISBN: 978-9966-076-79-3, [on-line available [https://ozone.unep.org/sites/default/files/Handbooks/MP-Handbook-2020-](https://ozone.unep.org/sites/default/files/Handbooks/MP-Handbook-2020-English.pdf)
1443 [English.pdf](https://ozone.unep.org/sites/default/files/Handbooks/MP-Handbook-2020-English.pdf)], 2020.
- 1444 Van Malderen, R., Allaart, M.A.F., De Backer, H., Smit, H.G.J., De Muer, D.: On instrumental errors and related correction
1445 strategies of ozonesondes: possible effect on calculated ozone trends for the nearby sites Uccle and De Bilt, *Atm. Meas.*
1446 *Tech.*, 9, 3793–3816, doi:10.5194/amt-9-3793-2016/, 2016.
- 1447 Vömel, H. and Diaz, K.: Ozone sonde cell current measurements and implications for observations of near-zero ozone
1448 concentrations in the tropical upper troposphere, *Atm. Meas. Tech.*, 3, 495–505, doi:10.5194/amt-3-495-2010,
1449 <http://www.atmos-meas-tech.net/3/495/2010/>, 2010.
- 1450 Vömel, H., Smit, H.G.J., Tarasick, D.W., Johnson, B.J., Oltmans, S.J., Selkirk, H.B., Thompson, A.M., Stauffer, R.M., Witte,
1451 J.C., Davies, J., Van Malderen, R., Morris, G.A., Nakano, T. and Stübi, R.: A new method to correct the ECC ozone sonde
1452 time response and its implications for “background current” and pump efficiency, *Atm. Meas. Tech.*, 13, 5667–5680,
1453 <https://amt.copernicus.org/articles/13/5667/2020/>, 2020.
- 1454 Wang, H. J. R., Damadeo, R., Flittner, D., Kramarova, N., Taha, G., Davis, S., Thompson, A.M., Strahan, S., Wang, Y.,
1455 Froidevaux, L., Degenstein, D., Bourassa, A., Steinbrecht, W., Walker, K.A., Querel, R., Leblanc, T., Godin-Beekmann, S.,
1456 Hurst, D., Hall, E.: Validation of SAGE III/ISS solar occultation ozone products with correlative satellite and ground based
1457 measurements, *J. Geophys. Res.*, 125, e2020JD032430, <https://doi.org/10.1029/2020JD032430>, 2020.
- 1458 Witte, J.C., Thompson, A.M., Smit, H.G.J., Fujiwara, M., Posny, F., Coetzee, G.J.R., Northam, E.T., Johnson, B.J., Sterling,
1459 C.W., Mohamad, M., Ogino, S.-Y., Jordan, A. and da Silva, F.R.: First reprocessing of Southern Hemisphere Additional
1460 Ozonesondes (SHADOZ) profile records (1998–2015): 1. Methodology and evaluation, *J. Geophys. Res.*, 122, 6611–6636,
1461 <https://doi.org/10.1002/2016JD026403>, 2017.
- 1462 Witte, J.C., Thompson, A.M., Smit, H.G.J., Vömel, H., Posny, F. and Stübi, R.: First reprocessing of Southern Hemisphere
1463 Additional Ozonesondes profile records: 3. Uncertainty in ozone profile and total column. *J. Geophys. Res.*, 123, 3243–
1464 3268. <https://doi.org/10.1002/2017JD027791>, 2018.
- 1465 Witte, J.C., Thompson, A.M., Schmidlin, F.J., Northam, E.T., Wolff, K.R. and Brothers, G.B.: The NASA Wallops Flight
1466 Facility digital ozonesonde record: Reprocessing, uncertainties, and dual launches. *J. Geophys. Res.*, 124, 3565–3582,
1467 [doi:10.1029/2018JD030098](https://doi.org/10.1029/2018JD030098), 2019.



- 1468 WMO/UNEP: Scientific Assessment of Ozone Depletion: 2022, Ozone Research and Monitoring – GAW Report No. 278,
1469 World Meteorological Organization, Geneva, 2023.
- 1470 Xu, X., Muller, R.P., Goddard, W.A.: The gas phase reaction of singlet dioxygen with water: A water-catalyzed mechanism,
1471 PNAS, 99 (6), 3376-3381, <https://doi.org/10.1073/pnas.052710099>, 2002.
- 1472 Zhang, J., Xuan, Y., Yan, X., Liu, M., Tian, H., Xia, X., Pang, L. and Zheng, X.: Development and preliminary evaluation of
1473 a double-cell ozonesonde, Adv. Atm. Sci., 31, 938–947, 2014a.
- 1474 Zhang, J.-Q., Xuan, Y.-J., Xia, X.-A., Liu, M.-Y., Yan, X.-L., Pang, L., Bai, Z.-X., and Wan, X.-W.: Performance evaluation
1475 of a self-developed ozonesonde and its application in an intensive observational campaign, Atm. Ocean. Sci. Lett., 7, 175–
1476 179, <https://doi.org/10.3878/j.issn.1674-2834.13.0089>, 2014b.
- 1477



1478 **Appendix A: KI + O₃ Chemistry in Presence of Phosphate-Buffer (NBKI after Saltzman & Gilbert, 1959)**

1479 Iodometric determination of ozone and the underlying oxidation of iodide ion by ozone to liberate iodine has long been
 1480 subject of controversy. The reaction of KI with O₃ may proceed through a variety of chemical pathways strongly depending
 1481 on pH, KI and O₃ concentrations, whether or not in presence of a pH-buffer. In this study the focus is on the NBKI method
 1482 and its application in the ECC-ozone sensor. Experimentally it was shown by several investigators (e.g. Saltzman and
 1483 Gilbert, 1959; Flamm and Anderson, 1975) that iodate (IO₃⁻) as intermediate can be excluded as long as ozone partial
 1484 pressures in the air are well below 100 mPa. This makes it most likely that much of the behaviour of the ECC and its slow
 1485 and fast sensor currents may be explained by the chemical reaction mechanisms for the NBKI (Neutral Buffered KI) and its
 1486 impact of the phosphate buffer as postulated by Saltzman and Gilbert (1959). It was experimentally shown that the fast and
 1487 slow reactions increase as KI concentrations increases, whereby the slow reactions increase with the buffer concentration.
 1488 Buffered solutions with no KI show no evidence of gaseous O₃ uptake into the sensing solution, indicating that the additional
 1489 reactions with O₃ are secondary reactions after the initial O₃ + KI reaction.

1490

1491 Primary reaction pathway:



1493 *In ion-notation:*



1495 Or in detail (postulated after Saltzman & Gilbert, 1959) :



1499 Losses of IO⁻, i.e. I₂:



1501

- 1502 • If all O₃ would be absorbed and react with KI in this primary reaction pathway, it would be expected that the
- 1503 stoichiometry for O₃/IO⁻ i.e. O₃/I₂ in neutral/acid solution is equal to one.
- 1504 • However, self-reaction of IO⁻ (R6) can be a loss mechanism, competing with the formation of I₂ (R4).
- 1505 • In general, loss mechanisms of IO⁻ might compete with (R4) and then the stoichiometry of primary reaction pathway is
- 1506 less than one.
- 1507 • ECC shows for 1% KI and no buffer a stoichiometry less than one (Johnson et al., JGR, 2002).
- 1508 • Dismutation (disproportioning) of IO⁻ into iodate (IO₃⁻) and I⁻ is extremely slow and is of no importance in case of the
- 1509 ECC-sensor. Iodate-chemistry plays first a role at significant higher KI or O₃ concentrations than are used in the ECC-
- 1510 sensor or encountered in the atmosphere, respectively.

1511

1512 Secondary Reaction Pathway: Impact of Phosphate Buffer



1516 But also losses of I₂ iodine (via IO⁻ losses):



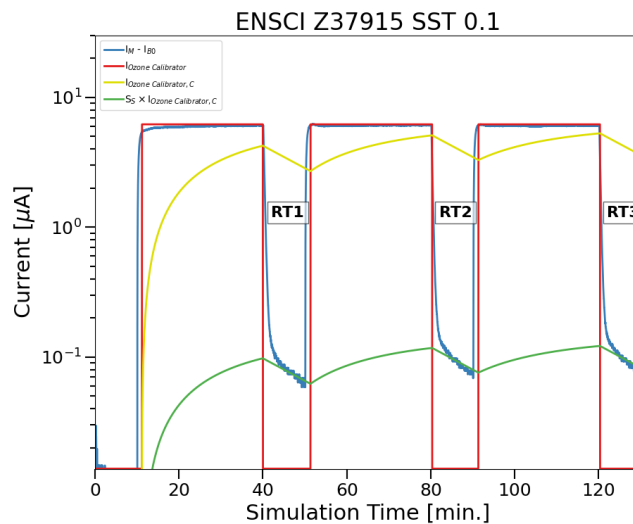
- 1519 • R7 is the key reaction to form extra IO⁻ that can react via (R4) into I₂ and is contributing in addition to the fast reaction
- 1520 pathway and thus adding to the stoichiometry causing the fast ECC signal.



- 1521 • H_2PO_5^- can be seen as the interim reactant that is formed fast but via (R8) decaying slowly to form extra IO^- . This latter
 1522 can produce in addition extra I_2 which is causing the slow part of the ECC current.
 1523 • It is known that H_2PO_5^- reacts similar as H_2O_2 to form IO^- , i.e. I_2 with typical time constant of about 25 minutes: this fits
 1524 to the slow, secondary response time of ECC of typical 25 minutes.

1525 **Appendix B: Laboratory Experiments to Determine S_s for EN-SCI SST0.1**

1526 As no time response tests are available during JOSIE campaigns for SST0.1 to determine S_s , we undertook laboratory
 1527 measurements under room conditions in Uccle (Belgium). During the experiments, 4 ozonesondes were simultaneously
 1528 exposed to ozone amounts generated by a photometric ozone calibrator Teledyne API T703 according to the following
 1529 scheme (3 times): 30 minutes of exposure to a value of $450 \mu\text{g}/\text{m}^3$ (around 225 ppb) ozone were preceded and succeeded by
 1530 10 minutes of ozone-free air, see Fig. B1. The value of $450 \mu\text{g}/\text{m}^3$ has been imposed by the upper limit ($6.5 \mu\text{A}$) of the
 1531 microcurrent meters used in the Forschungszentrum Jülich homemade ground calibration box for the 4 ozonesondes. These
 1532 microcurrents were read out digitally and, as in the JOSIE experiments, the S_s values were again estimated as the average
 1533 over a 50s time interval between 4 and 5 minutes after the end of the ozone exposure. As the time response test intervals in
 1534 these laboratory measurements are twice as long (10 minutes) as in the JOSIE 2009/2010 campaigns, we tried different
 1535 timings for the determination of the S_s values, but they did not give significantly different results for the slow stoichiometry
 1536 coefficients. Again, the differences between the S_s values obtained from the different time response test intervals in one
 1537 experiment were insignificant as well.



1538 **Figure B1.** Example of a series of three upward and downward ozone steps generated by a photometric ozone calibrator
 1539 Teledyne API T70 (represented by the generic $I_{\text{Ozone Calibrator}}$: red line) and the response of the measured cell current $I_{M-I_{B0}}$
 1540 (blue line) of an EN-SCI SST01 ozonesonde as function of time, the 25 min convolved $I_{\text{Ozone Calibrator, C}}$ (yellow line) and the
 1541 slow current after determination and application of S_s ($S_s \times I_{\text{Ozone Calibrator, C}}$: green line).
 1542

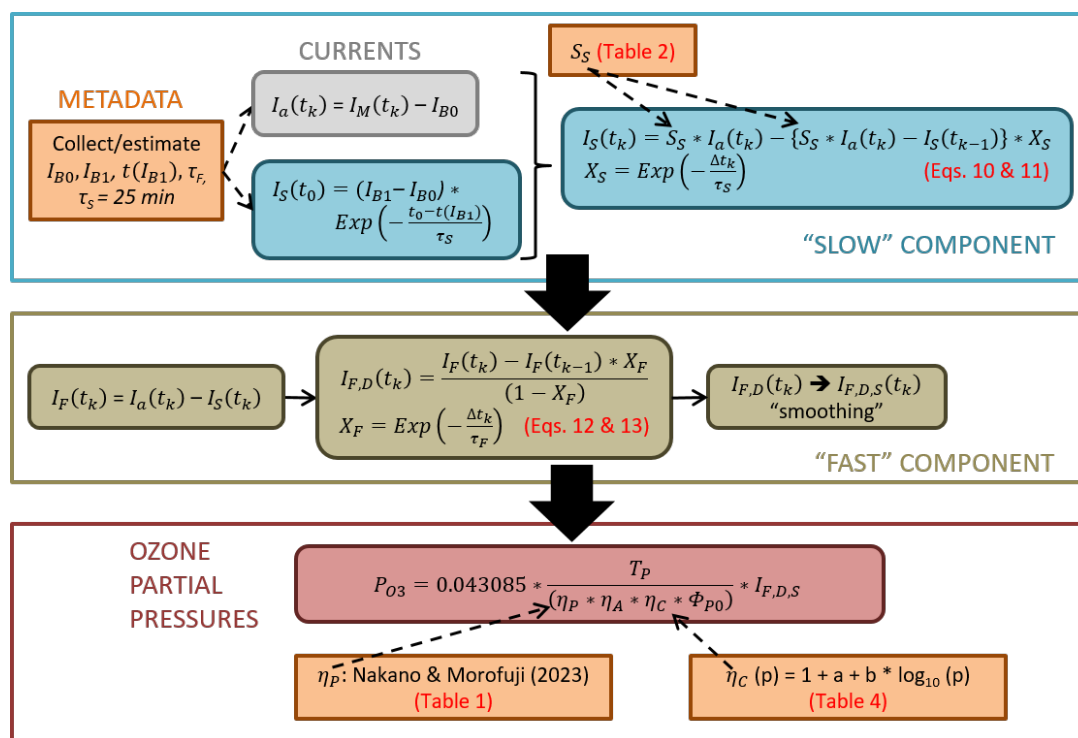
1543
 1544 In total, we have 8 S_s estimations with 4 EN-SCI ozonesondes filled with SST0.1 solutions coming from 3 different
 1545 experiment runs: 2 runs with each 2 (new) EN-SCI ozonesondes (with SST0.1), and a run with all 4 (re-used) EN-SCI
 1546 ozonesondes involved. These 4 ozonesondes, all with serial numbers Z379xxx, have been prepared by the same person,
 1547 according to the SOPs defined in GAW Report No.268, 2021. The median value for S_s for the 8 experiments, each including



1548 three time intervals, is 0.023 ± 0.005 . This value is very close to the value $S_S=0.017$ found for SST0.5 during the JOSIE
 1549 2009/2010 campaign, whereas a smaller value could be expected due to the lower buffer amount in SST0.1 (see Johnson et
 1550 al., 2002 and Sect. 3.2). However, the same Uccle experimental setup and method as described here above for EN-SCI
 1551 SST0.1 have been used to determine the S_S coefficient for 4 EN-SCI ozonesondes filled with SST0.5 (serial numbers
 1552 Z379xxx, but different from those used with SST0.1) during two experimental runs. The resulting median value,
 1553 0.022 ± 0.004 , is again in close agreement with the value determined for EN-SCI SST0.5 with the JOSIE 2009/2010 ($0.018 \pm$
 1554 0.004), confirming the consistency between the two instrumental setups to determine the stoichiometry coefficients.
 1555 Nevertheless, a JOSIE campaign is foreseen in 2023 to determine the S_S factors for SST0.1 for both EN-SCI and SPC
 1556 ozonesondes, using the same simulation setup as in JOSIE 2009/2010.

1557 **Appendix C: How to use TRC + calibration functions in practice: Practical Guidelines**

1558 In this appendix, we give a schematic overview of the different steps that need to be taken to implement the TRC +
 1559 calibration functions in the data processing of an ozonesonde time series in practice, displayed schematically in the flow
 1560 chart in Fig. C1.
 1561



1562
 1563
 1564 **Figure C1.** Flow chart summarizing the processing steps for the Time Responses Resolving Method (TRC) for correcting
 1565 ozonesonde data. The table and equation numbers in red refer to these in this paper.
 1566

1567 First, it should be noted that the TRC is applied on the currents measured by the ozonesonde. Hence, these ozonesonde’s raw
 1568 measurements should be available. Normally, when a site has been homogenized as part of the O3S-DQA activity, the
 1569 currents have been made available or have been converted back from the ozone partial pressures. Secondly, the TRC



1570 demands the knowledge of some metadata parameters that should have been measured during the preparation of the
1571 ozonesonde 0-1 day prior to launch (see also Fig. C1): I_{B0} , I_{B1} , the time of the I_{B1} measurement (relative to the launch time),
1572 and the sensor fast response time τ_F , measured as the time to drop from 4.0 to 1.5 μA (after the 5 μA test). If those metadata
1573 parameters are missing, these might be estimated as the means over a representative time period, e.g. using the same filter for
1574 determining the background currents, or the same batch of ozonesonde serial numbers or sensing solution for the fast
1575 response time.

1576 In a next step, the I_{B0} value is subtracted from the time series of measured currents of the sounding, resulting in $I_a(t_k)$, and all
1577 forthcoming calculations should be done with those currents $I_a(t_k)$. As the calculation for obtaining the slow component of
1578 the ECC signal is a recursive equation (Eq. 10), the slow component at launch time should be estimated first. Therefore, it
1579 suffices to start from the last measured value of the ozonesonde before launch, the I_{B1} , corrected for (i.e. subtract) the I_{B0}
1580 value, and convolve it with an exponential decay function with a slow time constant of 25 minutes. Hereby, the time
1581 difference between the I_{B1} measurement and the launch is used. If this time difference is large enough (GAW Report No. 268
1582) recommends a minimum 30-min time window), the exponential decay function will be close to zero, I_{B1} will approach the
1583 I_{B0} value, and the slow component at launch time will be zero, which is the allowed lower limit. Now, for every time step,
1584 the slow component of the ECC signal can be calculated from equations 10 and 11, using the stoichiometry factor S_s from
1585 the sonde–SST combination (see Table 2). This slow component can be seen as a time varying background current and
1586 should be subtracted from the currents $I_a(t_k)$, to be left over with the fast component I_F of the ECC signal.

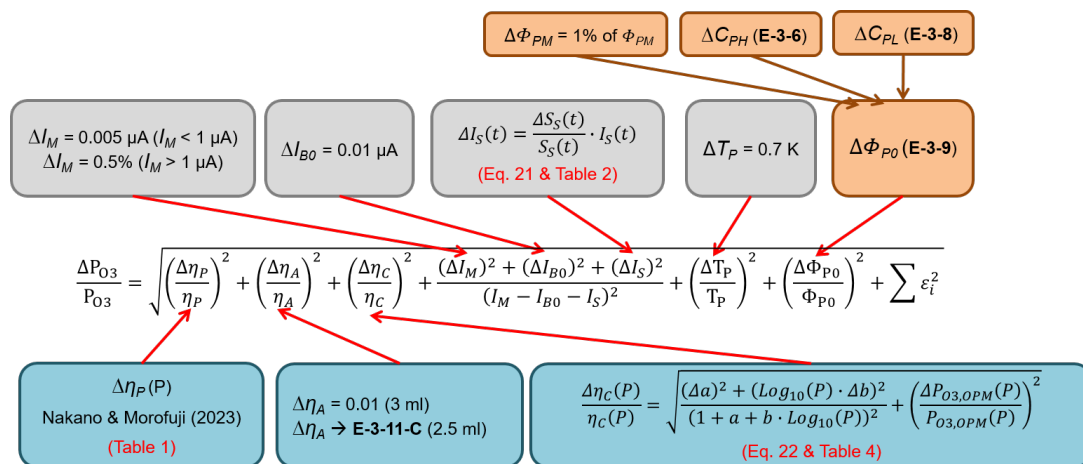
1587 To eliminate the 20 to 25 seconds response delay in the fast component, the latter can be deconvolved (Eqs. 12 and 13), i.e.
1588 corrected for the exponential decay of the signal with the fast sensor response time, measured before launch. This
1589 deconvolution will introduce a lot of noise in the signal, and therefore, a smoothing of the current, either before or after the
1590 deconvolution, will be necessary. Different smoothing algorithms can be considered, with different filter widths and/or time
1591 windows (e.g. for running averages). The choice of the smoothing algorithm depends on the application, e.g., to resolve
1592 steep vertical gradients and the profiles (smooth mid-latitude vs. upper-tropospheric tropical profile), as well as the
1593 measurement time interval (10 s versus 1s time resolution). At the end, a compromise between the smoothness of the profile
1594 and a full correction for the time response delay around strong vertical gradients should be sought.

1595 The smoothed, deconvolved time series of the fast component $I_{F,D,S}$ of the ECC signal is then used in the basic equation of
1596 the ozonesonde signal, converting the current to ozone partial pressure. In this equation, the recommended corrections for T_P ,
1597 η_A , and ϕ_{P0} in GAW Report No. 268 should be implemented as well: the conversion to the piston pump temperature [E-3-
1598 15], a correction for the absorption efficiency if the cathode cell was only filled with 2.5 cm^3 of solution before launch [E-3-
1599 11-A&B], and the humidification [E-3-4] and pump temperature [E-3-7] corrections for the pump flow rate at the ground. In
1600 comparison with the recommended processing in GAW Report No. 268, the pump efficiency corrections proposed by
1601 Nakano & Morofuji (2023) should now be used for all combinations of sonde type and SSTs, as these are the actual
1602 measured ones. The Komhyr (1986) and Komhyr et al. (1995) tables should be discarded, as these are empirical correction
1603 curves, as they actually combine pump efficiency and conversion efficiency. A last difference with the conventional method
1604 as proposed in GAW Report No. 268 is the use of the “calibration functions” defined in Sect. 6, Eq. 18: $\eta_C(p) = 1 + a + b * \log_{10}(p)$,
1605 with the coefficients a and b determined for every sonde type and SST combination separately (see Table 4), for the
1606 conversion efficiency, instead of adopting the value $\eta_C(p) = 1.00$. Using the calibration functions, the ozone sounding
1607 measurement should be traceable to the common reference of the ozonesonde network, the ozone photometer OPM in the
1608 simulation chamber of the World Calibration Centre for Ozonesondes in Jülich.

1609
1610 To calculate the uncertainties associated with the ozone partial pressure measurements of an ozonesonde, corrected with
1611 TRC + calibration functions, the uncertainty equation E-3-1 in GAW Report No. 268 (2021) forms the basis. With respect to



1612 this formula, the uncertainty equation for the TRC (see also Fig. C2) has one changed term, and the meaning of a couple
 1613 other terms has changed. We will only describe these 3 terms here.
 1614
 1615



1616
 1617

1618 **Figure C2.** Overview of the different data processing steps and input to derive the uncertainty of the ozone partial pressure
 1619 measured with an ozonesonde, using the TRC + calibration functions. Figure adapted from Fig. C-4 in GAW Report No. 268
 1620 (2021). The equation numbers also refer to equations in this GAW report. Table numbers in red refer to tables in the main
 1621 text of this paper.

1622

1623 First, as both the I_{B0} and slow component I_S are subtracted from the measurement background in the TRC, the uncertainties
 1624 of the I_{B0} and I_S should be included now. For I_{B0} , the uncertainty is estimated to be $0.01 \mu A$, and the (relative) uncertainty of
 1625 the slow component is, in a first order approximation, equal to the (relative) uncertainty of the stoichiometry coefficient S_S .
 1626 The uncertainties of S_S for the different SSTs can be found in Table 2.

1627 For TRC, the uncertainty of the pump efficiencies $\Delta \eta_P$ are now equal to the standard deviations of the pump efficiency
 1628 measurements reported in Nakano & Morofuji (2023), also shown in Table 1. Finally, the uncertainty of the conversion
 1629 efficiency is no longer estimated as a fixed value $\eta_C = 0.03$, but should take into account the uncertainty of the derived
 1630 calibration functions $\eta_C(p) = 1 + a + b \cdot \log_{10}(p)$ in Sect. 6 (see Table 4 for the uncertainties on the linear regression
 1631 coefficients a and b for the different combinations of sonde type and SST), as well as the uncertainty of the photometer
 1632 (OPM) to which the ozonesonde measurements are traced back. This latter (relative) uncertainty $\frac{\Delta P_{O_3,OPM}(P)}{P_{O_3,OPM}(P)}$ is estimated to

1633 be around 2%.

1634



1635 **Appendix D: Nomenclature of parameters**

| | | |
|------|---------------------------|--|
| 1636 | I_{B0} | Background Current before exposure with ozone (after 10 min flushing cathode cell with “zero” air) |
| 1637 | I_{B1} | Background Current after exposure with ozone (after 10 min flushing cathode cell with “zero” air) |
| 1638 | I_{B2} | Background Current at launch site just before flight |
| 1639 | I_B | Background Current used in data processing in Eq. (1). |
| 1640 | | |
| 1641 | S_F | Stoichiometry factor of fast reaction pathway of conversion of O_3 into I_2 |
| 1642 | S_S | Stoichiometry factor of slow reaction pathway of conversion of O_3 into I_2 |
| 1643 | I_M | Measured (cathode) cell current |
| 1644 | I_{OPM} | Ozone equivalent ECC current at time t derived from OPM |
| 1645 | I_F | Fast cell current |
| 1646 | $I_{F,D}$ | Fast cell current, deconvolved |
| 1647 | $I_{F,D,S}$ | Fast cell current, deconvolved, smoothed |
| 1648 | I_S | Slow cell current |
| 1649 | P_{O_3} | Ozone partial pressure |
| 1650 | R | Universal gas constant |
| 1651 | F | Faraday constant |
| 1652 | T_P | Pump temperature |
| 1653 | Φ_{P0} | Pump flowrate |
| 1654 | η_A | Absorption efficiency |
| 1655 | η_P | Pump efficiency |
| 1656 | η_C | Conversion efficiency |
| 1657 | η_T | Total (overall) efficiency |
| 1658 | τ_F | Response time of fast reaction pathway of conversion of O_3 into fast cell current component |
| 1659 | τ_S | Response time of slow reaction pathway of conversion of O_3 into slow cell current component |
| 1660 | RT1, RT2, RT3, RT4 | Response time tests in vertical ozone profile |
| 1661 | | |
| 1662 | | |



| | | |
|------|---|---|
| 1663 | Appendix E: List of Abbreviations (Green marked are mentioned in manuscript) | |
| 1664 | ASOPOS | Assessment of Standard Operating Procedures for OzoneSondes |
| 1665 | BESOS | Balloon Experiment on Standards for OzoneSondes |
| 1666 | CMDL | Climate Monitoring and Diagnostics Lab (formerly called GMD, now GML) |
| 1667 | ECC | Electrochemical Concentration Cell |
| 1668 | EN-SCI | Environmental Science Corporation; ECC ozonesonde manufacturer |
| 1669 | ESRL | Earth System Research Laboratories |
| 1670 | FZJ | ForschungsZentrum Jülich |
| 1671 | GAW | Global Atmospheric Watch |
| 1672 | GML | Global Monitoring Laboratory (division of NOAA's ESRL; formerly GMD) |
| 1673 | H₂O₂ | Hydrogen peroxide |
| 1674 | IAP | Institute of Atmospheric Physics, Beijing, China |
| 1675 | IPCC | Intergovernmental Panel on Climate Change |
| 1676 | JMA | Japanese Meteorological Agency |
| 1677 | JOSIE | Jülich OzoneSonde Intercomparison Experiment |
| 1678 | KI | Potassium Iodide |
| 1679 | NASA | National Aeronautics and Space Administration |
| 1680 | NBKI | Neutral-Buffered Potassium Iodide |
| 1681 | NDACC | Network for the Detection of Atmospheric Composition Change |
| 1682 | NOAA | National Oceanic and Atmospheric Administration |
| 1683 | NO_x | Nitrogen Oxides |
| 1684 | O3S-DQA | OzoneSonde-Data Quality Assessment |
| 1685 | OPM | Ozone PhotoMeter instrument (used as UV-reference at WCCOS) |
| 1686 | SHADOZ | Southern Hemisphere ADDitional OZonesonde |
| 1687 | SI²N | Ozone trend assessment study supported by SPARC, IOC, IGACO, and NDACC |
| 1688 | SOP | Standard Operating Procedure |
| 1689 | SPARC | Stratosphere-troposphere Processes And their Role in Climate |
| 1690 | SPC | Science Pump Corporation; ECC ozonesonde manufacturer |
| 1691 | SST | Sensing Solution Type |
| 1692 | SST0.1 | 1.0% KI & 1/10th buffer solution |
| 1693 | SST0.5 | 0.5% KI & half pH-buffer solution |
| 1694 | SST1.0 | 1.0% KI & full pH-buffer solution |
| 1695 | SST2.0 | 2.0% KI & non-pH-buffered solution with no KBr |
| 1696 | STP | Standard Temperature (=273.15 K) and Pressure (=1013.25 hPa) conditions |
| 1697 | TOAR | Tropospheric Ozone Assessment Report |
| 1698 | TRC | Time Responses Resolving Methodology |
| 1699 | UNEP | United Nations Environment Programme |
| 1700 | UV | Ultraviolet |
| 1701 | UWYO | University of Wyoming |
| 1702 | VOC | Volatile Organic Compound |
| 1703 | WCCOS | World Calibration Centre for OzoneSondes |
| 1704 | WMO | World Meteorological Organization |